Buoyant horizontal jets in an ambient flow

by

Merete Knudsen

Thesis supervisor:

Ian R. Wood

Professor of Fluid Mechanics

Supported by

National Water and Soil Conservation Organisation,
Ministry of Works
New Zealand

Department of Civil Engineering, University of Canterbury
Christchurch, New Zealand.

March 1988

ABSTRACT

Dimensional analysis has been used to derive formulae for dilution and trajectory for horizontal, buoyant, axisymmetric jets in still ambient, a coflow, a crossflow or a counterflow. The variation of the coefficients in the derived relationships are determined by analysing data obtained by the author and a number of other workers. The results have been presented in charts.

Further, a model to calculate the above flows which is based on the spreading concept has been outlined. The model is shown to describe simple cases well and is in these cases superior to models based on the entrainment hypothesis. However, work is still required to make the model cover the general case of a horizontal jet in an ambient flow.

A study has been made of the instability of jets in a counterflow. A number of behaviour modes are defined and described. On the basis of data from extensive experiments by the author a flow regime chart is presented which defines the occurrence of the different modes.

The frequencies of one type of unstable, oscillating behaviour of jets in a counterflow are studied. A functional relationship between Strouhal number and the ratio between exit velocity and ambient velocity is found from dimensional analysis and experimental data.

ACKNOWLEDGEMENTS

First and foremost, I would like to express gratitude and appreciation to my supervisor Professor Ian R. Wood for his guidance, encouragement and enthusiasm during this study.

For construction of laboratory equipment I am much indebted to Messrs. Alan Stokes, Harry Pearce and Ian Sheppard for their prompt and competent workmanship, Mrs. Val Grey for drafting some of the figures and Mr. Lionel Gardner for developing the photographs. Furthermore, the kind help and assistance from the staff in the Engineering Library and the Audiovisual Centre is very much appreciated.

Kris Ericksen and Institute of Data Technology, Technical University of Denmark deserve thanks for the loan of word processing equipment.

The kind friendship of Russell and Wendy Mein of Australia gave me a very good start here in New Zealand. Also the friendship and support from Alan and Cynthia Stokes, Kris Ericksen, my family and many others has been invaluable.

I would also like to thank University of Canterbury for providing the facilities which made this study possible.
The financial support was provided by National Water and Soil Conservation Organisation, Ministry of Works.

The thesis was submitted in March 1988 to University of Canterbury in fulfillment of the requirements for the degree of Doctor of Philosophy in Civil Engineering.

CONTENTS

Notation

Symbol	Definition	Appears in chapter
A	cross sectional area = volume per unit length in line thermals	4
A_Δ	buoyancy per unit length in line thermals	4
B	$= \pi/4\ d_p^2\ U_o\ \Delta_o$ initial discharge of buoyancy flux	4
b	distance from center line where $u_e = u_{em}\ e^{-1}$	4
C_{an}	where n=1,2,7 coefficients for still ambient case, see table 5.4	5
C_{bn}	where n=1,2,4,5,7,8,9,10 coefficients for coflow cases, see table 5.4	5
C_{cn}	where n=1,2,3,4,5,6,7,8,9,10 coefficients for crossflow cases, see table 5.4.	5
C_d	drag coefficient	6
C_{dn}	where n=1,2,4,5,7,8,9,10 coefficients for counterflow cases, see table 5.4.	5
C_o	initial tracer concentration	4
C^*	critical value for stability of counterflows ≈ 0.6 , cfr. sect. 7.3.	7
C_1	critical value for clinging parameter, cfr. sect. 7.3	7
C_1^*	critical value for clinging parameter ≈ 5.3 , cfr. sect. 7.3	7
c	local tracer concentration	4
c_m	center line tracer concentration	4
d_p	port diameter	4
d'	distance from the port to the free surface	7
E	entrainment function	6
E_o	initial value of entrainment function	6
f	$\Delta/\Delta_m = f(\eta)$ i.e. f is a function	6
f	frequency of type III oscillations	7
f_n	where n= 1-13 are unknown functions	4
Fr	$= U_o/(\Delta_o\ d_p)^{1/2}$ the densimetric Froude number	4
g	acceleration of gravity	4
h	$v_v/v_{vm} = h(\eta)$ i.e. h is a function	6
h	vertical distance from port to highest point of jet outline, cfr. fig. 7.10	7
h^*	unknown function in the analysis of frequencies in chapter 7	7
I_c	cross sectional constant, similar to I_Δ	6
I_q	cross sectional constant, defined by eq. (6.2.13)	6
I_{qc}	cross sectional constant, similar to $I_{q\Delta}$	6
$I_{q\Delta}$	cross sectional constant, defined by eq. (6.2.17)	6

I_m	cross sectional constant, defined by eq. (6.2.12)	6
I_{mv}	cross sectional constant, defined by eq. (6.2.14)	6
I_v	cross sectional constant, defined by eq. (6.2.15)	6
I_Δ	cross sectional constant, defined by eq. (6.2.16)	6
$\underline{i}$	unit vector in the direction of the x-axis	4
K_c	cell constant	3
k	$= db/ds \approx 0.109$ for pure jets in still ambient and pure plumes in still ambient	4
L_{HT}	horizontal distance from the port to the stagnation point in counterflows	7
L_{VT}	vertical distance from the port to the stagnation point in counterflows	7
$l_{BU\infty}$	$= B / U_\infty^3$ length scale	4
l_{vB}	$= \nu^{3/2} / B^{1/2}$ length scale	4
l_{MB}	$= M^{3/4} / B^{1/2}$ length scale	4
l_{MeB}	$= M_e^{3/4} / B^{1/2}$ length scale	4
$l_{MeBU\infty}$	$= M_e U_\infty / B$ length scale	4
$l_{MeU\infty}$	$= M_e^{1/2} / U_\infty$ length scale	4
l_{QB}	$= Q^{3/5} / B^{1/5}$ length scale	4
$l_{QU\infty B}$	$= Q U_\infty^2 / B$ length scale	4
l_{QM}	$= Q / M^{1/2}$ length scale	4
l_{QMe}	$= Q / M_e^{1/2}$ length scale	4
M	$= \pi/4\ d_p^2\ U_o^2$ initial momentum flux	4
M_e	$= \pi/4\ d_p^2\ U_o\ \lvert \underline{U}_o - \underline{U}_\infty \rvert$ initial excess momentum flux	4
M_{eo}	$= M_e$ initial excess momentum flux	4
M_{ex}	the x-component of the excess momentum flux	4
M_y	the y-component of the excess momentum flux	4
m	$= db/dy$ for line thermals and $= db/dx$ for line momentum puffs	4
Q	$= \pi/4\ d_p^2\ U_o$ initial discharge	4
q	local volume flux	6
q_{inflow}	entrainment per unit length in the s' direction	6
R	some large, finite value of r	6
r	radial coordinate in cross sections	4
	(or visible half width of dyed thermals, eq. (4.4.1))	4
s	coordinate along the center line of the jet	4
s'	coordinate perpendicular to the cross section	6
S_{CL}	$= \Delta_o/\Delta_m$ for buoyant jets and $= C_o/c_m$ for non-buoyant jets (C_L dilution)	4

t	time	4
$t_{AA\Delta}$	$= A^{3/4} / A_\Delta^{1/2}$ time scale	4
$t_{A\mu}$	$= A^{3/2} / \mu$ time scale	4
U_{eo}	initial excess velocity = $\lvert \underline{U}_o - \underline{U}_\infty \rvert$	4
U_o	initial velocity at the port	4
$\underline{U}_\infty$	ambient velocity	4
u	local velocity in the jet	4
u_e	local excess velocity	4
u_{em}	center line excess velocity	4
u_{entr}	inwards velocity at the distance b from the center line, entraining velocity	6
u_m	center line velocity	4
u_s	component of u_e perpendicular to the cross section	6
u_{sm}	component of u_{em} perpendicular to the cross section	6
v_v	component of u_e parallel to the cross section	6
v_{vm}	component of u_{em} parallel to the cross section	6
x	coordinate in the direction of discharge	4
x_{max}	maximum value of x in still ambient and cross flows (see table 5.4)	5
x_o	integration constant	6
y	coordinate in the direction of buoyancy (depth)	4
y_o	integration constant	6
z	coordinate perpendicular to x and y such that a right hand system is formed	4
α	entrainment coefficient	6
β	angle from the X-axis to u_{sm}	6
δ	angle from u_{sm} to u_{em}	6
Δ	$= (\rho_r - \rho_\rho)g/\rho_r$ local buoyancy of the jet	4
Δ_m	center line buoyancy in the jet	4
Δ_o	initial buoyancy of the jet	4
Φ	unknown function	4 & 6
Φ^*	unknown function	4
ϕ	angle between horizontal and the center line	6
γ	angle between u_{em} and cross section	6
η	$= r/b$	6
λ	spreading coefficient	4
μ	initial instantaneous kinematic momentum input per unit length of line	

	momentum puff	4
ν	kinematic viscosity	4
ρ	local density of the jet	4
ρ_r	reference density, e.g. the density of the ambient fluid	4
Ψ	unknown function	4
Ψ^*	unknown function	4
ζ	some jet parameter such as b, u_{em}, S_{CL}, x,y	4
ζ^*	ζ non-dimensionalised with appropriate parameters, e.g. u_{em}/U_∞ etc.	4

Abreviations.

BDFF	buoyancy dominated far field	5
BDNF	buoyancy dominated near field	5
CL	center line	4
CV	control volume	6
IZ	initial zone	5
MDFF	momentum dominated far field	5
MDNF	momentum dominated near field	5
ZFE	zone of flow establishment	4

Other symbols.

~	proportional to, of the order of magnitude of	4
$\rightarrow$	tends towards, transition to	5

Note: For technical reasons it has not been possible to print subscripts of subscripts in the main text (but it has been possible in the equations). Also for technical reasons it has not always been possible to print equation numbers on the same line as the equations. The number has then been given on the following line.

CHAPTER 1
INTRODUCTION

With the increasing urbanisation and industrialisation there is an increasing production of waste water. The modern practise for dealing with this waste water consists of some treatment followed by discharge through an outfall into either a lake or the ocean.
Lakes and coastal areas are of a great recreational value. It is therefore important no damage be done by the amounts of waste water which are being discharged into these waters.
The protection of the receiving water areas is important in the design of a waste water disposal scheme and it is necessary to consider the aesthetic as well as the hygienic and ecological impact of a planned discharge.

In most countries there is legislation which clearly outlines maximum limits of the discharge of certain hazardous substances. These substances accumulate in the environment and subsequently accumulate in the food chains. Ideally, enforced trade waste regulations should prevent the discharge of such substances. Indeed, New Zealand legislation gives limits for the amount of both toxic substances and biodegradables that can be discharged into the receiving waters.
To minimise the impact on the environment of the waste water the best possible dilution is sought obtained. This is achieved by discharging via outfalls which consist of a long pipe on the bed of the ocean or lake (see fig. 1.1). Some outfalls discharge the waste water through a single opening at the end of the pipe. Where optimum dilution is required a series of ports placed alternatingly on each side of the pipe (a diffusor) ensure additional dilution.

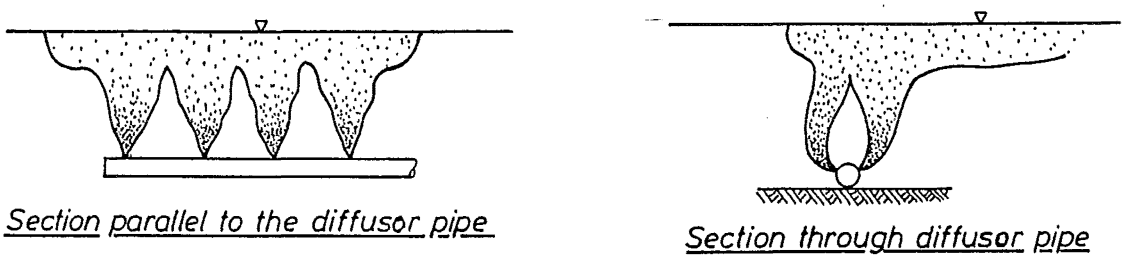

Fig. 1.1. Sketch of multiport diffusor.

On many outfalls the ports are sufficiently spaced so that the plumes do not merge. The plumes rise to the surface and the dilution over this rise is called the initial dilution. At the surface the plumes become surface plumes and are advected and there is further dilution.
This study deals only with the initial dilution from a single port in an ambient flow (coflow, crossflow or counterflow) with negligible turbulence in the ambient.

Chapter 2 is a review of relevant literature. In the following chapters further references to other work will be made, so chapter 2 is kept brief.

In chapter 3 a description is given of the experimental equipment and procedures.

In chapter 4 a discussion of 5 limiting types of jets is given. The character of these jets is such that dimensional analysis can be used to derive formulae for quantities such as local velocities, width of the jet, dilution and trajectory.

These results are applied in chapter 5 to the more general case of a horizontal buoyant jet in an ambient flow (co-,cross- or counterflow) . On the basis of this design charts have been produced from which the approximate value of trajectory and dilution as a function of depth can be found for any given type of jet.

In chapter 6 a numerical model is outlined. The model is based on a so-called spreading closure rather than the more commonly used entrainment closure and predicts data well in all limiting cases and some more complex flows. However, further work is required to make the model applicable to the general case.

During experimentation it was found that several different modes of instability can occur in counterflowing jets. This was further investigated and has been discribed and classified in chapter 7.

Finally, conclusions and references are given in chapters 8 and 9.

CHAPTER 2
LITERATURE STUDY

2.1. General.

Previous investigators have concentrated on the study of vertical buoyant jets in still ambient (Fan [1967] , Papanicolaou [1984] , Noutsopoulos & Yannopoulos [1985] and others) and pure jets in a perpendicular crossflow (Keffer & Baines [1963] , Pratte & Baines [1967] , Margason [1968] , Platten & Keffer [1968] and others) and for the latter group the main interest has been to determine the trajectories.

Most modern outfalls consist of horizontal buoyant jets in an ambient flow and only work which relates to this type of flows can be used directly in the design of ocean outfalls.

2.2. Methods of solution.

In early attempts to solve simple jet problems so-called constitutive relations were specified. The constitutive relations were relations (not necessarily linear) between the Reynold's stress tensor and the deformation tensor for the fluid. They were specified for the turbulent transport terms in the equations for the conservation of mass, momentum, energy and tracer. This method has not generally been considered for more complex jets in an ambient flow (or in density stratification).

Another method of solution has been to derive relations for mean flow properties from dimensional analysis of the given problem.Wright [1977] used this method to make a comprehensive analysis of vertical buoyant jets in a crossflow. Bühler & Hauenstein [1979] used a similar method to analyse horizontal buoyant jets in a crossflow.
To the knowledge of the author no comprehensive analysis has been made of horizontal buoyant jets in an ambient flow from an arbitrary horizontal angle using this method.

The third and most commonly used method has been to consider the integrated conservation equations for mass, momentum flux and buoyancy or tracer flux. The flow has usually been assumed to be self similar in cross sections perpendicular to the center line . The distribution of velocity, buoyancy and tracer has been assumed Gaussian and the equations have been integrated over these cross sections. Thereby the equations have been greatly simplified.

This 'integral method' was proposed by Morton, Taylor & Turner [1956].
A thorough discussion of the development of the general equations for a buoyant jet in a (density-stratified) crossflow is given by Hirst [1971].

The general equations contain one more variable than the number of equations. An additional equation is therefore required in order to obtain a closed system of equations.
The most commonly used closure is the entrainment hypothesis in which it is assumed that the rate of entrainment per unit length of the jet is proportional to the local maximum excess velocity on the center line and the local width of the jet. This closure was first suggested by Morton, Taylor & Turner [1956] and has subsequently been used and modified by other workers. Some workers have assumed that the ambient flow exerts a 'drag' on the jet as if it were a solid body. In those cases a drag term has been included in the momentum equations.

The basic equations are derived in chapter 6 and a more detailled discussion of the entrainment hypothesis is also given there.

There exists an alternative to the 'integral method' which is the so-called differential method. In this approach no assumptions have been made about axisymmetry of the flow or about the distribution of velocity, buoyancy or tracer. The equations are therefore more applicable to different types of flows. However, more assumptions have been made and the system of equations is also much more complicated to solve. Only one model, Hirst [1971], has been based on this method.

2.3. Existing models for round buoyant jets in an ambient flow.

Fan [1967] derived a model for vertical round buoyant jets in a stratified crossflow. He assumed Gaussian profiles throughout the flow . He also had a drag term in the horizontal momentum equations. It will be described in more detail in chapter 6 how Fan performed the integration over the cross sections such that an additional term incorrectly appeared in the momentum equations. Fan fitted the drag coefficient and a variable entrainment coefficient such that the model predicted the available data.
Abraham [1970] developed a model for the discharge of a vertical round buoyant jet into a constant density ambient fluid with a horizontal flow field. Abraham used a semi-empirical two parameter entrainment relationship and had also a drag term in the momentum equations. Abraham's equations had the same incorrect additional term in the momentum flux equations as Fan.

Hirst [1971] developed a model for vertical buoyant jets in a crossflow. He used a three parameter entrainment coefficient and had no drag term in the momentum equations. His model was as mentioned of the differential type. According to Schatzmann [1976] there are also mistakes in the derivations in Hirst's analysis.

Ayoub [1971] developed a model for horizontal round jets in a coflow and a crossflow. He fitted a complex entrainment coefficient function, a drag coefficient and a spreading coefficient function λ to data(λ is a factor that accounts for the fact that buoyancy spreads out faster than momentum in a jet, and which is normally considered a constant in other models) . Ayoub used the same incorrect approach as Fan in deriving the momentum flux equations, so the data-fitting concealed the fact that the model was based on incorrect equations.

Schatzmann [1976] developed a comprehensive model for buoyant round jets in an ambient stratified flow with two-dimensional trajectories (i.e. the only horizontal jets which can be described by Schatzmann's model are buoyant jets in still ambient, coflow and possibly counterflow). The model allows for large density differences between effluent and ambient. It contains a drag term and the entrainment function is derived from the kinetic energy equation. The five constants in the entrainment function are determined by letting it match 5 different limiting cases. No further data fitting was done. The model predicts a wide range of data well.

2.4. Data for round buoyant horizontal jets in an ambient flow.

Below in table 2.1 a list has been given of some of the available data for round buoyant horizontal jets in an ambient flow. (Pure plume data are also listed but they will of course be vertical jets.)

Type of jet	Author	Measured quantities
Buoyant jet in still ambient	Fan [1967]	trajectory
	Hansen & Schrøder [1968]	dilution
Pure jet in coflow	Forstall & Shapiro [1950]	velocity
	Antonia & Bilger [1974]	velocity
	Challen [1968]	velocity
	Present work	width, dilution
Buoyant jet in coflow	Ayoub [1971]	width, dilution, trajectory

Type of jet	Author	Measured quantities
	Present work	width,dilution trajectory
Pure jet in still ambient	Albertson et al. [1950]	velocity, width
	Wygnanski & Fiedler [1969]	velocity
	Crow & Champagne [1971]	velocity, width
	Present work	width, dilution
Pure plume in still ambient	Nakagome & Hirata [1976]	velocity, width
Hor. buoyant jet in crossflow	Ayoub [1971]	width, dilution, trajectory
	Chu [1975]	trajectory

Table 2.1.

CHAPTER 3
EXPERIMENTAL EQUIPMENT AND PROCEDURES

3.1. Introduction.

Three types of experiments were performed. They are briefly described in the following:

1) The experiments were carried out to study the two phenomena which will be described in chapter 7 , jet oscillations in counterflow and clinging to a free surface by a jet discharged close to it. These experiments were the basis for determining the regime chart in fig. 7.12. This is a chart which shows regimes where the flow types shown in fig. 7.3-7.5 occur.
   The experiments were recorded on video. From the video recordings the individual flows were classified. In those cases where oscillations without clinging occured (type III flows, cfr. fig. 7.5b) the average frequency of the oscillations was also found from the video recording.
   The frequency was plotted as a function of the other flow parameters in fig. 7.13.
   The counterflow cases are described in more detail in chapter 7.

2) In the second set of experiments the trajectories of various jet flows were recorded. The majority of these were for jets in still ambient or in a coflow. The trajectories were found by recording the flows on video. The camera was either in a fixed position or moving along the tank, following the jet. By 'freezing' the recording of the experiments at different times and trace these the trajectories could be found.

3) In the third and last set of experiments concentration measurements were made in various cross sections of a jet. This was carried out for still ambient, coflowing and counterflowing jets.
   These measurements gave information about the density or tracer distribution, the position of the points of maximum concentration (which per definition are on the centerline) and the width in the cross sections considered.

In the following sections of this chapter a description will be given of the experimental equipment and setup.
Finally the sources of error will be mentioned.

3.2. Experimental equipment and procedures.

The buoyant and nonbuoyant jet experiments were made by discharging dyed salt/sugar or fresh water from a constant head tank through a port into a 6 by 1.5 by 1 metre glass tank containing quiescent fresh water (see fig. 3.1).

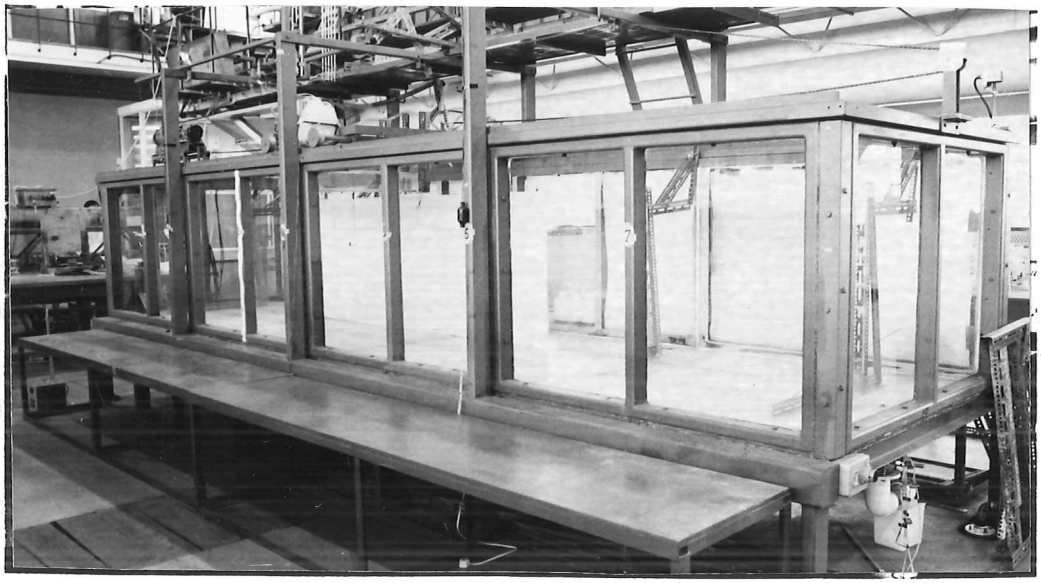

Fig. 3.1. Photograph of experimental tank.

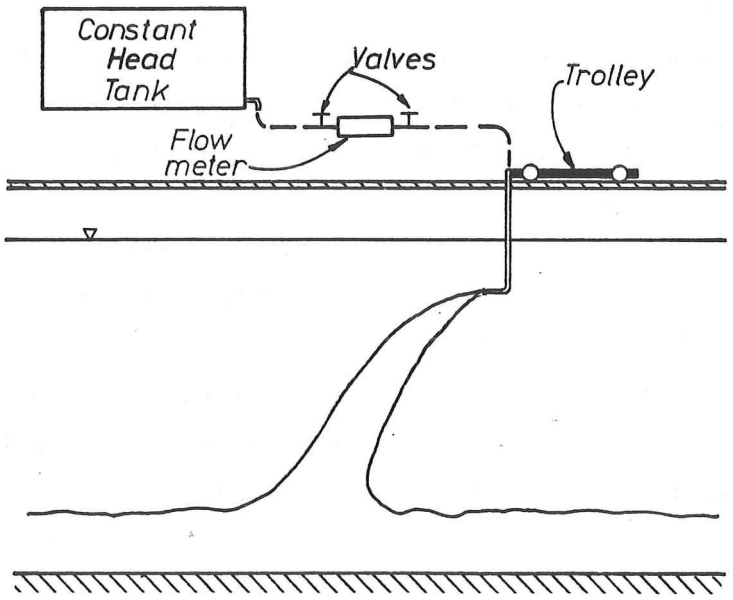

Fig. 3.2. Trolley with attached port.

This is the exact opposite situation of ocean outfalls where fresh water is discharged into salt

water. However, it is only the density difference that is important when studying these flows .

The port was attached to a trolley and to model a moving environment (coflow or counterflow) the port was towed through the stationary ambient fluid. By altering the direction of discharge the direction at which the ambient flow approaches the port could be changed. (See fig. 3.2)

Red food colour, William's certicol carmoisine, was used to dye the effluent.

In non-buoyant experiments fresh water containing dye was used as effluent. For the effluent to behave as non-buoyant it was found that the temperature had to deviate less than 2/10 of a degree Celcius from the temperature of the ambient water.

In the buoyant experiments a 3% salt water solution containing dye was used. This gave a density corresponding to that of sea water, 1.025×10^3 kg/m^3.

In a few experiments densities higher than the above were used. It was found that the dye did not dissolve completely in salt solutions much above 3%. However, the dye dissolved well in very strong sugar solutions. Sugar was therefore used in those few experiments requiring particularly high densities (exp. 192-197). (A few experiments were carried out with sugar solutions that had the same density as seawater to make sure that experiments with sugar were comparable to those made with salt, exp. 190-191 and exp. 198-205). Finally, in a few experiments requiring very high Froude numbers smaller values of the density difference was used.

Five different rotameters were used with the flow ranges 0.15-0.7 ml/s, 0.5-3.5 ml/s, 2.0-20 ml/s, 7.5-32 ml/s and 30-140 ml/s.

The trolley shown in fig. 3.1 and 3.2 was driven by a motor that could be mounted with 2 different sprockets yielding trolley speeds in the ranges 0.007-0.044 m/s and 0.044-0.30 m/s.

The port diameters ranged between 2.0 and 9.3 mm.

In experiment types 1 and 2 either a photographic camera (Olympus OM-1 with 28 mm wide angle lens) or a video camera (either Canon with TV zoom lens or Hitachi VK-C1600 autofocus) were mounted either on a tripod or on a trolley which could move along the tank in tandem with the port.

For the type 1 experiments the photographs or (better) the video recordings could be studied after the experiment. Since the length of the tank and the speed of the trolley on the tank were known, information on the frequencies and length scales of possible periodical phenomena could be found.

Also, the qualitative behaviour of the jet could be studied in more detail. For this, the 'SLOW' and 'STILL FRAME' feature on the video recorder was of great value.

In experiments where direct recordings of the trajectory were made a grid with 10x10 cm grid width was submerged into the tank (filled with water) at the jet center line prior to the experiment and was recorded/photographed. Afterwards the experiment was performed and recorded/photographed. The grid was copied from the photographs. The photographs were

then copied onto the tracing of the grid. This determined the trajectory of the jet. The centerline was defined as being mid between the visual boundaries of the jet.

A similar method was used in the cases where the experiments had been recorded on video ; a piece of plastic sheet was taped onto the screen of the monitor. The recording was played back and by using still frame ('freezing' the picture) the grid and subsequently the shape of the jet at various times could be traced on the plastic sheet with a marker.

This method was very satisfactory.

In coflow runs where the trajectory was short enough to be seen in its entire length on the screen, the camera was moved along the tank with the port. In this method a picture of the jet averaged over a long period of time was obtained.

However, in coflow experiments where the trajectory was long ('stretched out') all of it could not be seen at the same time on the screen without losing a lot of detail. It was decided in those cases to use the camera in a fixed position and let the jet move past. An electronic clock was placed in front of the tank and appeared on the recording. Since the speed of the trolley on the tank was known, the postion of the port at any time after it first had appeared on the recording was known.

The trajectories in all still ambient and counterflow runs were short enough to be seen on the screen in their entire length.

For the concentration measurements the equipment in fig. 3.3 was used.

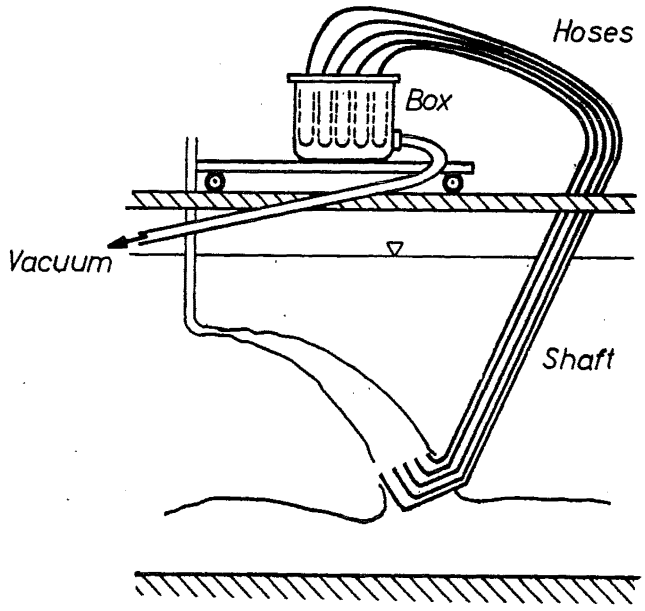

Fig. 3.3. Probe system for sampling.

First the trajectory of a given jet flow was found by using the methods mentioned above.

When the trajectory was known a cross section in which the concentration distribution should be measured was chosen.

The concentration measurements were then made with the equipment shown in fig. 3.3.

A set of probes was attatched to the trolley in such a position that their plane would be in the cross section of the jet where the measurements were to be made. The probes consisted of 40 1.1 m long metal tubes that were shaped as shown in fig. 3.3.

The tubing in the probes was stainless steel with a diameter of 2 mm.

Three different sets of probes were made with different spacing between the probes. The dimensions were 8x8 cm, 15x15 cm and 30x30 cm.

The 8x8 cm probes were used for very thin jets or close to the port, 15x15 cm was an all-round size and was the one that was most used. The 30x30 cm probes were used in thick jets or far from the port.

The upper part of the tubes formed a shaft which via 40 lengths of plastic tubing were connected to a sealed box on top of the trolley.

Prior to an experiment compressed air was applied to the sealed box through a valve. The air then moved through the 40 hoses and out through the probes. This was done to remove the water that would otherwise have been sitting in the part of the probes that was below the water surface. The compressed air also removed the majority of small droplets in the hoses, left from previous experiments.

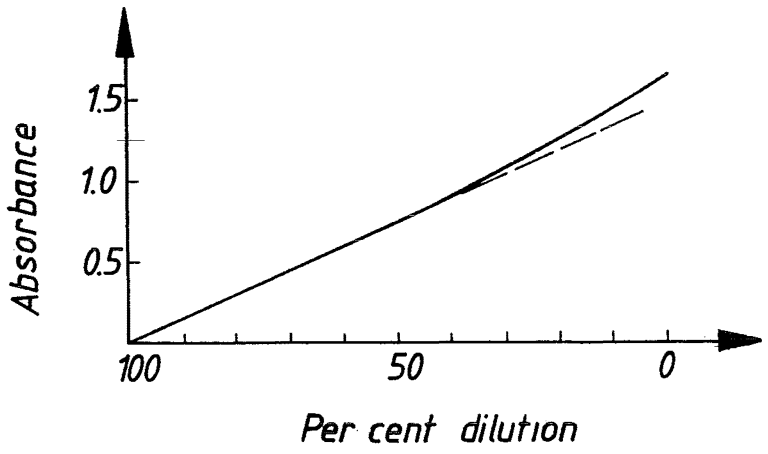

Fig. 3.4. The qualitative variation of absorbance with concentration.

The overpressure stayed in the system until samples were taken when a vacuum was applied to the sealed box and the effluent was withdrawn. The box contained 40 test tubes. Each of these was connected to one of the 40 tubes in the set of probes. By subsequently analysing the

samples concentration profiles could be obtained.

In the non-buoyant experiments the dye was used as a tracer. The absorbance of the samples was measured by using a spectrophotometer (Unicam SP600 series 2). The wavelength was 515 nm which corresponds to a peak absorbance.

As shown in fig. 3.4 there is a linear relationship between absorbance and concentration for absorbances less than 1.0. All samples in the present experiments had absorbances well below 1.0.

It was not necessary to convert the measured absorbances into concentrations because only relative concentrations were needed as data; to draw concentration profiles the local concentrations relative to the centerline concentrations were only required. To find the dilution in a given cross section, the centerline concentration relative to the effluent concentration was required. The absorbance for the effluent was too high to be measured directly. It usually had an absorbance around 20. To measure an equivalent absorbance of the effluent, corresponding to that the curve in fig. 3.4 had been perfectly straight, a sample was diluted as 1:50 with distilled water and the absorbance was then measured. The equivalent absorbance was then the measured absorbance multiplied by 50.

The spectrophotometer was also used for concentration measurements in those buoyant experiments where the effluent was sugar solutions.

In the buoyant experiments where the effluent was salt solutions a faster and easier method could be used to measure the concentration distribution. In those cases the conductivity of each sample was measured with a Radiometer conductivity meter, CDM 83.

The conductivity of a sample is a direct function of the salt concentration and for diluted solutions the conductivity is proportional to the salt concentration. In fig. 3.5 the relationship between conductivity and concentration is shown. For conductivities less than 1 mS/cm the relationship is linear. There was a strong dependency on temperature. The conductivity meter therefore internally transformed the readings to corresponding conductivities at a reference temperature. In a set of samples there could easily be a variation of temperature of 1 ^{o}C or more.This would have been a large source of error. (The temperature dependency as given by the temperature coefficient was 2.2%/^{o}C). A reference temperature was usually chosen which was close to the average temperature of the samples.

A cell constant of K_c=1.345 cm^{-1} was used and was found by callibration.

As for the absorbance measurements it is not necessary to convert the measured conductivities to concentrations. We are only interested in relative concentrations. However, since the relationship between conductivity and concentration is not linear for conductivities greater than 1 mS/cm, values higher than these had to be transformed into equivalent conductivities corresponding to that the conductivity - concentration curve had been a straight line. An

example of this is shown in fig. 3.5 (with a reference temperature of 16 °C).

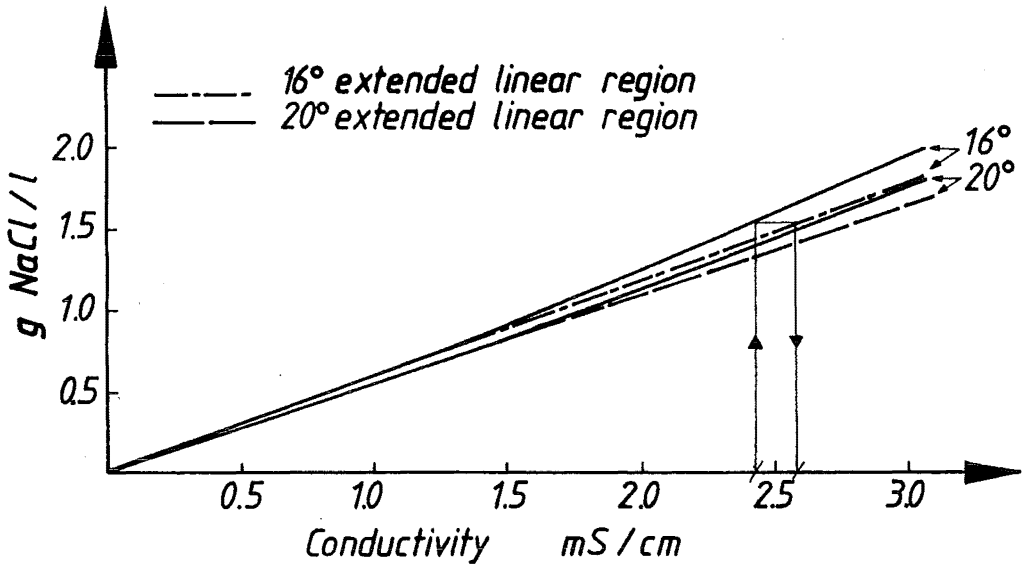

Fig. 3.5. The relationship between concentration and conductivity at 16 °C and 20°C.

The effluent was diluted 1:100 prior to measuring the conductivity. The measured conductivity was then multiplied by 100 to obtain the equivalent conductivity.
For seawater concentrations the conductivity was found to be around 50-60 mS/cm.

3.3. Sources of error.

The discussion of the errors of measurement will be divided up in the 3 categories that were used in the introduction of this chapter, sect. 3.1.

3.3.1. Sources of error in type 1 experiments.

Sources of error in these experiments were:

a) Air pockets in the supply hose
b) Interaction with the bottom
c) Uneven motion of the trolley on the tank / vibrations of port.
d) The subjective nature of some of the measurements.
e) Secondary currents.
f) The short time period studied / short tank.
g) Usage of free surface rather than solid surface to cling to.

a) If air bubbles were discharged this meant an uneven discharge through the port but more importantly: if some kind of periodic behaviour of the jet was present then release of air

bubbles might modify or escalate the behaviour. Care was taken, however, to remove air bubbles from the supply system prior to each run. Before a run commenced, the effluent was discharged at a very high speed before being adjusted to the desired level. This way all air was discharged. The big cloud of initially discharged effluent could cause some problems. A trap was designed to keep most of this effluent in the beginning of the tank.

b) In some runs effluent would run on the bottom underneath or faster than the port. The effluent on the bottom seemed to force the jet upwards to cling to the surface.
In experiments where this was observed the experiment was repeated with greater distance from the port to the bottom.

c) The motor and chain drives caused vibrations and some unevenness in the motion of the trolley. Care was taken to keep this at a minimum. It is possible that unevenness and vibrations could trigger an instability in the jet flow that might otherwise not have been noticed.
The frequency of the vibrations was however very different from the frequency of the observed oscillations whereas the unevenness at times were of a similar frequency.

d) In some cases it was a matter of subjective judgment whether a flow should be called e.g. type III or IV and often intermediate cases occured, e.g. type III and IV alternatingly or type III in the first half of the tank and type IV in the last half of the tank. This lead to a slight difficulty in the classification.

e) The tank was usually left at least half an hour after it had been filled with fresh water. This was done so that currents caused by filling would decay. However, it was not always possible to make these disappear completely. If the water was left in the tank for too long then a weak stratification (especially on warm days) started building up.
Another and in some cases probably stronger source of secondary currents was the motion of the port and the motion of the effluent that was initially discharged.
Secondary currents were most significant in runs with low exit or ambient velocities.

f) The short time spans over which the flows were observed must certainly be a source of inaccuracy. Because the initial part of the tank where the flow became established could be up to 2 metres it meant that some of the runs were observed over as little as 10-20 secs.

h) In the present experiments the clinging phenomenon to a free surface were studied. In ocean outfalls the clinging would be near a solid surface. Although the velocity profiles of the ambient water of course are different at the free surface or near the bottom it is believed that the free surface experiments are also applicable to flows near solid boundaries.

A few qualitative experiments were made in which a positively buoyant jet was discharged near a solid surface and the results from these experiments confirmed what had been found for the free surface experiments.

Error sources d) and f) are probably the most significant ones.
It is estimated that there is approximately an accuracy of up to 50% in the frequencies found in these experiments.

3.3.2. Sources of error in recording of trajectories.

The main sources of error in these measurements were assumed to be the following:

a) The three-dimensionality of the jet as viewed in perspective from one point - parallax errors.
b) Inaccuracies from tracing from a video screen.
c) For very pale or diluted jets - difficulty in defining the jet boundary.
d) For stationary camera - end wall effects.
e) For very uneven jet boundaries - difficulties in defining an average boundary.
f) For stationary camera - lack of time averaging in coflows.

a) The picture of the jet we get is not a parallel projection as could be desired but rather a perspective view. This introduces some inaccuracy.

b) Because of the thickness of the glass on a video screen the position of the lines in the tracings depends on the position of the viewer's eye. For example, if the viewer's head was moved 10 cm downwards, a given line on the screen might be traced 2-3 mm lower. This might represent as much as 1 cm compared to the grid. To minimise this effect it was attempted to trace grids and jets as consistently as possible.

c) Very pale jets could be difficult to define. This was mainly the problem where the port diameter was small (ca. 2mm) and U_0/U_∞ was very small (near 1).

d) The initially discharged effluent would fall and form a cloud that was slowly travelling forwards along the bottom of the tank. In experiments with a stationary camera and where the recording took place over a fairly long time (over one minute) the cloud would almost reach the visible field moving under the jet and thus 'lifting' its end part (see fig. 3.6). Experiments where this effect was strong had to be discarded because of inconsistent

trajectories. In other experiments it could cause scatter of the data. The effluent trap which was mentioned earlier was a way of reducing this source of error.

e) Far from the port the jet boundaries were quite uneven and it was at times a matter of judgment where the average boundary would be.

f) In coflow experiments with a stationary camera we were basically observing a segment of jet falling with time. There were inevitably instability changes in the jet outline. With

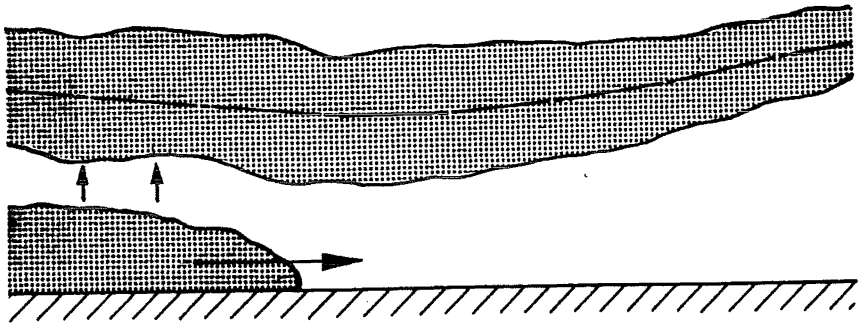

Fig. 3.6. The effect on the trajectory of effluent running along the bottom.

these irregularities in it it could be difficult to get a consistent trajectory from the observations since only a small part of the jet was observed. This problem or source of error did not occur in experiments where the camera followed the jet and a good time average for the trajectory could be made.

In general the inaccuracy was roughly of the order of magnitude plus minus 1.5 port diameters. This had the greatest effect near the port where the x- and y-values were small. When tracing and plotting trajectories it was attempted to do this as consistently as possible. If any trajectories looked inconsistent then they were replotted and if still inconsistent then the experiment was repeated.
For those few cases where photographs rather than video recordings were used, b) does not apply.

3.3.3. Sources of error in concentration measurements.

Here the main sources of error or inaccuracy were:

a) The sampling velocity was too high.
b) Only 40 points to define a profile.
c) The presence of the probes might affect the flow.
d) Inaccuracies in concentration measurement methods.
e) A small amount of fresh water in the probes prior to the run.

a) Because the pressure in the sampling box with the test tubes was somewhat difficult to adjust smoothly the withdrawal could be uneven in some of the experiments. This is a further source of error.

b) There were 40 probes in each set of probes so the resulting concentration contours were based on a maximum of 40 points. When finding the maximum concentration in a cross section by drawing a curve through 5 points there could sometimes be up to 10% inaccuracy. For complicated contours like the ones for the advected thermal from a continuous source more points than 40 would have been useful.

c) The physical presence of the probes may have affected the flow. This is probably a minor effect.

d) Spectrophotometer measurements:
To get optimum accuracy in those measurements the absorbance should be between 0.3 and 0.8. In most of the measurements the maximum absorbance was between 0.05 and 0.6 with about 2/3 over 0.3. The absorbance of the samples decreased to 0 when moving away from the centerline. However, the results were reproduceable. Great care was taken to remove all lint or droplets on cuvettes (glass sample containers) which could have a considerable effect. The inaccuracy was probably plus minus 0.005 for absorbances less than 0.8. This therefore mainly affected the low absorbance samples and has therefore only limited effect as it is really the centreline value that is important.

e) As mentioned above, the system was blown through with compressed air and left with the overpressure until sampling commenced. This means that the water level inside the probes was at the level of the top probes. The bottom probes may have contained 0.5 ml of water each which is neglegible compared with the sample size of 30-50 ml.

The conductivity measurements were reproduceable to plus minus 10 µS/cm. For unknown reasons a few samples with low reproduceability occured. A background conductivity of 100-120 µS/cm had to be subtracted from the readings. This would affect the accuracy of the low-conductivity readings but again, they were not very important.
The straight line calibration curve for conductivities <1 mS/cm in fig. 3.5 indicates that the

readings are very consistent.

A source of error was the temperature correction as mentioned earlier in this chapter. The temperature coefficient is a fairly crude way of correcting for temperature variations. Ideally, the samples should be kept in a bath at constant temperature while being analysed. However, as long as the actual and reference temperature were not too far away from each other and reasonably close to 16-20^{o}C then it was assumed to be acceptable. The error introduced was probably 5% or less.

Another source could be dust from the air which would affect the conductivity of a sample.

If a sample with low conductivity was analysed after a sample with high conductivity had been analysed, remnants of the stronger solution left on the measuring electrodes could contaminate the weaker solution and give a too high reading. Care was taken to minimise this effect.

Of the sources of error mentioned above a) and b) are probably the most important.

CHAPTER 4
DESCRIPTION OF BASIC JET TYPES.

4.1. Introduction.

In fig. 4.1 the coordinate system which has been used in this work is shown. The X-axis is horizontal and is in the direction of the discharge. The Z-axis is also horizontal and is perpendicular to the X-axis. The Y-axis is vertical and goes in the direction of the buoyant forces. The system formed by the X, Y and Z-axis is a right hand system.

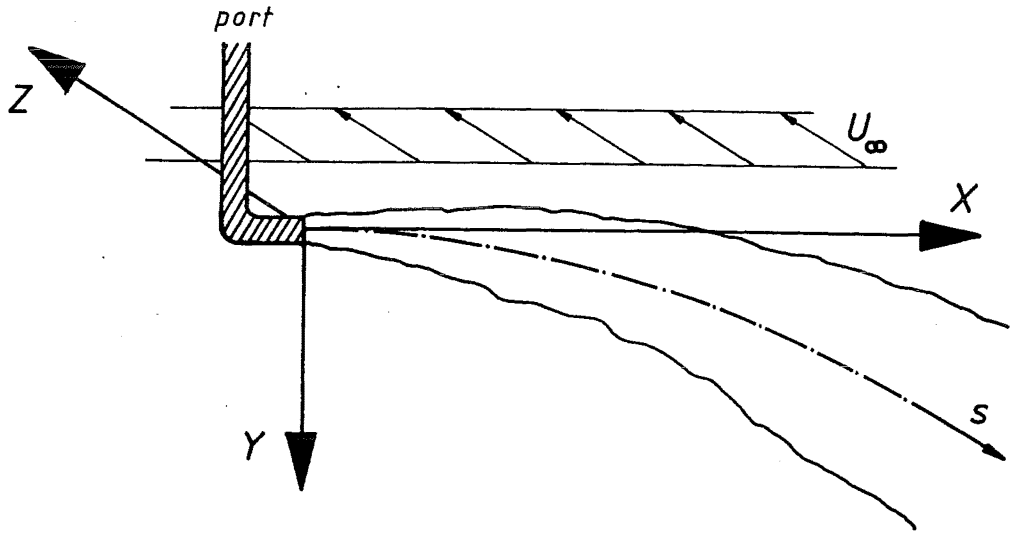

Fig. 4.1. Definition sketch (crossflow).

The ambient flow will either be coflowing, counterflowing or crossflowing.
In a coflow the ambient velocity $\underline{U}_\infty$ is in the positive direction of the X-axis and $|\underline{U}_\infty| = U_\infty$ is a positive number.
In a counterflow $\underline{U}_\infty$ is in the negative direction of the X-axis and U_∞ is negative.
For a crossflow $\underline{U}_\infty$ is in the direction of the Z-axis.

A horizontal buoyant jet in an ambient flow is completely defined when the following initial conditions are specified:

d_p : port diameter

U_0 : initial velocity

Δ_0 : initial buyoancy

$\underline{U}_\infty$: ambient velocity

where $\Delta_0 = (\rho_r - \rho_0)g/\rho_r$

ρ_0 : initial density of the jet

ρ_r : reference density, usually chosen to be the density of the ambient fluid.

g : acceleration of gravity

$\underline{U}_0$ is a vector in the direction of the X-axis, i.e. $\underline{U}_0 = U_0\underline{i}$, where $\underline{i}$ is a unit vector for the X-axis.

In co- and counterflows $\underline{U}_\infty$ and $U_0\underline{i}$ are parallel and in crossflows they are perpendicular.

The traditional approach to describing jets has been to specify d_p, U_0, Δ_0 and $\underline{U}_\infty$.

Let ζ represent some flow variable such as width, centerline velocity etc.

ζ's dependence on the given parameters can then be expressed:

$$\zeta = \Phi(s, d_p, U_0, \Delta_0, U_\infty) \tag{4.1.1}$$

where Φ is an unknown function. (4.1.1) can in accordance with Buckingham's π theorem also can be written as

$$\zeta^* = \Phi^*\left(\frac{s}{d_p}, Fr, \frac{U_0}{U_\infty}\right) \tag{4.1.2}$$

where $Fr = U_0/(\Delta_0 d_p)^{1/2}$ is the densimetric Froude number and ζ^* is ζ non-dimensionalised with some of the other parameters.

Thus a buoyant jet is completely described by specifying Fr and U_∞/U_0 (and of course the angle between U_0 and U_∞).

However, List and Imberger [1973] and others found that it was much more convenient to use the following parameters to define a jet flow:

$$Q = \frac{\pi}{4} d_p^2 U_0 \tag{4.1.3}$$

$$B = \frac{\pi}{4} d_p^2 U_0 \Delta_0 \tag{4.1.4}$$

$$M_e = \frac{\pi}{4} d_p^2 U_0 \, |\underline{U}_0 - \underline{U}_\infty| \tag{4.1.5}$$

U_∞ (4.1.6)

Where Q is the initial discharge, B is the intial buoyancy flux and M_e is the initial excess momentum flux.

[List and Imberger actually used the absolute momentum flux $M = (\pi/4)d_p^2U_0^2$ rather than the excess momentum flux M_e as defined above. It can be seen from the equations of motion in chapter 6 that M_e and not M is conserved. M_e is therefore the important momentum parameter].

When d_p , U_0 , Δ_0 and $\underline{U}_\infty$ are given then Q , B , M_e and U_∞ can be found from the definitions given above (eqs. (4.1.3) - (4.1.6)). On the other hand, if Q , B , M_e and $\underline{U}_\infty$ are given then d_p , U_0 , Δ_0 and $\underline{U}_\infty$ can be found by solving the system of equations, eqs. (4.1.3) - (4.1.6) that is formed by the definitions of Q , B , M_e and $\underline{U}_\infty$.

The two sets of parameters are therefore equivalent.

A similar type of equation as eq. (4.1.1) can be written with these parameters:

$$\zeta = \psi(s, Q, B, M_e, U_\infty) \tag{4.1.7}$$

where Ψ is an unknown function.

It will be shown later that in many cases Q can be ignored. This corresponds to considering the flow as coming from a virtual origin with initial volume flux equal to zero but with excess momentum flux M_e and buoyancy flux B.

When Q can be ignored there is one less variable in eq. (4.1.7) and the dimensional analysis therefore becomes simpler as compared to eq. (4.1.7).

It is intended to use dimensional analysis with either (4.1.1) or (4.1.7) to find solutions for the flow. The paramaters Q , M_e , B and U_∞ are parameters that physically directly describe the processes that take place in the jet as it will be seen in the following and are therefore quantities that enter directly into the arguments in the dimensional analysis.

It can be shown that in the general case of a buoyant jet in an ambient flow the jet consists of regions in which one or two of the parameters Q , M_e , B or U_∞ dominate. The non-dominant parameters can be neglected in these regions.

The dimensional analysis of eq. (4.1.7) is then greatly simplified.

The parameters Q , M_e , B and U_∞ as used in (4.1.7) are therefore used as the basis for the following discussions.

Now where a region is dominated by one or two flow parameters and followed by a region dominated by other flow parameters then a length scale can be computed using the dominant parameters in the two regions.

This length scale is a measure of the distance from the source to where the transition between the two regions occurs.

To illustrate the concept of length scales let us consider a horizontal buoyant jet in still ambient. This flow contains both momentum and buoyancy.
Close to the source where the flow is still affected by the source geometry the discharge Q is important. The initial horizontal momentum $M = M_x$ is conserved throughout the flow. The buoyancy continuously generates vertical momentum M_y. Since M_y initially equals zero we have $M_y<M_x$ in the initial part of the flow.
In this part of the flow the initial momentum therefore dominates over buoyancy. At a certain distance from the port M_y has increased so much that $M_y = M_x$. After this point $M_y>M_x$ and the buoyancy generated vertical momentum then dominates over the initial horizontal momentum.
It follows from the above that there is first a region dominated by initial discharge Q, then a region dominated by initial momentum flux M and finally a region dominated by the buoyancy flux B.
The parameters Q and M can be combined into the length scale $l_{QM} = Q/M^{1/2}$ ($\approx d_p$) which is the approximate distance from the source where the flow becomes dominated by M rather than Q. I.e. for $s<<l_{QM}$ the flow is dominated by Q and the effect of M is negligible and for $l_{QM}<<s$ the flow is dominated by M and the effect of Q is negligible. Since $l_{QM}\approx d_p$ the effect of Q will be negligible in the flow except for the first few initial port diameters.

The parameters M and B can be combined into the length scale $l_{MB} = M^{3/4}/B^{1/2}$ and for $l_{QM}<< s <<l_{MB}$ the flow is dominated by M and B is negligible and for $s >> l_{MB}$ the flow is dominated by B and M is negligible.
Each region is then dominated by one parameter only.
In the special case where $l_{MB} < l_{QM}$ there is only a Q-dominated region followed by a B-dominated region. There can not exist a M-dominated region because buoyancy dominates over momentum before the end of the Q-dominated region. In this case a length scale combining Q and B is relevant : $l_{QB} = Q^{3/5}/B^{1/5}$. For $s << l_{QB}$ Q dominates and for $s >> l_{QB}$ B dominates.

The above discussion of a buoyant jet in still ambient can be extended to the case where there is also an ambient flow U_∞.

[Now it is necessary to look at excess momentum rather than absolute momentum; the flow is thus momentum dominated when $M_{ex} = M_e >> M_y$, where M_{ex} is the excess momentum in the x-direction equal to the initial excess momentum flux and M_y is as before the vertical

momentum flux generated by buoyancy.

The flow similarly is buoyancy dominated when $M_y >> M_e$.]

There will exist regions dominated by U_∞ (which is when $u_{em} << U_\infty$). A distinction has to be made whether the flow becomes dominated by U_∞ within a discharge -, excess momentum- or buoyancy dominated part of the flow.

The ambient flow by itself can not drive the jet flow and therefore there will be a secondary, important parameter, Q, M_e or B in the regions dominated by U_∞.

Q can however be ruled out as a parameter secondary to U_∞ because a flow driven mainly by Q and U_∞ is simply an advected cylinder of fluid and is therefore not a real jet flow.

If the flow becomes dominated by U_∞ in the excess momentum dominated part of the flow then it will be dominated by M_e before the transition and by U_∞ and M_e after the transition. The relevant length scale is therefore $l_{MeU_\infty} = M_e^{1/2}/U_\infty$ and this is the approximate distance from the source where there is a transiton from the flow being dominated by M_e to being dominated by U_∞ and M_e.

Similarly, if the flow becomes dominated by U_∞ in the buoyancy dominated part of a flow then $l_{BU_\infty} = B/U_\infty^3$ is the approximate distance from the port where there is a transition from the flow being dominated by B to being dominated by U_∞ and B.

From the above discussion it has now been seen that in the general case of a buoyant jet in an ambient flow it is possible to have regions dominated by:

$$Q, M_e, B, U_\infty \& M_e \text{ or } U_\infty \& B.$$

The Q dominated region is very short and of little practical interest.

Then there remains 4 possible ways in which a region can be dominated.

A jet which apart from a short initial region is dominated entirely by M_e, B, U_∞ & M_e or U_∞ & B is called a basic jet.

A jet which consists of several regions is called a composite jet.

Basic jets have sufficiently few parameters in eq. (4.1.7) for us to obtain the form of the solution with dimensional analysis. Once solutions have been obtained for the basic jets the solutions can be applied to regions in the general, composite jets which have the same dominating parameter(s).

Below is shown the basic jets that correspond to the relevant dominating parameter(s):

Basic jet	Dominating parameter(s)
1. Pure jet in still ambient	M
2. Pure plume in still ambient	B
3.Advected momentum line puff from continuous source / weak jet	U_∞ & M_e
4.Advected line thermal from continuous source	U_∞ & B

The flow in the 4 basic jets will be completely solved in the following sections.

In the next chapter the solutions will be used as a basis to achieve solution for the general

case of a composite jet.

4.2. Pure jet in a still ambient fluid.

(also called simple jet, non-buoyant jet or momentum jet)

A pure jet is created by a continous source of momentum (see fig. 4.2). It is one of the simplest cases of free turbulent flows and as such has been investigated extensively.

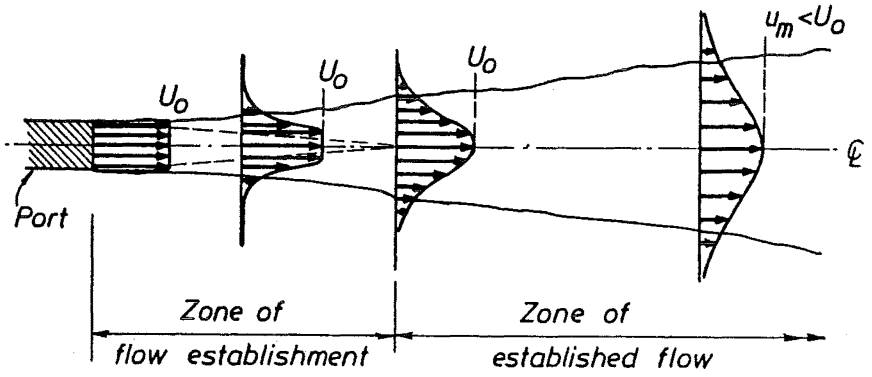

Fig. 4.2. Sketch of the initial region and flow development in a pure jet in still ambient.

The flow at the port has the same velocity distribution as inside the pipe, i.e. approximately rectangular (apart from the boundary layer). There will then be a velocity difference between the jet fluid and the still ambient. As described first by Albertson et al.[1950] this forms a region of high shear in which eddies are formed. The eddies produce lateral diffusion of the jet fluid by entraining and bringing into motion the surrounding fluid. At the same time the fluid in the jet is decellerated.

In the short region downstream of the nozzle the turbulence penetrates inwards to the axis/centreline of the jet. The cenral part of this region is a wedge-like region of undiminished mean velocity, equal to the nozzle velocity U_0. This wedge is known as the potential core and the entire region as zone of flow establishment (ZFE), flow development region or potential zone (see fig. 4.2). It is given the latter name because the velocity in the potential core is constant ($=U_0$) and the turbulence in the core is relatively low.

The length of the zone has been found to be 6.2 port diameters, Albertson et al.[1950] , Chan & Kennedy[1972], Gordier [1959] , Keffer & Baines [1963] and Pratte & Baines [1967]. This is comparable to the length scale l_{QM} which is of the order of magnitude of the distance from the port in which the flow becomes fully developed, cfr. previous section.

At the end of this zone the initially rectangular velocity profile at the port has been transformed into a bell shaped profile (see fig. 4.2) with an apex velocity equal to U_0.
After this point the flow can be considered fully established and this part of the flow is called the zone of established flow. Experimental results from the 1920's to 1980's have shown that the shape of the velocity profile remained the same in this region and the jet is thus said to be self similar or self preserving.
This is illustrated in fig. 4.3 where non-dimensionalised velocity profiles as measured by Papanicolaou[1984] are compared with each other. They are seen indeed to be self similar.

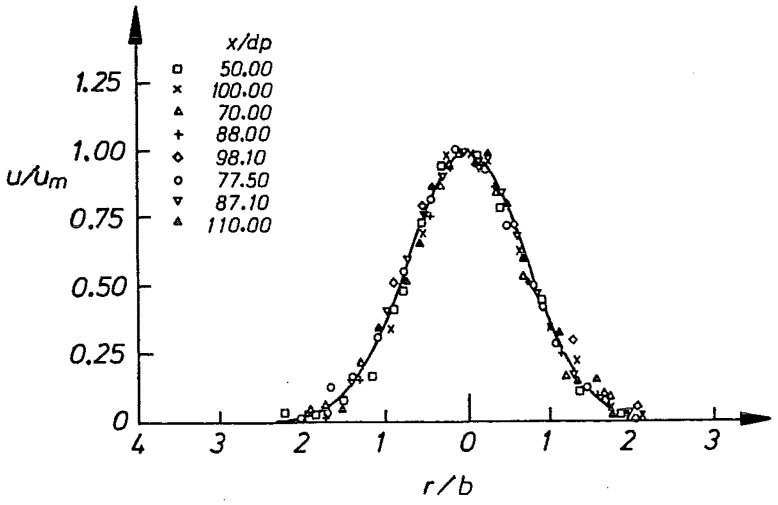

Fig. 4.3. Velocity distribution in a pure jet in still ambient.

Papanicolaou's and others' experiments also showed linear expansion of the nominal jet boundary defined by the width b such that

$$db/dx = k \quad \text{or} \quad b \sim x \tag{4.2.1}$$

where b is defined as the distance from the center line where
the longitudinal velocity $u=e^{-1}u_m$
x is a coordinate along the center line
k is a constant =0.109 (Papanicolaou)

The velocity profile was shown to follow a Gaussian distribution closely (except near the edges)

$$u = u_m e^{-\left(\frac{r}{b}\right)^2} \tag{4.2.2}$$

where r is a radial coordinate
u_m is the velocity at the center line

The distribution of tracer concentration was found to be given by

$$c = c_m e^{-\left(\frac{r}{\lambda b}\right)^2} \tag{4.2.3}$$

where c is the local tracer concentration

c_m is the center line concentration

λ is a spreading coefficient

Papanicolaou found λ to be equal to 1.275 for a pure jet.

The Gaussian distributions can be shown to be compatible with an assumption of a mixing length proportional to the width of the jet (Cederwall[1968])

The pure jet in still ambient is discharging initial momentum M and initial volume flux Q. From Q and M the length scale l_{QM} is formed:

$$l_{QM} = \frac{Q}{M^{1/2}} \tag{4.2.4}$$

Since u_m has the ~~unit~~ dimension length per unit time we must have

$$\frac{u_m Q}{M} = f_1\left(\frac{x}{l_{QM}}\right) \tag{4.2.5}$$

where f_1 is some as yet unknown function

For $x >> l_{QM}$ Q should not enter and the only possible solution is

$$\frac{u_m Q}{M} \sim \left(\frac{x}{l_{QM}}\right)^{-1} \tag{4.2.6}$$

Similar arguments give us

$$\frac{bQ}{M^{1/2}} = \frac{b}{l_{QM}} \sim \frac{x}{l_{QM}} \tag{4.2.7}$$

which confirms (4.2.1).

If we call the local tracer flux q_c and the initial tracer concentration C_o then $q_c=QC_o$.
Dimensional reasoning then yields $c_m/q_c \sim (M^{1/2}x)^{-1}$ and thus

$$S_{CL} = \frac{C_o}{c_m} \sim \left(\frac{x}{l_{QM}}\right) \qquad (4.2.8)$$

Since $l_{QM} \approx d_p$ this means that (4.2.6) and (4.2.7) hold over almost the entire range of the flow.
The results from this analysis, eqs. (4.2.6)-(4.2.8) apply to pure jets but also to pure jet-like flows as it will be shown in next chapter.

4.3. Vertical pure plume in a still ambient fluid.

(also called simple plume)

A pure plume is the turbulent flow that is generated by a continuous source of buoyancy. Ideally initial momentum and volume flux should be zero but in practical experiments it usually has some very small value.
Although the momentum flux initially is zero (or almost zero) it increases with increasing height because the bouyant forces generate momentum.
A simple example of a pure plume would be the flow that is generated above a heated plate. The heat creates a density difference relative to the surrounding fluid and the heated fluid moves upwards under the action of buoyancy.
The maintenance of the heat source sustains a flux of buoyancy which thus can be seen as a pure plume.
In a similar manner as in pure jets, the velocity differences cause turbulent eddies and lateral spreading of the plume fluid , see fig. 4.4.
A zone of flow establishment can be defined in terms of the density profiles in the plume, see fig. 4.5. The turbulence will cause both excess density and velocity to be spread.

Papanicolaou[1984] and Rouse, Yih & Humphreys[1952] found experimentally that the velocity profiles as well as the density profiles are similar at all horizontal cross sections after the ZFE.
Further, it was found that

$$b \sim y$$

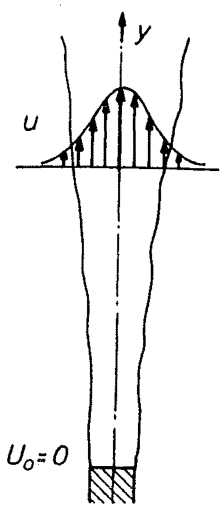

Fig. 4.4. Velocity distribution in a pure plume in still ambient

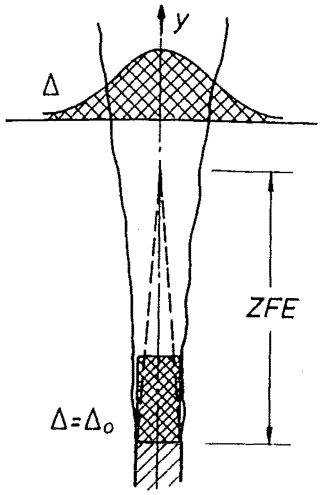

Fig. 4.5. Buoyancy distribution in a pure plume in still ambient.

The growth of width of the pure plume is thus linear

$$\frac{db}{dy} = k \tag{4.3.1}$$

The value for k is the same as for pure jets, 0.109 (Rodi[1982])

The velocity and buoyancy profiles can be represented by Gaussian profiles as pointed out by Rouse et al. :

$$u = u_m e^{-\left(\frac{r}{b}\right)^2} \tag{4.3.2}$$

$$\Delta = \Delta_m e^{-\left(\frac{r}{\lambda b}\right)^2} \tag{4.3.3}$$

where $\Delta = (\rho - \rho_r)g / \rho_r$

ρ_r is a reference density

ρ is the local density

g is the acceleration of gravity

λ is a spreading factor

Δ_m is center line buoyancy in the jet

The Gaussian distribution for buoyancy in (4.3.3) differs from the Gaussian distribution for

velocity in (4.3.2) by a spreading factor λ similar to the spreading factor for tracer concentration in pure jets (eq.(4.2.3)).

Rouse et al[1952] found experimentally the value 1.16. Papanicolaou [1984] found λ=1.067 . It seems then that an average value of λ=1.2 for pure plumes is reasonable.

Since λ>1 it means that buoyancy spreads further out than velocity.

There is no initial volume flux or momentum flux so the only parameters that are relevant in the dimensional analysis is initial buoyancy flux B, kinematic viscosity ν and vertical distance from the source, y.

[Viscosity is included since the flow is starting from zero velocity and therefore there must be a region where viscosity is important.]

The only possible length scale is then

$$l_{\nu B} = \frac{\nu^{3/2}}{B^{1/2}} \tag{4.3.4}$$

All properties in the plume must be a function of B, ν and $y/l_{\nu B}$.

When $y >> l_{\nu B}$ then the effect of the viscosity is negligible in the comparison with the buoyant forces. In other words, when $y >> l_{\nu B}$ then all properties are defined solely in terms of y and B.

The center line velocity and the width of the jet and center line dilution must be given by the following expressions:

$$\frac{u_{e\,m}\,\nu^{1/2}}{B^{1/2}} = f_2\left(\frac{y}{l_{\nu B}}\right) \tag{4.3.5}$$

$$\frac{b}{l_{\nu B}} = f_3\left(\frac{y}{l_{\nu B}}\right) \tag{4.3.6}$$

$$\frac{\Delta_m Q}{B} = f_4\left(\frac{y}{l_{\nu B}}\right) \tag{4.3.7}$$

where f_2, f_3 and f_4 are some as yet undetermined functions.

Since ν must disappear from (4.3.5) and (4.3.6) when $y >> l_{\nu B}$ then

$$\frac{u_m \nu^{1/2}}{B^{1/2}} \sim \left(\frac{y}{l_{\nu B}}\right)^{-1/3} \tag{4.3.8}$$

$$\frac{b}{l_{\nu B}} \sim \frac{y}{l_{\nu B}} \tag{4.3.9}$$

$$\frac{\Delta_m}{B} \sim B^{-1/3} y^{-5/3} \tag{4.3.10}$$

which becomes

$$S_{CL} = \frac{\Delta_o}{\Delta_m} \sim \left(\frac{y}{l_{\nu B}}\right)^{5/3} \tag{4.3.11}$$

Equations (4.3.8) - (4.3.9) and (4.3.11) describe the flow in pure plumes but also as it will be shown in next chapter in pure plume-like flows.

4.4. Advected line thermal from a continous source.

In the two previous sections, sections 4.2 and 4.3 two jet flows were studied which both had only one length scale defining the transition between a negligible initial region and a main region dominated by one parameter only.

It was seen how this fact made it possible to use very simple dimensional analysis to derive information about the flows.

In this and the following section, sections 4.4 and 4.5, jet flows in an ambient flow are studied. The extra parameter U_∞ means that two length scales rather than one exist for these cases.

It can be seen directly from the dimensional analysis in the two previous chapters that the method used there where u_{em}, b or S_{CL} could be written as a function of s/l only, where l was the length scale for the flow, can not be used when there is more than one length scale.

In this section the problem has been solved by studying a similar type of flow, the line thermal in still ambient, which has only one time scale. The simple dimensional analysis from the previous sections can then be used to completely describe this type of flow. The results can then be used to describe the flow in an advected line thermal from a continuous source by considering the line thermal as merely being advected by the ambient flow U_∞ and being continuously discharged rather than instantly.

4.4.1. Line thermal in still ambient.

A line thermal in still ambient is formed when a cylinder of fluid with a density different from the surrounding fluid is released. At the instant of release the thermal is at rest and has thus zero initial momentum.

The thermal will move in the direction of the buoyant forces, and the shear stress which acts round the circumference of the thermal causes a pair of counter rotating vortices to form in the thermal (see figs. 4.6 and 4.7). Richards[1963] has made extensive measurements in line thermals.

Fig. 4.7 is reproduced from Richards [1963] and shows stream lines/isotachs in a cross section of a thermal. The vortex pair is seen quite clearly. Because of the symmetry of the flow there is self similarity in the longitudinal direction.

Experiments (Richards [1963]) have shown that the flow is also roughly self similar with respect to time, i.e. in the vertical direction in vertical cross sections perpendicular to the center line. It is the latter self similarity that is of relevance in this context because it goes in the direction of motion.

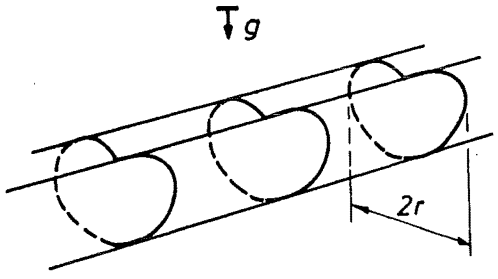

Fig. 4.6. Sketch of line thermal in still ambient.

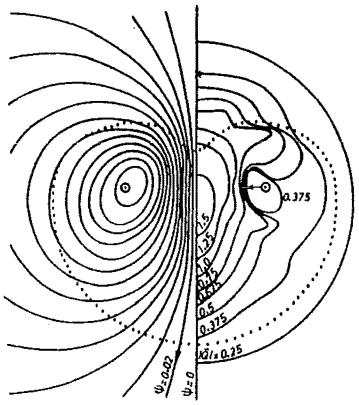

Fig. 4.7. Stream lines and isotachs in a line thermal from Richards [1963].

Richards [1963] and Scorer [1959] found that the width of the line thermal was proportional to the distance travelled:

$$y = nr \tag{4.4.1}$$

where n is a constant

r is half the visible width of the thermal

(when the thermal is dyed)

Richards found the value of n to vary between 1.86 and 3.17. The value varied strongly with the method of release.

In this type of flow there are 3 relevant parameters:

the initial volume per unit length thermal, A,

the initial amount of buoyacy per unit lenght, A_Δ,

and vertical distance y or alternatively time t from the thermal was released.

One time scale can be derived

$$t_{AA_\Delta} = \frac{A^{3/4}}{A_\Delta^{1/2}} \tag{4.4.2}$$

$t_{AA\Delta}$ is the time it takes for the line thermal to fall till the flow is fully developed and the originally uniform distribution of buoyancy and vertical velocity (which is originally zero) to transform into the vortex pair distribution shown in fig. 4.7.

For $t >> t_{AA\Delta}$ we can ignore A and consider the thermal as originating from a line of cross sectional area zero with finite buoyancy A_Δ.

This idea is similar to the 'virtual origin' of pure jets and pure plumes.

For $t >> t_{AA\Delta}$ we have that all properties in the line thermal must be a function of A_Δ and $t_{AA\Delta}$.

In the case of a line thermal we choose to define u_m as the velocity in the centres of the vortices and the width b as the average radius in which $u=e^{-1}u_m$.

We must have

$$\frac{u_m A_\Delta^{1/2}}{A_\Delta^{1/4}} = f_5\left(\frac{t}{t_{AA_\Delta}}\right) \tag{4.4.3}$$

$$\frac{b}{A^{1/2}} = f_6\left(\frac{t}{t_{AA_\Delta}}\right) \tag{4.4.4}$$

$$S_{CL} = f_7\left(\frac{t}{t_{AA_\Delta}}\right) \tag{4.4.5}$$

where f_5, f_6 and f_7 are some as yet unknown functions.

For $t >> t_{AA\Delta}$ (which is the case in virtually all of the flow except in an initial zone) A must cancel out and then we find

$$\frac{u_m A^{1/4}}{A_\Delta^{1/2}} \sim \left(\frac{t}{t_{AA_\Delta}}\right)^{-1/3} \tag{4.4.6}$$

$$\frac{b}{A^{1/2}} \sim \left(\frac{t}{t_{AA_\Delta}}\right)^{2/3} \tag{4.4.7}$$

Since S_{CL} is dimensionless we can not derive it with dimensional analysis. However, it is possible to find the variation of the quantity A_Δ/Δ_m:

$$\frac{A_\Delta}{\Delta_m} \sim (A_\Delta t^2)^{2/3} \tag{4.4.8}$$

Then

$$S_{CL} = \frac{\Delta_o}{\Delta_m} \sim \left(\frac{t}{t_{AA_\Delta}}\right)^{1/3} \tag{4.4.9}$$

Since $u_m = dy/dt$ then (4.4.6) yields by integration

$$\frac{y}{A^{1/2}} \sim \left(\frac{t}{t_{A A_\Delta}}\right)^{2/3} \qquad (4.4.10)$$

and (4.4.10) combined with (4.4.7) then gives

$$b \sim y$$

which confirms (4.4.1) since b ~ r.

[(4.4.10) gives with (4.4.6) and (4.4.7):

$$u_m \sim t^{-1/3} \sim y^{-1/2} \qquad (4.4.11)$$

$$b \sim t^{2/3} \sim y \qquad (4.4.12)$$

$$s_{CL} \sim t^{4/3} \sim y^2 \qquad (4.4.13)]$$

4.4.2. The advected thermal from a continous source.

An advected thermal from a continous source is the turbulent flow that results when buoyant fluid is discharged through the port with the same velocity U_0 as that of the ambient fluid U_∞.

As a result, a cylinder of buoyant fluid is laid out and convected away by the ambient flow (see fig. 4.8). This type of jet is characterised by having no initial excess momentum. The flow is thus driven entirely by buoyancy. The horizontal component of the excess velocities in the jet will everywhere be zero. There is therefore no momentum or buoyancy flux between neighbouring vertical cross sections.

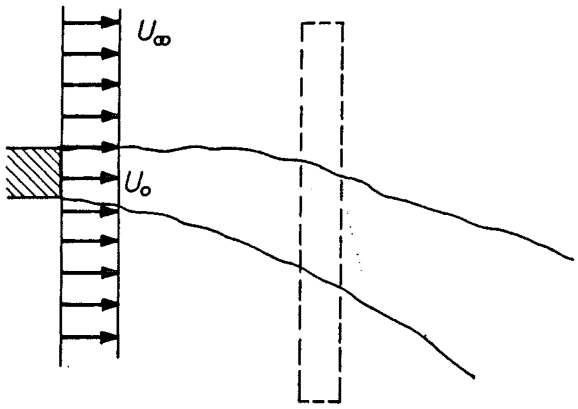

Fig. 4.8. Sketch of an advected line thermal from a continuous source.

This gives us virtually the same physical situation as in the line thermal and we can therefore expect the equations for line thermals to be valid for advected thermals too.
Line thermals in still ambient (sect. 4.4.1) can be seen as a special case of this type of jets where U_0 and U_∞ tend towards infinity because then the trajectory becomes virtually horizontal. Because of the close analogy with line thermals it is reasonable to expect self similarity in vertical cross sections. Experiments by the author have confirmed that there is roughly self similarity in the vertical direction (see fig. 4.9). Because there is an infinitesimal velocity difference between neighbouring sections there is virtually no vertical shear between them.
The contours in fig. 4.9 are similar to the contours in line thermals (fig. 4.7) .

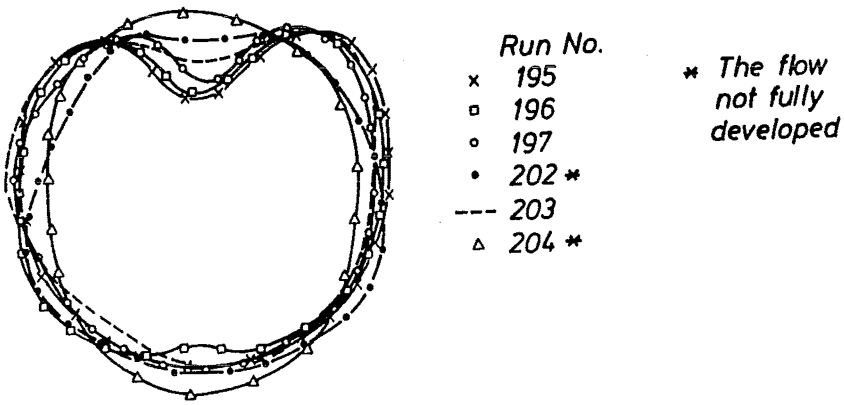

Fig. 4.9. Concentration contours in an advected line thermal from a continuous source.

The similarity with line thermals leads to

$$b = my \tag{4.4.14}$$

where m is a constant.

Equation (4.4.14) is equivalent to (4.4.1).
(4.4.14) was confirmed experimentally by the author (see fig. 4.11).

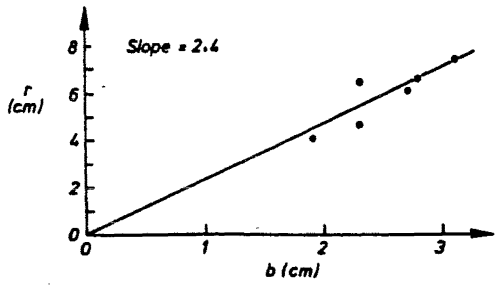

Fig. 4.10.Visible versus measured width of an advected line thermal from a cont. source.

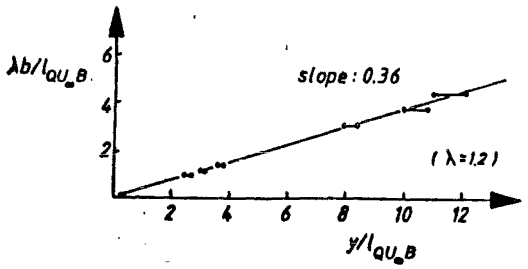

Fig. 4.11. Width versus depth for an advected line thermal from a cont. source.

In each run the jet was recorded from the side and the concentration profile was measured in a vertical cross section.
A relationship between Richards' visible width r and our width b could therefore be found (see fig. 4.10). The proportionality factor was approximately 2.4. That gives a n-value of about $(0.24 \times 2.4)^{-1}=1.7$ in equation (4.4.1) because m in (4.4.14) was found experimentally to be about 0.30 (see fig. 4.11).

It is worth noting that these experiments are more repeatable than the normal line thermal experiment as it is simpler to obtain initial conditions which have little variation.
(Richards' results depended on the method of release but here there is only one method of release).
The relevant parameters for the flow in an advected thermal from a continous source are discharge Q , buoyancy flux B , ambient velocity U_∞ and vertical distance from the port, y. A few port diameters from the port Q becomes negligible. M_e is equal to zero and can therefore also be neglected.
y has to be the important distance parameter because the motion in the X- or Z-direction is purely advective and does not affect any of the flow variables.

From the 3 initial parameters Q , B and U_∞ two length scales can be formed:

$$l_{QB} = \frac{Q^{3/5}}{B^{1/5}} \qquad (4.4.15)$$

$$l_{BU_\infty} = \frac{B}{U_\infty^3}$$

(4.4.16)

It can be shown by inserting eqs. (4.1.3)-(4.1.5) that for Fr > 1 then $l_{QB} > l_{BU_\infty}$.

Since l_{QB} is the approximate distance from the port where the flow goes from being dominated by Q to being dominated by B and l_{BU_∞} is the approximate distance where the flow goes from being dominated by B to being dominated by U_∞ it can be concluded that for Fr>1 all advected thermals from a continuous source will go directly from being dominated by Q to being dominated by U_∞. Since the effect of B cannot be completely neglected this means that a length scale containing both Q , U_∞ and B will be a measure of the distance from the port in which this transition occurs:

$$l_{QU_\infty B} = \frac{Q U_\infty^2}{B}$$

(4.4.17)

For Fr>1 $l_{QU_\infty B}$ is the only significant length scale for the flow and it can be considered a basic flow, dominated only by one parameter.

$l_{QU_\infty B}$ is the order of magnitude of the distance from the port where the flow has become fully established and the counter rotating vortex pair is set up (cfr. fig. 4.7). At this point the flow starts ressembling an advected line thermal.

The flow is driven by U_∞ and to a lesser extent B.

The line thermal was driven by B only. By considering U_∞ as being merely advective it can be seen that the results found for a line thermal in still ambient can be adapted to the present case.

Then $x = U_\infty t$ for co- and counterflows where U_∞ is in the direction of the X-axis and $z = U_\infty t$ for crossflows where U_∞ is in the direction the Z-axis.

The trajectory is not horizontal in this case as it was in the line thermal case but each vertical infinitesimal 'slice' corresponds to a similar 'slice' in a line thermal at the same depth y.

A can be replaced by Q/U_∞ and A_Δ by B/U_∞.

Then the equivalents to (4.4.11)-(4.4.13) become after some rearrangement:

$$\frac{u_{em}}{U_\infty} = \left(\frac{y}{l_{BU_\infty}}\right)^{-1/2}$$

$$\frac{b}{l_{BU_\infty}} \sim \frac{y}{l_{BU_\infty}} \tag{4.4.18}$$

$$\frac{S_{CL}\,Q}{l_{BU_\infty}^2\,U_\infty} \sim \left(\frac{y}{l_{BU_\infty}}\right)^2 \tag{4.4.19}$$

(4.4.20)

The trajectory can be found for co- and counterflows by using $u_{em}=dy/dt$ and $U_\infty=dx/dt$ with equation (4.4.17):

$$\frac{y}{l_{BU_\infty}} \sim \left(\frac{x}{l_{BU_\infty}}\right)^{2/3} \tag{4.4.21}$$

For crossflows $u_{em}=dy/dt$ and $U_\infty=dz/dt$ and with (4.4.17) that gives

$$\frac{y}{l_{BU_\infty}} \sim \left(\frac{z}{l_{BU_\infty}}\right)^{2/3} \tag{4.4.22}$$

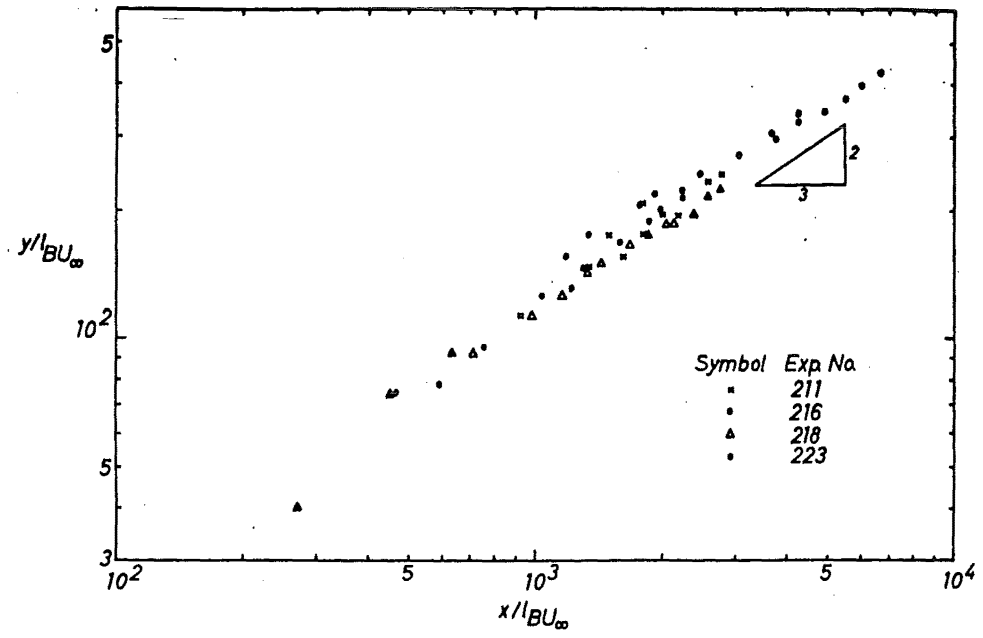

Fig. 4.12. Advected line thermal from a continuous source trajectories.

Equations (4.4.18)-(4.4.22) describe the flow in an advected line thermal from a continous source. However, they also apply to regions in composite jets that behave like an advected line thermal from a continous source.

In fig. 4.12 the trajectories for advected line thermals from a continuous source have been plotted on log/log paper and they can be seen to confirm (4.4.21).

4.5. Advected momentum line puff from a continous source and weak jet.

In this section jets which are dominated by an ambient flow U_∞ and to a lesser extent the initial excess momentum , M_e, are discussed.

However, the behaviour of such jets depends on whether the excess momentum M_e is parallel with the ambient velocity U_∞ (as in co- and counterflows) or M_e is perpendicular to U_∞ (as in crossflows).

To make this distinction it is therefore necessary to study two different types of basic jets in this section:

1. The advected momentum line puff from a continuous source, which is a jet dominated by U_∞ and M_e and with M_e perpendicular to U_∞

and

2.The weak jet which is a jet dominated by U_∞ and M_e with M_e parallel to U_∞ .

Both advected momentum line puffs from a continuous source and weak jets have more than one length scale and the simple dimensional analysis used in sections 4.2 and 4.3 can therefore not be used.

For advected momentum line puffs from a continuous source an approach similar to the one used in previous section is applicable : there exists an equivalent, simpler type of flow in still ambient with only one time scale : a momentum line puff.

This flow can easily be investigated and the results can be applied to the case of the advected momentum line puff from a continuous source by considering it as merely being advected by the ambient flow and being continuously discharged rather than instantly.

In the case of a weak jet the flow is such that it is not equivalent to a simpler flow which is being advected by U_∞.

In a weak jet U_∞ interacts with the flow. The dimensional analysis for this case therefore requires additional information in the form of equations of motion. The equations which will

be used are derived in chapter 6 and reference therefore has to be made to that chapter.

A momentum line puff is the momentum dominated parallel to a buoyant line thermal. Both are 2-dimensional flows with velocities perpendicular to the axis. However, in buoyant line thermals the velocities are generated by buoyant forces whereas in momentum line puffs the velocities are related to the initial momentum of the line thermal.
Like buoyant thermals only the momentum line puff in still ambient has been described previously (Wright[1977]).

Therefore a description is first given here for the momentum line puff in still ambient. The results are then extended to the case of an advected momentum line puff from a continuous source.

For co- or counterflowing jets the basic jet of interest in this category can be likened to the flow in a weak non-buoyant jet in a co- or counterflow. Here the excess velocities in the jet are in the direction of the axis of the jet. It is sufficient to analyse the weak jet in a coflow because the results apply for a counterflow with a change of sign of the excess velocities in the jet.

4.5.1. Momentum line puff in still ambient.

This flow is initiated when a cylinder of fluid with initial momentum μ per unit length of the cylinder is injected into a stagnant fluid of the same density. The momentum is perpendicular to the axis of the momentum thermal. It is expected that a similar type of velocity distribution as in buoyant line thermals will develop, see fig. 4.13.

The significant initial parameters are

A : initial cross sectional area=volume per unit length
μ : initial instantaneous kinematic momentum input per unit length
x : the coordinate in the direction of motion
or t : time from release

One time scale can be formed from A and μ:

$$t_{A\mu} = \frac{A^{3/2}}{\mu} \qquad (4.5.1)$$

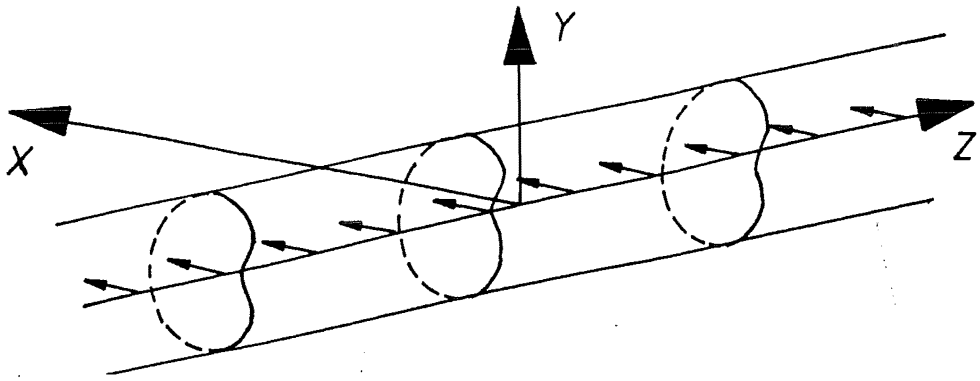

Fig. 4.13. Sketch of a momentum line puff in still ambient.

$t_{A\mu}$ is the time it takes for the momentum line puff from its injection till the flow is fully developed and no longer dependent on the method of injection.

The velocity will then have transformed from the originally uniform velocity distribution into a velocity distribution presumably similar to the vortex pair distribution for buoyant thermals as shown in fig. 4.7. The velocity distribution is also assumed self similar with respect to time.

For $t>>t_{A\mu}$ we can ignore A and consider the momentum line puff as originating from a line of cross sectional area zero and momentum per unit length μ.

The properties in the momentum line puff can be written in the following way:

$$\frac{u_m A}{\mu} = f_8\left(\frac{t}{t_{A\mu}}\right) \tag{4.5.2}$$

$$\frac{b}{A^{1/2}} = f_9\left(\frac{t}{t_{A\mu}}\right) \tag{4.5.3}$$

$$S_{CL} = f_{10}\left(\frac{t}{t_{A\mu}}\right) \tag{4.5.4}$$

where f_8, f_9 and f_{10} are unknown functions, and for $t>>t_{A\mu}$ A must cancel out which yields:

$$\frac{u_m A}{\mu} \sim \left(\frac{t}{t_{A\mu}}\right)^{-2/3} \tag{4.5.5}$$

$$\frac{b}{A^{1/2}} \sim \left(\frac{t}{t_{A\mu}}\right)^{1/3} \tag{4.5.6}$$

To find S_{CL} we can write from dimensional reasoning

$$\frac{A C_o}{c_m} \sim (\mu t)^{2/3} \tag{4.5.7}$$

and then

$$S_{CL} = \frac{C_o}{c_m} \sim \left(\frac{t}{t_{A\mu}}\right)^{2/3} \tag{4.5.8}$$

Using u_m=dx/dt with equation (4.5.5) gives

$$\frac{x}{A^{1/2}} \sim \left(\frac{t}{t_{A\mu}}\right)^{1/3} \tag{4.5.9}$$

(4.5.9) used with (4.5.5), (4.5.6) and (4.5.9) yields:

$$\frac{u_m A}{\mu} \sim \left(\frac{x}{A^{1/2}}\right)^{-2} \tag{4.5.10}$$

$$\frac{b}{A^{1/2}} \sim \frac{x}{A^{1/2}} \tag{4.5.11}$$

$$S_{CL} \sim \left(\frac{x}{A^{1/2}}\right)^{2} \tag{4.5.12}$$

Using U_∞ = dz/dt with (4.5.9) yields

$$\frac{x}{A^{1/2}} \sim \left(\frac{z}{A^{1/2}}\right)^{1/3} \tag{4.5.13}$$

4.5.2. Advected momentum line puff from a continuous source in an ambient flow.

An advected momentum line puff can be obtained if at some vertical section of an extensive horizontal flow a short cylinder of the flow is given an impulsive force perpendicular to its axis and the horizontal flow, see fig. 4.14 and an advected momentum line thermal from a

continuous sorce in an ambient crossflow can be created as shown in fig. 4.15.

The jet is discharged into the ambient flow such that $U_{eo} << U_\infty$ and U_{eo} is perpendicular to U_∞. In this manner there will be an excess momentum discharged perpendicular to the ambient flow. Because the excess velocity is so small compared to U_∞ the trajectory will be almost completely aligned with the ambient flow.

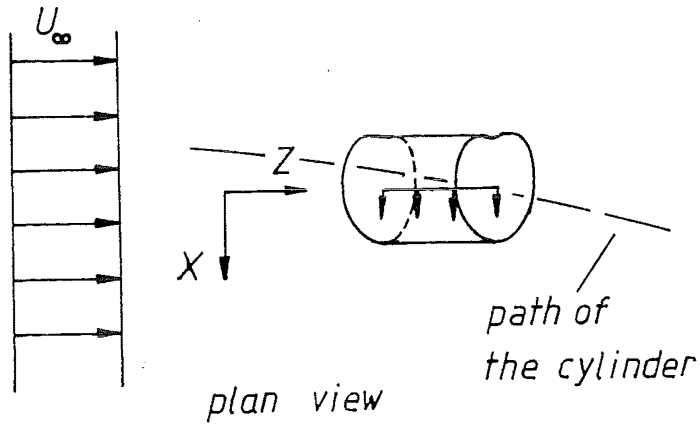

Fig. 4.14 Short momentum cylinder in an ambient flow.

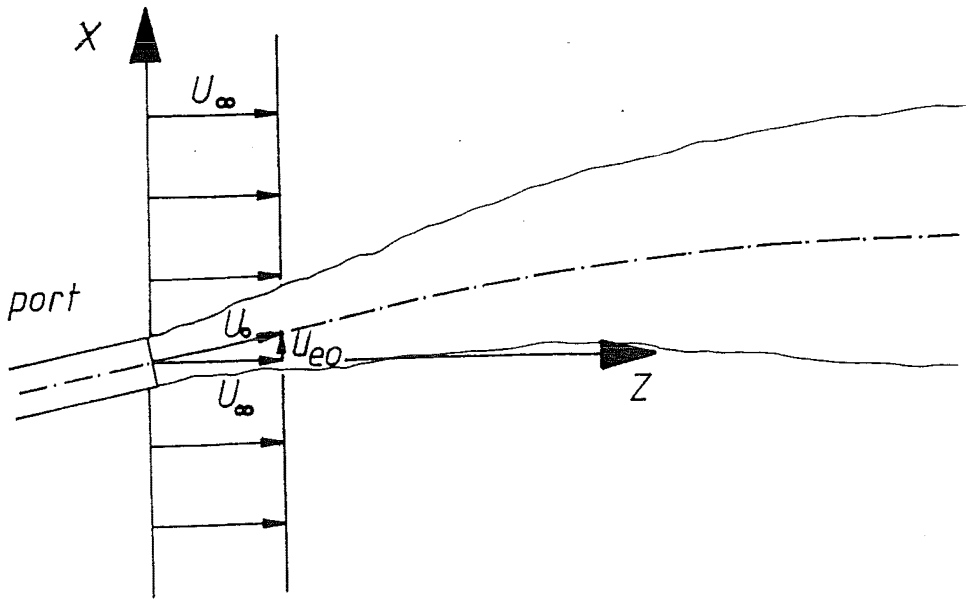

Fig. 4.15. Sketch of advected momentum line puff from a continuous source.

Since this jet corresponds to the far field of a jet discharged perpendicularly into an ambient flow it is reasonable to choose the X-axis perpendicular to U_∞.

It is assumed that the ambient flow advects the momentum line puff from the continuous source. In that case the equations derived in previous section apply.

The jet has the initial discharge Q , initial excess momentum flux M_e and the ambient velocity U_∞. The buoyancy flux B is equal to zero.

The equivalent to A in previous section is Q/U_∞ and the equivalent to μ is M_e/U_∞.

Two length scales can be formed:

$$l_{QM_e} = \frac{Q}{M_e^{1/2}} \tag{4.5.14}$$

$$l_{M_eU_\infty} = \frac{M_e^{1/2}}{U_\infty} \tag{4.5.15}$$

l_{QMe} is as usual of the order of magnitude d_p. Because $U_{eo} << U_\infty$ $l_{MeU\infty}$ will be $<< d_p$.

By inserting $A=Q/U_\infty$ and $\mu=M_e/U_\infty$ in equations (4.5.10)-(4.5.12) and rearranging it is found:

$$\frac{u_{em}}{U_\infty} \sim \left(\frac{x}{l_{M_eU_\infty}}\right)^{-2} \tag{4.5.16}$$

$$\frac{b}{l_{M_eU_\infty}} \sim \frac{x}{l_{M_eU_\infty}} \tag{4.5.17}$$

$$\frac{S_{CL}\,Q}{l_{M_eU_\infty}^2\,U_\infty} \sim \left(\frac{x}{l_{M_eU_\infty}}\right)^{2} \tag{4.5.18}$$

The trajectory can be found from (4.5.9) by using $dz/dt=U_\infty$:

$$\frac{x}{l M_e U_\infty} \sim \left(\frac{z}{l M_e U_\infty}\right)^{1/3} \qquad (4.5.19)$$

Equations (4.5.14)-(4.5.16) now describe the flow in an advected momentum line puff from a continuous source and also regions in composite jets where the effect of buoyancy is negligible, the flow is dominated by the ambient flow and there is a small momentum flux perpendicular to the axis of the jet.

4.5.3. Weak jets.

A weak jet is like an advected momentum line puff from a continuous source characterised by being dominated by the ambient flow U_∞ , the momentum being of some importance and the buoyancy being negligible.

However, in weak jets the excess momentum in the jet goes in the direction of the axis of the jet whereas it in an advected momentum line puff from a continuous source went in a direction perpendicular to both U_∞ and the axis of the jet.

It can then be seen that weak jets are co- or counterflowing jets.

A weak jet discharging into a coflowing ambient fluid is shown in fig. 4.16.

A weak coflowing jet is here defined as a jet whose exit velocity U_0 is only slightly greater than the ambient velocity U_∞. This implies that the initial excess velocity U_{e0} is $<<U_\infty$.

There is then a small excess momentum flux in the direction of the ambient flow. Experiments with weak jets have shown the flow to be self similar.

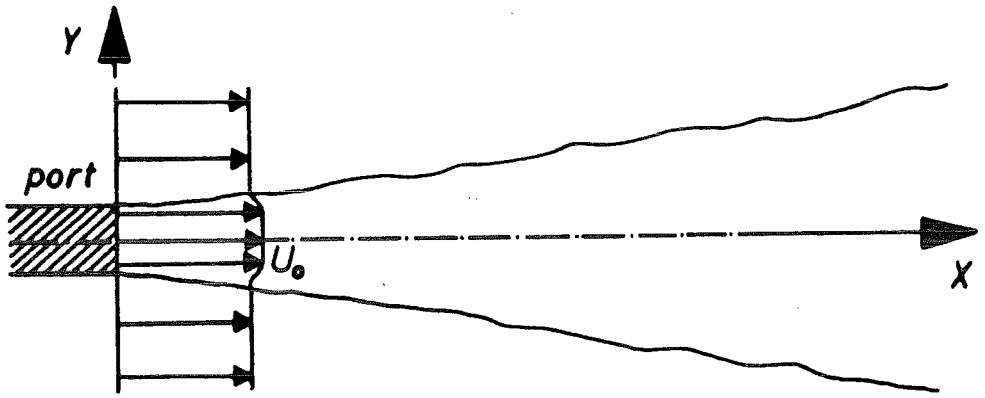

Fig. 4.16. Sketch of a weak jet.

The jet has the initial discharge Q , initial excess momentum M_e and the ambient velocity U_∞. The buoyancy flux is equal to zero.

Two length scales can be formed:

$$l_{QM_e} = \frac{Q}{M_e^{1/2}} \tag{4.5.20}$$

$$l_{M_eU_\infty} = \frac{M_e^{1/2}}{U_\infty} \tag{4.5.21}$$

l_{QMe} is as usual the order of magnitude d_p and because $U_{eo} << U_\infty$ then $l_{MeU\infty} << d_p$.

In this case we can not assume that the jet behaves like a similar type of flow in still ambient but then advected by the ambient velocity U_∞.

When the ambient flow goes in the direction of the excess velocity it does not merely advect the flow. This can be seen from the X-momentum conservation equations for e.g. a pure jet in a coflow (see chapter 6 for details) : a change of coordinate system to one moving at the velocity U_∞ in the direction of the X-axis does not cause the equation to become similar to the one for a pure jet in still ambient.

It is therefore necessary to adopt another approach to derive equations for u_{em}, b and S_{CL} for this type of flow:

We will need additional information from the equations of motion and we have to make a reference to chapter 6 to get this.

For $x>>l_{MeU\infty}$ and $x>>l_{QMe}$ M_e and U_∞ are the important parameters with U_∞ being the dominating one. Then

$$\frac{u_{em}}{U_\infty} = f_{11}\left(\frac{x}{l_{M_eU_\infty}}\right) \tag{4.5.22}$$

$$\frac{b}{l_{M_eU_\infty}} = f_{12}\left(\frac{x}{l_{M_eU_\infty}}\right) \tag{4.5.23}$$

$$\frac{S_{CL}Q}{U_\infty l^2_{M_eU_\infty}} = f_{13}\left(\frac{x}{l_{M_eU_\infty}}\right) \tag{4.5.24}$$

where f_{11}, f_{12} and f_{13} are unknown functions.

Additional information is required.

With $\delta \approx \beta \approx 0^o$, $u_{sm} \approx u_{em}$, $v_{vm} \approx 0$ and $s' \approx x$ the X-momentum conservation equation becomes (cfr. chapter 6 for derivation) :

$$I_m u_{em}^2 b^2 + I_q U_\infty u_{em} b^2 = M_{eo} \tag{4.5.25}$$

where I_m and I_q cross sectional constants

M_{eo} is the initial excess momentum flux

The tracer conservation equation becomes (cfr. chapter 6):

$$I_q u_{em} c_m b^2 + I_\Delta U_\infty c_m b^2 = Q C_o \tag{4.5.26}$$

where I_q and I_c are cross sectional constants

c_m is the center line tracer concentration

C_o is the initial tracer concentration

Finally, a closure equation (cfr. (6.3.4)) :

$$\frac{db}{dx} = k \frac{u_{em}}{u_{em} + U_\infty} \tag{4.5.27}$$

where k is the constant growth rate for pure jets and pure plumes
(cfr. sections 4.2 and 4.3)

We assume

$$u_{em} \sim x^{a'} \tag{4.5.28}$$

$$b \sim x^{b'} \tag{4.5.29}$$

$$S_{CL} \sim x^{c'} \tag{4.5.30}$$

where a', b' and c' are unknown constants

Since $U_{eo} << U_\infty$ then $u_{em} << U_\infty$ which implies that first term in (4.5.25) can be ignored. First term in (4.5.26) can similarly be ignored and equation (4.5.27) becomes

$$b \sim \frac{u_{em} x}{U_\infty} \tag{4.5.31}$$

Using eqs. (4.5.28)-(4.5.30) with (4.5.25) and (4.5.26) (both without first term) and (4.5.31) yields:

$$\frac{u_{em}}{U_\infty} \sim \left(\frac{x}{l_{M_e U_\infty}}\right)^{-2/3} \tag{4.5.32}$$

$$\frac{b}{l_{M_e U_\infty}} \sim \left(\frac{x}{l_{M_e U_\infty}}\right)^{1/3} \tag{4.5.33}$$

$$\frac{S_{CL} Q}{U_\infty l^2_{M_e U_\infty}} \sim \left(\frac{x}{l_{M_e U_\infty}}\right)^{2/3} \tag{4.5.34}$$

Equations (4.5.32)-(4.5.34) describe the flow in weak jets in a coflow and in similar regions in composite jets.

A weak counterflowing jet is shown in fig. 4.17. U_0 is slightly greater numerically than the ambient velocity U_∞ to avoid backflow into the nozzle. A wake-like flow similar to the coflowing case is formed except that the excess velocities are negative.

The equations derived for coflow would be expected to hold with a change of sign of u_{em} and x will have to be replaced by -x because otherwise the powers in eqs. (4.5.32)-(4.5.34) would be undefined.

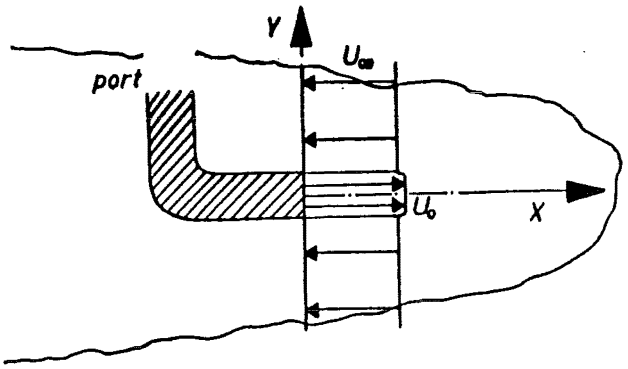

Fig. 4.17. Sketch of a weak jet in a counterflow.

All four basic jet types have now been discussed and equations for width, velocity and center line dilution have been derived.

We have then in principle studied

1. Momentum driven jet in still ambient
2. Buoyancy driven jet in still ambient
3. Buoyancy driven jet in a strong (dominating) ambient flow
4. Momentum driven jet in a strong (dominating) ambient flow

and the results will be used to predict the behaviour of a composite jet in next chapter.

CHAPTER 5

EMPIRICAL FORMULAE FOR DILUTION AND TRAJECTORY

5.1. Introduction.

In this chapter the general case of a buoyant jet discharging horizontally into either a stationary fluid or an ambient flow which is co-, cross- or counterflowing will be discussed. The discussion is based on the results of the dimensional analysis in previous chapter.

A length scale, as mentioned in previous chapter is an indication of the distance from the port where the flow goes from being dominated by one or two flow parameters to being dominated by another set of one or two flow parameters.
The length scale is a combination of these parameters with the dimension length. Length scales can therefore also be viewed as the approximate distance from the port where a transition in the flow occurs.
If a flow has more than two initial parameters then several length scales can be formed and they will define several regions in the jet, each dominated by one single or a combination of two parameters only. Such a jet is called composite.

The basic jets as discussed in previous chapter were all characterised by having only one significant length scale and being dominated by one or a set of two initial parameters throughout virtually the entire flow. The flow in the regions of a composite jet must therefore each ressemble the flow in a basic jet which has the same dominating initial parameter or parameters. By first identifying the various regions in a composite jet with the help of its length scales and then applying the results found in previous chapter for the corresponding basic jets with the same dominating parameter to each of the regions, a complete description of the composite jet can be obtained.

This method has been used by Wright [1977] for vertical jets in a cross flow, by Fisher et al. [1979], also for a vertical jet in a crossflow , and finally by Bühler & Hauenstein [1979] for a horizontal jet in still ambient and a cross flow. All three workers have looked at a jet in still ambient or in a perpendicular crossflow only, not flows from other angles.
In this work horizontal jets in still ambient and in a co-, cross- and counterflow are treated. Since crossflows have already been studied by Bühler & Hauenstein the case of a horizontal jet in a coflow will be discussed in detail in this introduction and will then be followed by a brief reference to the corresponding results for cross- and counterflows. It will be shown in the following sections that counterflows are very similar to coflows.

From the discussion in the previous chapter it was seen that it was possible to have regions dominated by one parameter (a - c as listed below) or a pair of parameters (d - e) :

a) Q

b) M_e

c) B

d) U_∞ and M_e

e) U_∞ and B

The following length scales describing transitions between two regions can directly be derived because they only contain two parameters:

Parameter		Transition	
l_{QMe}	$= Q/M_e^{1/2}$	$Q \rightarrow M_e$	(5.1.1)
l_{QB}	$= Q^{3/5}/B^{1/5}$	$Q \rightarrow B$	(5.1.2)
l_{MeB}	$= M_e^{3/4}/B^{1/2}$	$M_e \rightarrow B$	(5.1.3)
$l_{MeU\infty}$	$= M_e^{1/2}/U_\infty$	$M_e \rightarrow U_\infty \& M_e$	(5.1.4)
$l_{BU\infty}$	$= B/U_\infty^3$	$B \rightarrow U_\infty \& B$	(5.1.5)

It is not possible directly to find e.g. the length scale containing U_∞ & M_e and U_∞ & B, i.e. U_∞, M_e and B , $l_{U\infty Me,U\infty B}$. The length scale must be a power product of the form $M_e^a B^b U_\infty^c$ where a, b and c are powers chosen such that the dimension of the product is length. Because there are three unknowns, a,b and c, but the factors only contain two dimensions, length and time, there is one degree of freedom and thus an infinity of solutions.

Additional information is therefore required and for that purpose it is necessary to make a reference to chapter 6 where the x- and y-momentum equations and the buoyancy flux conservation equations are derived.(Eqs. (6.2.9)-(6.2.11) (coflow), eqs. (6.2.26)-(6.2.28) (crossflow) and eqs. (6.2.36)-(6.2.38) (counterflow)).

For a coflow, the x-momentum equation is (cfr. eq. (6.2.9))

$$(I_m u_{sm}^2 + I_q U_\infty u_{sm} \cos\beta)\cos\beta\, b^2 - (I_{mv} u_{sm} v_{sm} + I_v U_\infty v_{vm} \cos\beta)\sin\beta\, b^2 = M_e \qquad (5.1.6)$$

And the y-momentum equation is (cfr. eq. (6.2.10))

$$\frac{d}{ds'}[(I_m u_{sm}^2 + I_q U_\infty u_{sm}\cos\beta)\sin\beta\, b^2] +$$

$$\frac{d}{ds'}[(I_{mv} u_{sm} v_{vm} + I_v U_\infty v_{vm}\cos\beta)\cos\beta\, b^2] = I_\Delta \Delta_m b^2$$

(5.1.7)

The buoyancy conservation equation is (cfr. (6.2.11))

$$I_{q\Delta}\Delta_m u_{sm} b^2 + I_\Delta \Delta_m U_\infty b^2 \cos\beta = B$$

(5.1.8)

When the local excess velocity u_{em} and any components of it is much smaller than U_∞then U_∞ is dominating the flow , and this is said to be the far field of the flow.

Similarly, when u_{em} is much greater than U_∞ , then this is called the near field of the flow.

The parts of the flow where U_∞ is not dominating have already been dealt with (eqs. (5.1.1) - (5.1.3)) so the case where $u_{em} << U_\infty$ is the case of interest here. It can be seen from eqs. (5.1.6), (5.1.7) and (5.1.8) that in that case the terms which do not contain U_∞ become negligible as compared with the terms which contain U_∞.

Eq. (5.1.6) then becomes

$$(I_q u_{sm}\cos\beta - I_v v_{vm}\sin\beta)\cos\beta\, b^2 \sim \frac{M_e}{U_\infty}$$

(5.1.9)

Eq. (5.1.7) becomes

$$\frac{d}{ds'}[U_\infty u_{sm}\cos\beta\sin\beta\, b^2 + U_\infty v_{vm}\cos^2\beta\, b^2] \sim \Delta_m b^2$$

(5.1.10)

And eq. (5.1.8) becomes

$$b^2 \Delta_m \sim \frac{B}{U_\infty}$$

(5.1.11)

Inserting (5.1.11) in (5.1.10) yields

$$\frac{d}{ds'}[u_{sm}\cos\beta\sin\beta\, b^2 + v_{vm}\cos^2\beta\, b^2] \sim \frac{B}{U_\infty^2}$$

(5.1.12)

From (5.1.9) and (5.1.12) it can be seen that in the U_∞ & M_e dominated part of a flow the important parameter is M_e/U_∞ and in the U_∞ & B dominated part of a flow the important parameter is B/U_∞^2.

It is now possible to derive the remaining length scales:

Length scale		Transition	
$l_{QU_\infty Me}$	: can not be derived	$Q \rightarrow U_\infty \& M_e$	(5.1.13)
$l_{QU_\infty B} = Q/(B/U_\infty^2)$		$Q \rightarrow U_\infty \& B$	(5.1.14)
$l_{MeU_\infty B}$	: can not be derived	$M_e \rightarrow U_\infty \& B$	(5.1.15)
$l_{BU_\infty Me} = (M_e/U_\infty)^{3/5}/B^{1/5}$		$B \rightarrow U_\infty \& M_e$	(5.1.16)
$l_{U_\infty Me,U_\infty B} = (M_e/U_\infty)/(B/U_\infty^2)$		$U_\infty \& M_e \rightarrow U_\infty \& B$	(5.1.17)

The length scale $l_{U_\infty Me,U_\infty B}$ is for convenience referred to as l_{MeBU_∞} in the following.
Two of the length scales can not be obtained and thus the transitions they describe can not occur. Further, a buoyancy dominated region can not be followed by a momentum dominated region because the x- excess momentum of the jet is conserved and equal to M_e and the y-excess momentum grows steadily because of the buoyant forces. Thus, once M_{ey} has become greater than M_{ex} (i.e. the flow has gone from being momentum dominated to buoyancy dominated) it can never again become smaller than M_{ex}, i.e. the jet remains buoyancy dominated after this point. This implies that although an expression for $l_{BU_\infty Me}$ can be derived it describes a transition that can not take place.

Equations (4.1.3) - (4.1.5) define Q, B and M_e.

According to (4.1.5) M_e is given by $M_e = (\pi/4)\, d_p^2\, U_0\, |\underline{U}_0 - \underline{U}_\infty|$. (This definition originates from the equations of motion, cfr. chapter 6).

M_e then becomes for a horizontal jet in a coflow (see fig. 5.1)

$$M_e = \pi/4\ d_p^2\, U_0\, (U_0 - U_\infty) \qquad (5.1.18)$$

(It is worth noting that both Wright (1977), Fisher et al. (1979) and Bühler & Hauenstein (1979) incorrectly used the absolute momentum flux M rather than the excess momentum flux M_e, this will be discussed in more detail later in this section).

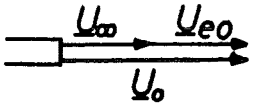

$$U_{eo} = U_o - U_\infty$$

Fig. 5.1. Sketch of U_{eo} in coflow.

Using equations (5.1.1) - (5.1.5) , (5.1.14) and (5.1.17) with (5.1.18) the length scales take the form as shown in table 5.1:

Length scale	Equation	General expression	Horizontal jet in coflow
l_{QM_e}	(5.1.1)	$\dfrac{Q}{M_e^{1/2}}$	$\left(\dfrac{\pi}{4}\right)^{1/2} d_p \left(1-\dfrac{U_\infty}{U_o}\right)^{-1/2}$
l_{QB}	(5.1.2)	$\dfrac{Q^{3/5}}{B^{1/5}}$	$\left(\dfrac{\pi}{4}\right)^{2/5} d_p Fr^{2/5}$
l_{M_eB}	(5.1.3)	$\dfrac{M_e^{3/4}}{B^{1/2}}$	$\left(\dfrac{\pi}{4}\right)^{1/4} d_p Fr \left(1-\dfrac{U_\infty}{U_o}\right)^{3/4}$
$l_{M_eU_\infty}$	(5.1.4)	$\dfrac{M_e^{1/2}}{U_\infty}$	$\left(\dfrac{\pi}{4}\right)^{1/2} d_p \left(\dfrac{U_\infty}{U_o}\right)^{-1} \left(1-\dfrac{U_\infty}{U_o}\right)^{1/2}$
l_{BU_∞}	(5.1.5)	$\dfrac{B}{U_\infty^3}$	$\dfrac{\pi}{4} d_p Fr^{-2} \left(\dfrac{U_\infty}{U_o}\right)^{-3}$
$l_{QU_\infty B}$	(5.1.14)	$\dfrac{QU_\infty^2}{B}$	$d_p \left(\dfrac{U_\infty}{U_o}\right)^2 Fr^2$
$l_{M_eBU_\infty}$	(5.1.17)	$\dfrac{M_e U_\infty}{B}$	$d_p Fr^2 \left(\dfrac{U_\infty}{U_o}\right)\left(1-\dfrac{U_\infty}{U_o}\right)$

Table 5.1. Length scales in a coflow.

The length scale $l_{\nu B} = \nu^{3/2}/B^{1/2}$ as introduced in the discussion of pure plumes in still ambient is not included in table 5.1. The viscosity ν was important in the pure plume because the plume started from initially at rest. In the initial laminar region ν would therefore be

expected to affect the flow.

In practice, however, it is difficult to create pure plume flows without some initial momentum. In those cases $l_{MeB} = M_e^{3/4}/B^{1/2}$ then becomes the relevant length scale for the 'pure' plume flows and for this scaling the form of the equations for pure plume previously derived is valid.

For convenience, the 5 possible regions will in the following be referred to as:

Q-dominated	: Initial zone	(IZ)
M_e-dominated	: Momentum dominated near field	(MDNF)
U_∞ & M_e-dominated	: Momentum dominated far field	(MDFF)
B-dominated	: Buoyancy dominated near field	(BDNF)
U_∞ & B-dominated	: Buoyancy dominated far field	(BDFF)

In the general case of jets discharging both M_e and B all five regions IZ, MDNF, MDFF, BDNF and BDFF can (but not necessarily will) exist.

When the possible length scales for the flow are calculated (according to table 5.1) then their order of magnitude relative to each other indicate the extent of the existence of the regions MDNF, MDFF, BDNF and BDFF.

This can be illustrated as in fig. 5.2.

Fig. 5.2 shows a plot of the various length scales for a jet in a coflow (cfr. table 5.1) when $M_e \neq 0$, $B \neq 0$ and $U_\infty \neq 0$.

As an example, U_∞/U_0 has been given the value of 0.2. The abscissa is the distance from the port non-dimensionalised with d_p and it is at the same time also the value of the various length scales, divided by d_p.

Note that the lines representing l_{QB}, $l_{QU_\infty B}$ and l_{BU_∞} intersect in the same point A. The lines representing l_{MeBU_∞}, l_{BU_∞} and l_{MeB} intersect in the point B and the lines representing l_{QB}, l_{MeB} and l_{QMe} intersect in the point C. A and B are both on the line for l_{BU_∞}.

Consider the case Fr = 50. This corresponds to a horizontal line through 50 on the y-axis.

For all finite values of Fr the flow must eventually become BDFF [buoyancy dominated regions follow after momentum dominated regions (because M_{ey} increases, M_{ex} is constant) and far fields follow after near fields(u_{em} decreases constantly, U_∞ is constant)].

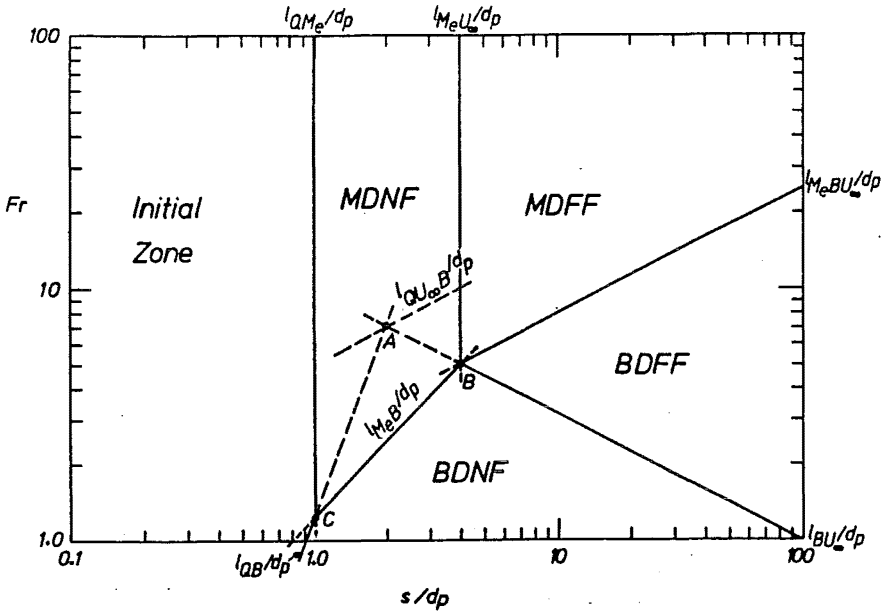

Fig. 5.2. The variation of the length scales in a coflow with $U_\infty/U_0 = 0.2$.

When the length scales are compared relative to each other to identify the regions that can occur in a flow then it becomes much easier if one starts in the far right end of the s/d_p scale and then works to the left towards what must ultimately become the initial zone (IZ).

If this is done for Fr=50 (and $U_\infty/U_0 = 0.2$ as in fig. 5.2) then the first line that is encountered is $l_{MeBU\infty}$ which indicates a transition from BDFF to MDFF.

Next line to be intersected is $l_{QBU\infty}$ which is an indication of a transition from BDFF to IZ. However, we are now in MDFF and it is not applicable. Next line to intersect is $l_{MeU\infty}$ which indicates a transition from MDFF to MDNF. Next line to intersect is l_{QB} which indicates a transition from BDNF to IZ. Since we are in MDNF it does not apply. Next line is l_{QMe} which indicates a transition from MDNF to IZ. The last line to intersect is $l_{BU\infty}$ which indicates a transition from BDFF to BDNF but it does not apply since we are in IZ.

It can then be concluded that for Fr=50 and $U_\infty/U_0 = 0.2$ the following regions exist: IZ, MDNF,MDFF and BDFF.

It can be shown from the formulae in table 5.1 that when $0 \leq U_\infty/U_0 < 0.5$ then points A,B and C have positions relative to each other as in fig. 5.2 and the diagrams will then be of a similar type as fig. 5.2.

For $U_\infty/U_0=0.5$ point A,B and C in fig. 5.2 coincide, see fig. 5.3. The region called 2 in fig. 5.3 can be both IZ and MDFF. This can be seen by comparing the length scales in a similar manner

as it was done for fig. 5.2. Region 2 must be said to be undefined.

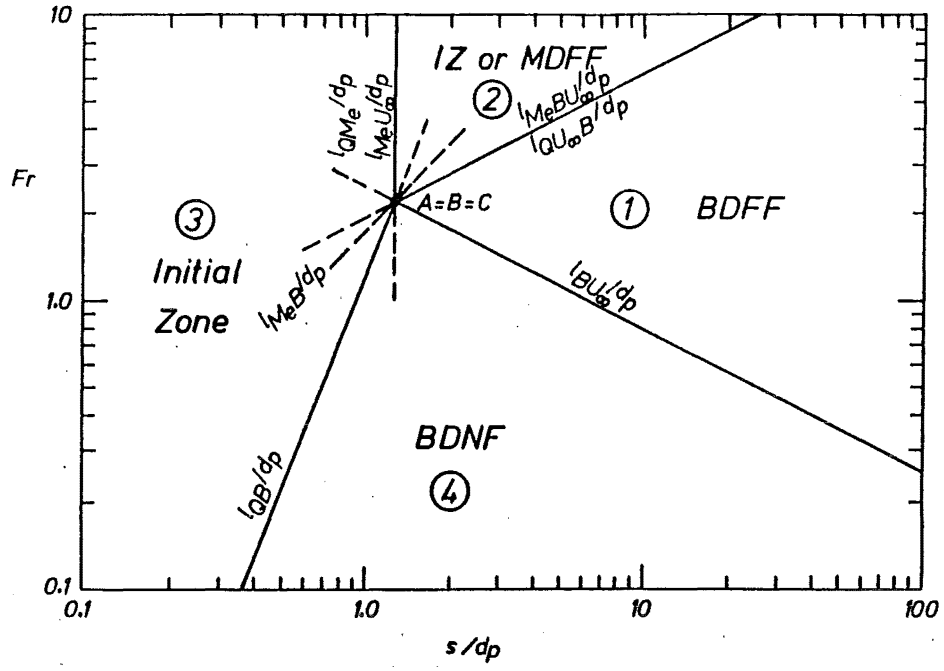

Fig. 5.3. Length scales in a coflow with $U_\infty/U_0 = 0.5$.

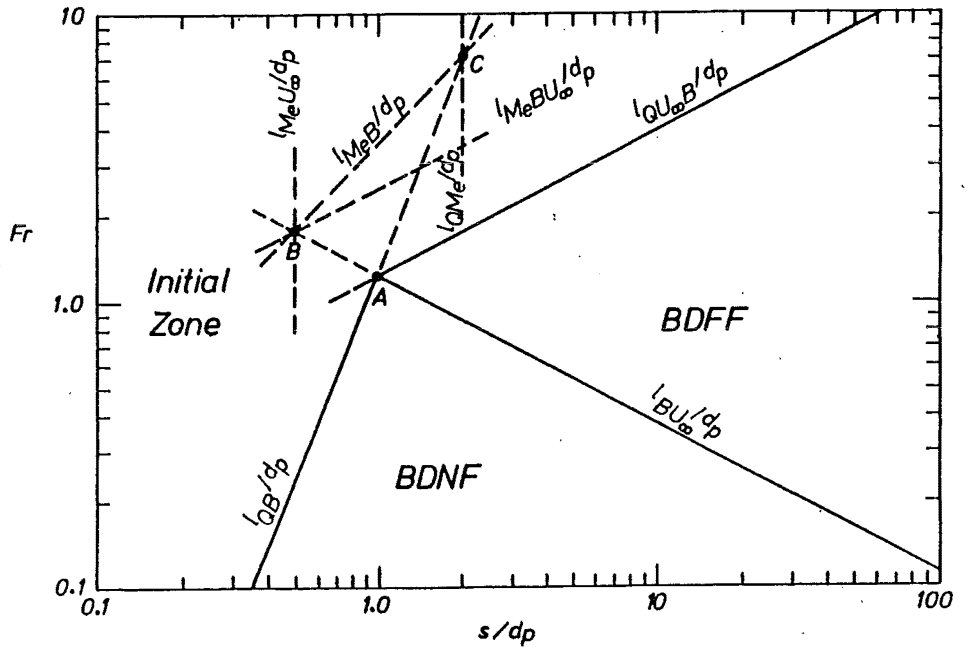

Fig. 5.4. Length scales in a coflow with $U_\infty/U_0 = 0.8$.

For $0.5<U_\infty/U_0\leq 1$ (U_∞/U_0 can not become greater than 1 in coflows because then it is no longer a jet flow) the diagrams typically look like fig. 5.4. which has $U_\infty/U_0 = 0.8$. Note that

points A,B and C now have a different position relative to each other. Here the momentum dominated regions have completely disappeared. For high Froude numbers the flow ressembles an advected cylinder of non-buoyant fluid (i.e. the length of IZ→ ∞) and for very small values of Fr the flow ressembles an advected plume (i.e. the length of BDNF →∞).
Fig. 5.2 (with $0 \leq U_\infty/U_0 < 0.5$) has been generalised to include U_∞/U_0 = 0.001, 0.005, 0.1, 0.2, 0.3 and 0.4 in fig. 5.5.

When $U_\infty/U_0 \rightarrow 0$ then point C will not change much but point A and B will move infinitely to the left, as indicated by the trend in fig. 5.5. This confirms that only IZ, MDNF and BDNF can exist in still ambient.

When Fr → ∞ corresponding to B → 0 then the approximate distance from the source where the flow becomes buoyancy dominated will →∞ as it also can be seen from fig. 5.5.

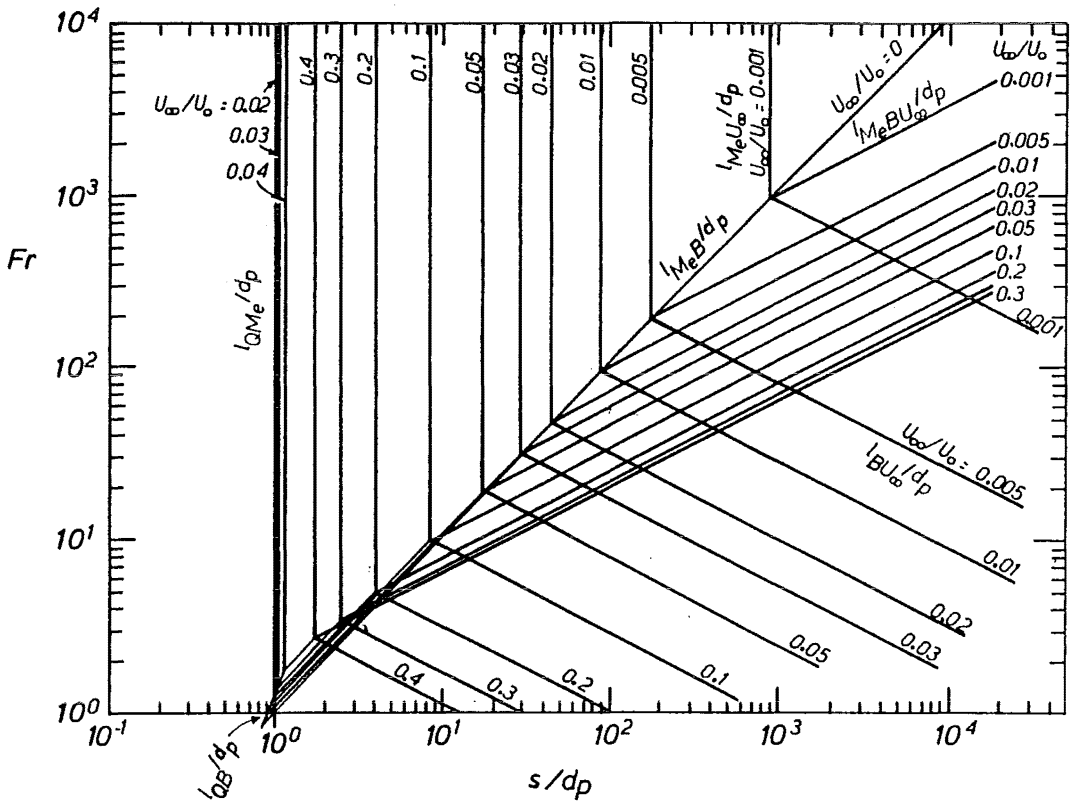

Fig. 5.5. General plot of length scales in a coflow with $0 < U_\infty/U_0 < 0.5$.

A generalised form of fig. 5.4. (with $0.5 < U_\infty/U_0 \leq 1$) is shown in fig. 5.6. for the values U_∞/U_0=0.6, 0.7, 0.8, 0.9 and 1.0.

The above discussion and classification of flow regions (MDNF, MDFF, BDNF and BDFF) for horizontal jets in a coflow can easily be extended to horizontal jets in a crossflow and horizontal jets in a counterflow.
For crossflows, M_e is given by (see fig. 5.7)

$$M_e = \pi/4\ d_p^2\ U_0(U_0^2 + U_\infty^2)^{1/2} \qquad (5.1.19)$$

In crossflows U_∞ can be greater than U_0. It can be shown from the equations of motion (which are derived in next chapter) for jets in a crossflow that also in this case M_e/U_∞ and B/U_∞^2 are the relevant parameters in MDFF and BDFF respectively. This leads to length scales of a similar form as for coflows, and the length scales become as shown in table 5.2.

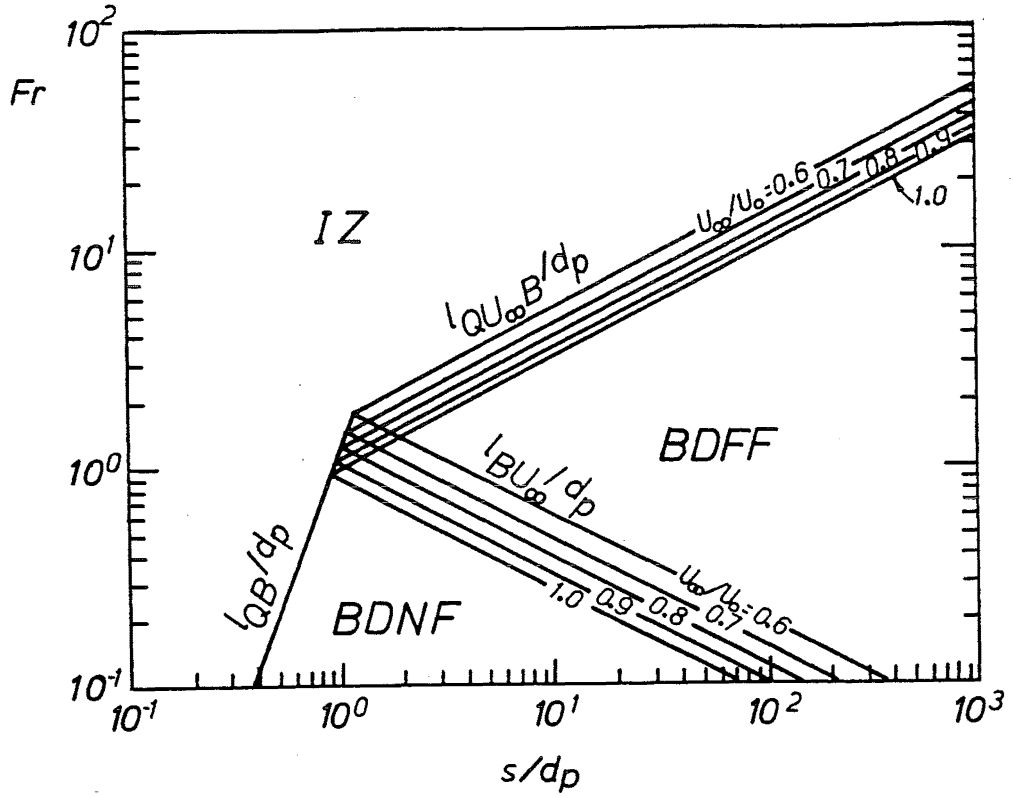

Fig. 5.6. General plot of length scales in a coflow with $0.5<U_\infty/U_0\leq 1.0$.

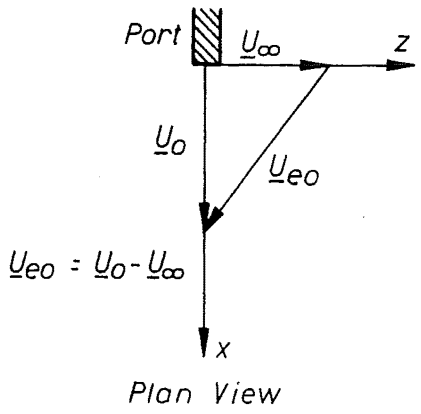

Fig. 5.7. Sketch of U_{eo} in a crossflow.

Length scale	Expression for a jet in a crossflow
l_{QM_e}	$\left(\frac{\pi}{4}\right)^{1/2} d_p \left(1+\left(\frac{U_\infty}{U_o}\right)^2\right)^{-1/4}$
l_{QB}	$\left(\frac{\pi}{4}\right)^{2/5} d_p Fr^{2/5}$
l_{M_eB}	$\left(\frac{\pi}{4}\right)^{1/4} d_p Fr \left(1+\left(\frac{U_\infty}{U_o}\right)^2\right)^{3/8}$
$l_{M_eU_\infty}$	$\left(\frac{\pi}{4}\right)^{1/2} d_p \left(\frac{U_\infty}{U_o}\right)^{-1} \left(1+\left(\frac{U_\infty}{U_o}\right)^2\right)^{1/4}$
l_{BU_∞}	$\frac{\pi}{4} d_p Fr^{-2} \left(\frac{U_\infty}{U_o}\right)^{-3}$
$l_{QU_\infty B}$	$d_p Fr^2 \left(\frac{U_\infty}{U_o}\right)^2$
$l_{M_eBU_\infty}$	$d_p Fr^2 \left(\frac{U_\infty}{U_o}\right) \left(1+\left(\frac{U_\infty}{U_o}\right)^2\right)^{1/2}$

Table 5.2 Length scales for horizontal jet in a crossflow.

All of the discussion of the coflow case applies to crossflowing jets. Furthermore, the behaviour of buoyancy dominated flows is exactly the same in co-, cross- and counterflows; in buoyancy dominated flows the initial excess momentum M_e is negligible. Since the angle between $\underline{M_e}$ and $\underline{U_\infty}$ defines whether it is a co-, cross- or counterflow the initial angle of discharge is therefore unimportant too. The length scales in table 5.2 are plotted in fig. 5.8 in a way similar to the way the length scales were plotted for coflows.

From table 5.2 it can be seen that $l_{MeU\infty} > l_{QMe}$ for all values of U_∞/U_0 and the equivalent to point A in fig. 5.2 is to the left of the equivalent to point B for all values of U_∞/U_0. The type of diagram as shown in fig. 5.3 and 5.4 is thus not possible for crossflows. The length

scales are plotted for the values U_∞/U_0 = 0.001, 0.01, 0.1, 0.2, 0.3, 0.4, 0.5, 0.6, 0.7, 0.8 and 0.9.

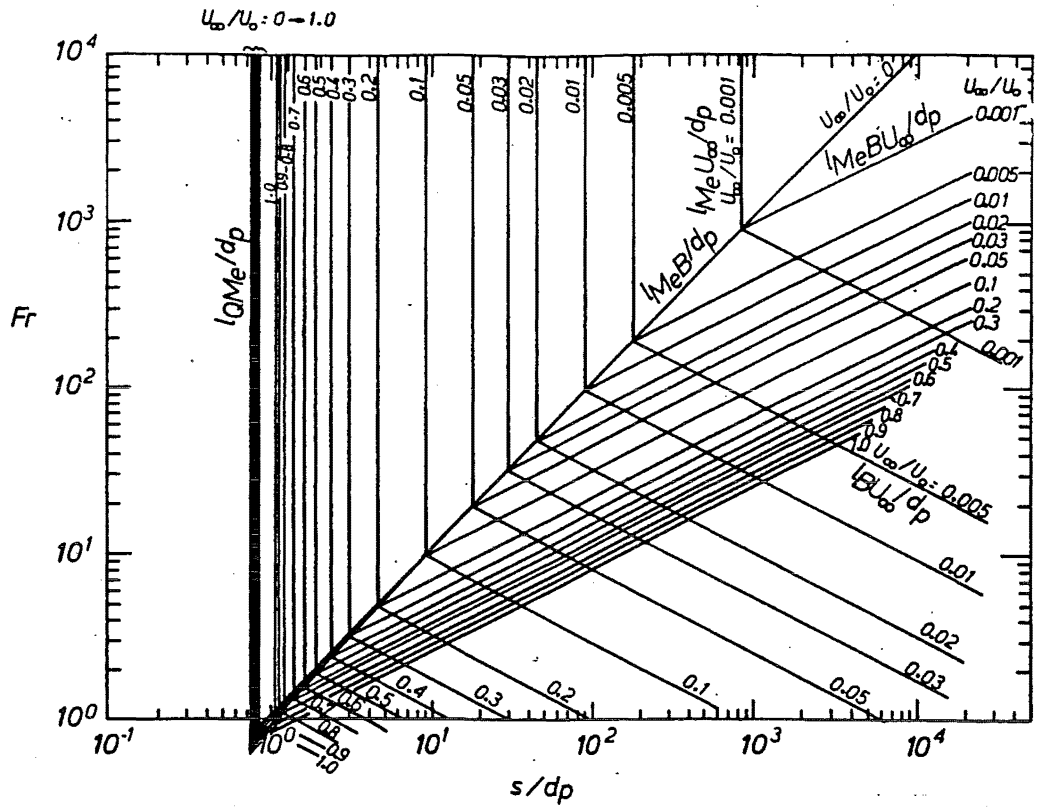

Fig. 5.8. General plot of length scales in a crossflow.

For counterflows M_e is given by (see fig. 5.9) :

$$M_e = \pi/4\ d_p^2\ U_0(U_0-U_\infty) \qquad (5.1.20)$$

This expression is the same as for coflows but in counterflows U_∞ is negative.

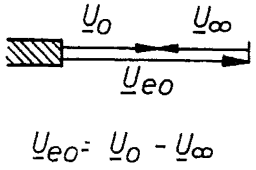

$$\underline{U}_{eo} = \underline{U}_0 - \underline{U}_\infty$$

Fig. 5.9 Sketch of U_{eo} in a counterflow.

The absolute value of U_∞ must be smaller than U_0 because otherwise there will be entrainment into the nozzle. The expressions for the length scales are therefore the same as for coflows and table 5.1 must also apply for counterflows. However, because U_∞/U_0 is negative l_{MeU_∞} and l_{BU_∞} would become negative. This is inappropriate since they are

compared with s and the other length scales which are all positive. The absolute values of the length scales $l_{MeU\infty}$ and l_{MeB} are therefore used in the following.

It can be shown that only the type of curve as shown in fig. 5.5 is possible.

The length scales for the counterflow cases are plotted in fig. 5.10 in a similar way as for coflows ($U_\infty/U_0<0.5$) and crossflows. The values of $|U_\infty/U_0|$ are 0.001, 0.01, 0.1, 0.2, 0.3, 0.4, 0.5, 0.6, 0.7, 0.8 and 0.9.

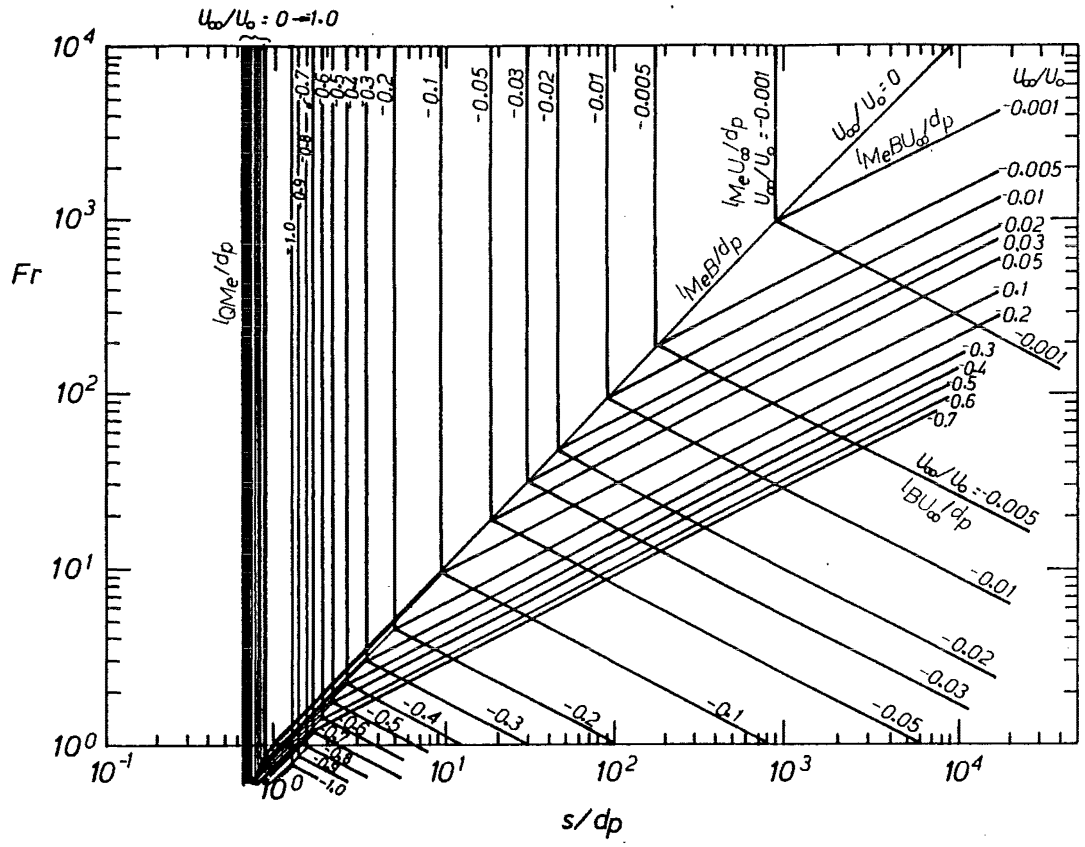

Fig. 5.10. General plot of length scales in a counterflow.

Note that although the boundaries between the different regions in the figures above are shown as a line the transition from one region to another takes place over some distance.

In the following sections each of the 4 flow regions MDNF, MDFF, BDNF and BDFF and momentum dominated/buoyancy dominated in still ambient will be discussed individually. The results from the analysis in chapter 4 will be applied and extended. This applies to jets in still ambient, co-, cross- and counterflow.

Formulae are derived for center line dilution S_{CL} and trajectories.

The flows which were analysed in chapter 4 were characterised by consisting of one infinitely long region only (apart from a very short initial region). Figs. 5.5, 5.6, 5.8 and 5.10 show that in many cases a region in a composite jet can be relatively short. The influence from the adjacent regions means that the results from chapter 4 for infinitely long regions are

only approximate for the limited regions in a composite jet.

The functional relationships derived in chapter 4 apply in the relevant regions but the influence of the adjacent regions can be seen in that the coefficients in the equations may depend slightly on the proximity of the adjacent regions, i.e. the ratios of the length scale of a given region and the length scales of the adjacent regions. However, once a region is sufficiently long, see region A-B in fig. 5.11, then the coefficients must have their 'real' value corresponding to an infinitely long region. For comparison, region A'-B' in fig. 5.11 is very short and the coefficients may depend strongly on the ratios between the relevant length scale of the region and the length scales of the adjacent regions.

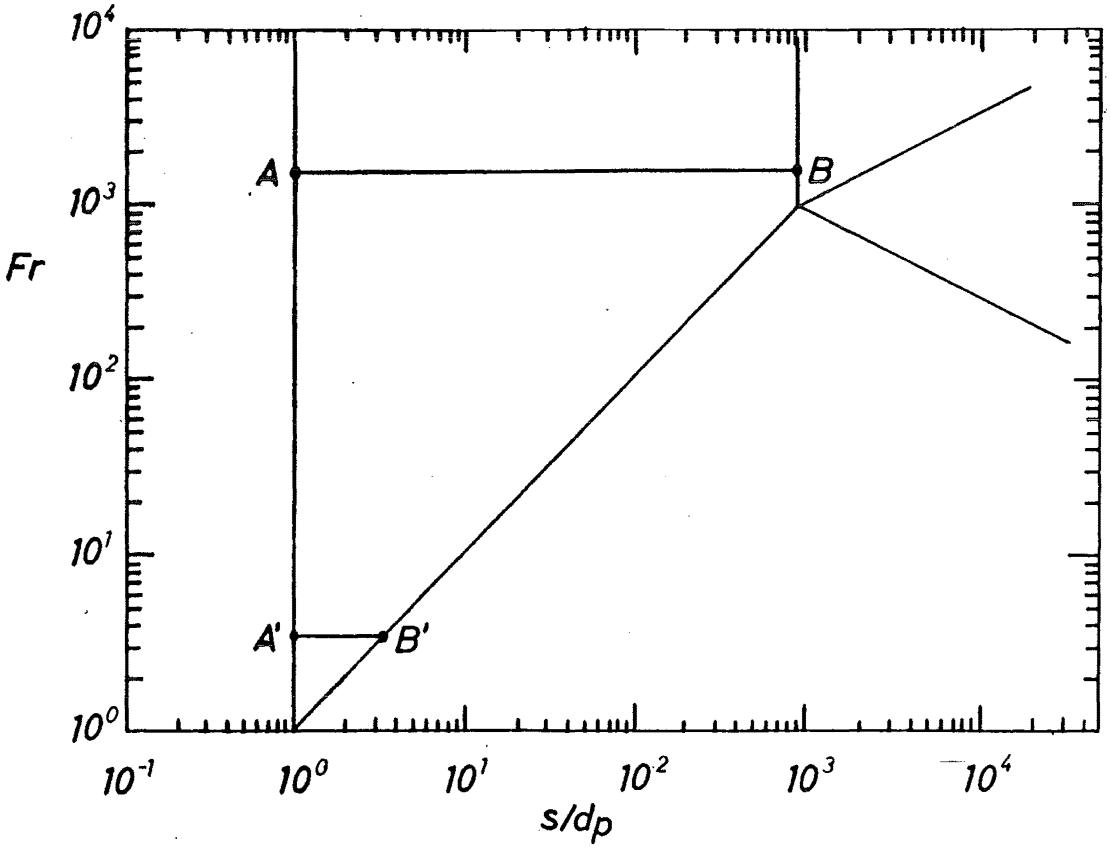

Fig. 5.11. Sketch of length of different regions.

Experimental data obtained by Ayoub [1971], Brown [1984], Abraham [1963], Hansen & Schrøder [1968], HRS [1977] , Fan [1968] , Chu [1975] and the author are compared with the formulae for S_{CL} and trajectories as derived in the following sections to find the coefficients in the formulae.

It should be emphasised that both Wright [1977], Fisher et al. [1979] and Bühler & Hauenstein[1979] incorrectly used the absolute momentum flux M rather than the excess momentum flux M_e (cfr. also comment in section 4.1) in their analysis.

However, it can be shown that the errors in the values of the length scales within the range of the parameters in their experiments caused by this is less than 0.3 % with only a few exceptions. The resulting error in the coefficients as found by them would be expected to be of

a similar order of magnitude.
Within their limits (which will be stated where they are used) Wright's and Bühler & Hauenstein's results can therefore be considered fully applicable.
In appendix D the values of the coefficients are found theoretically from the basic equations in chapter 6. Those values correspond to infinitely long regions and are also considered in the analysis of the data.

The results from the 6 analyses in the following section are used to produce charts for the dilution and trajectory in the general cases where there are several significant length scales.

5.2. Flow regions in buoyant jets in still ambient.

The MDNF and BDNF in a jet in still ambient behave in a similar manner as the MDNF and BDNF in jets in an ambient flow. However, since $U_\infty=0$ then U_∞ can not enter into the analysis. The still ambient case is therefore treated separately in this section.

The source discharges volume flux M and bouyancy flux B. From these parameters the three length scales l_{QM}, l_{QB} and l_{MB} can be formed.
l_{QM} and l_{QB} relate to the initial zone and will be ignored.
For $s << l_{MB}$ (but outside the initial zone) the jet behaves like a pure jet in still ambient with almost horizontal trajectory and center line dilution given by (cfr. eq. (4.2.8))

$$S_{CL} \sim x/l_{QM}$$

Which is equivalent to

$$\frac{S_{CL}\,Q}{l_{MB}\,M^{1/2}} \sim \frac{x}{l_{MB}} \quad \text{or} \quad \frac{S_{CL}\,Q}{l_{MB}\,M^{1/2}} = C_{a1}\,\frac{x}{l_{MB}} \tag{5.2.1}$$

(Cfr. the definitions of l_{QM} and l_{MB})

where C_{a1} is a coefficient.

Abraham [1963] showed that in the momentum dominated region the trajectory gently bends in the direction of the buoyant forces and the trajectory there is given by

$$\frac{y}{l_{MB}} \sim \left(\frac{x}{l_{MB}}\right)^3 \qquad \text{or} \qquad \frac{y}{l_{MB}} = C_{a2}\left(\frac{x}{l_{MB}}\right)^3 \tag{5.2.2}$$

It has also been derived in appendix B.

Analysis of Ayoub's data produces the curve as shown in fig. 5.12. The value of C_{a1} possibly depends slightly on the ratio l_{QM}/l_{MB}. Bühler & Hauenstein[1979] gave the value C_{a1} = 0.17 based on Hansen & Schrøder [1968] and Abraham's [1963] data which according to them is a generally accepted value. The theoretical value of C_{a1} as derived in appendix D is 0.185. Ayoub's data could not serve to give an estimate of the value of C_{a2} but Bühler & Hauenstein [1977] gave 0.05 which is also based on Hansen & Schrøder and Abraham's data.

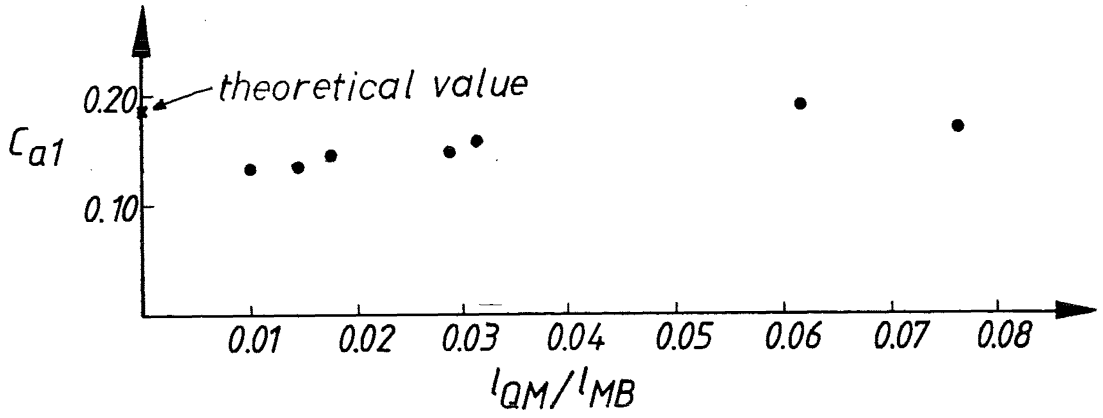

Fig. 5.12. The coefficient C_{a1} as a function of l_{QM}/l_{MB}.

For $s >> l_{MB}$ the jet behaves like a pure plume in still ambient. Then the dilution relationship for pure plumes must be expected to apply:

$$S_{CL} \sim y^{5/3}$$

That can be written as

$$\frac{S_{CL}\,Q}{l_{MB}\,M^{1/2}} = C_{a7}\left(\frac{y}{l_{MB}}\right)^{5/3} \qquad (5.2.3)$$

The trajectory will have a vertical tangent as $s \rightarrow \infty$, i.e. the abscissa of the trajectory reaches a maximum value asymptotically:

$$\frac{x}{l_{MB}} \rightarrow \frac{x_{max}}{l_{MB}} \qquad (5.2.4)$$

Ayoub's data do not go far enough but indicate a value of $C_{a7} \approx 0.11$. Bühler & Hauenstein give $C_{a7} = 0.091$ and this is according to them a generally accepted value. The theoretical value of C_{a7} is 0.102.

Bühler & Hauenstein found $x_{max} \approx 5.0\, l_{MB}$. The theoretical value as found in section 6.5 is $8.4\, l_{MB}$.

5.3. Flow regions in coflowing jets.

5.3.1. Momentum dominated near field in coflowing jets.

The momentum dominated near field in a coflowing jet can be located by using figs. 5.5 or 5.6. It can be seen from the figures that there is not always a MDNF in a coflowing jet.
It can also be seen that a MDNF is either followed by a MDFF or a BDNF (there is a special case: for each value of U_∞/U_0 there is one value of Fr where MDNF can go directly to BDFF. That value of Fr corresponds to the ordinate of point A). The transitions MDNF $\rightarrow$ MDFF and MDNF $\rightarrow$ BDNF correspond to the length scales $l_{MeU\infty}$ and l_{MeB} so it is reasonable to use one of these length scales in the analysis. $l_{MeU\infty}$ is chosen.

Because the flow in the MDNF region ressembles the flow in a pure jet in still ambient the dilution and xy-trajectory formulae from section 4.2 are expected to apply.
The dilution S_{CL} is 'non-dimensionalised' with $l_{MeU\infty}$, M_e , U_∞ and Q:

$$\frac{S_{CL}Q}{U_\infty l^2_{M_eU_\infty}}$$

Q is used above since the product $S_{CL}Q$ can be written as (C_0Q/c_m) so that the above expression is in fact c_m non-dimensionalised with the initial tracer flux (C_0Q), U_∞ and $l_{MeU\infty}$.

For coflowing jets in MDNF the dilution equation is given by (cfr. eq. (4.2.8):

$$\frac{S_{CL}Q}{U_\infty l^2_{M_eU_\infty}} = C_{b1}\left(\frac{x}{l_{M_eU_\infty}}\right) \tag{5.3.1}$$

The trajectory in the xy-plane is similar to the one in the momentum dominated part of a jet in still ambient because U_∞ is not important since $s<<l_{MeU\infty}$. The formula has been derived in appendix B.

$$\frac{y}{l_{BU_\infty}} = C_{b2}\left(\frac{x}{l_{M_eU_\infty}}\right)^3 \tag{5.3.2}$$

$$\frac{z}{l_{M_eU_\infty}} = 0 \tag{5.3.3}$$

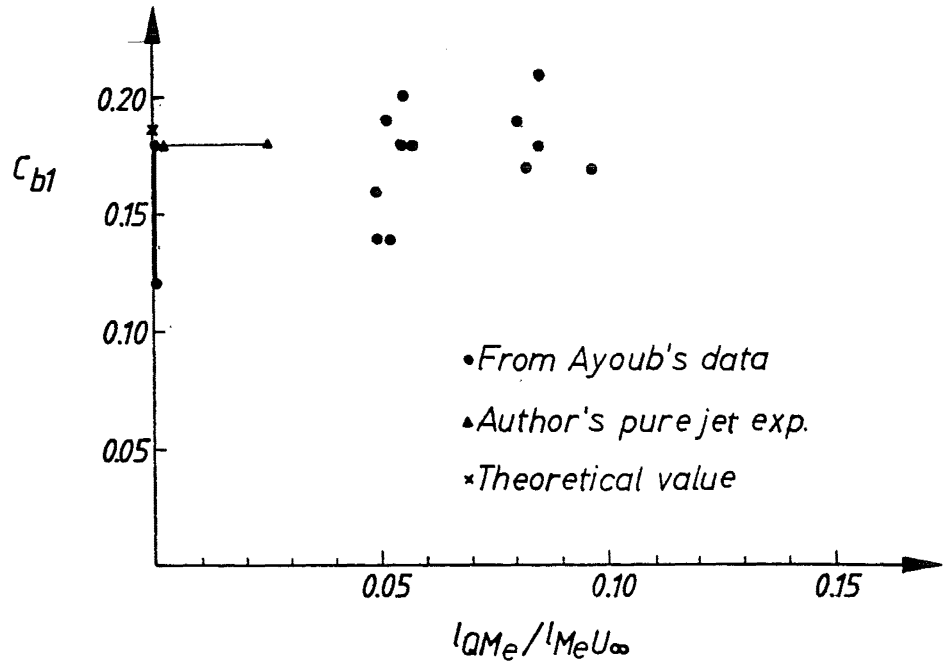

Fig. 5.13. The coefficient C_{b1} as a function of $l_{QMe}/l_{MeU\infty}$.

Ayoub's data for coflows and the author's measurements in pure coflowing jets yielded the values of C_{b1} as shown in fig. 5.13. There did not seem to be any dependency on $l_{QMe}/l_{MeU\infty}$ or $l_{QMe}/l_{MeBU\infty}$. The average value of C_{b1} was around 0.18 and the theoretical value is 0.185.

Only one set of Ayoub's data in MDNF could be used to find the value of C_{b2}. A value of $C_{b2} \approx$ 0.08 was indicated. The theoretical value was 0.048.

5.3.2. Momentum dominated far field in coflowing jets.

The momentum dominated far field in a coflowing jet can be located by using figs. 5.5 or 5.6. It can be seen from these figures that there is not always a MDFF in a jet. It can also be seen that a MDFF is followed by a BDFF (provided that B≠0).

The transition MDFF → BDFF corresponds to the length scale $l_{MeBU\infty}$. However, it is preferable to choose using the length scale $l_{MeU\infty}$ in this analysis because this is consistent with the choice for the analysis of MDNF in previous section.

The flow is driven by the ambient flow U_∞ and to a very small extent by M_e. The buoyancy B is negligible. We will therefore expect the equations derived in section 4.5.3, eqs. (4.5.32), (4.5.33) and (4.5.34) to apply.

As for the MDNF the relevant dilution parameter is $S_{CL}\, Q/(\, U_\infty\, l_{MeU\infty}{}^2\,)$ and the coordinates are non-dimensionalised by dividing by $l_{MeU\infty}$.

For the MDFF region in a coflowing jet eq. (5.4.34) then becomes:

$$\frac{S_{CL}\, Q}{U_\infty\, l^2_{M_eU_\infty}} = C_{b4}\left(\frac{x}{l_{M_eU_\infty}}\right)^{2/3} \qquad (5.3.4)$$

The trajectory in the xy-plane as derived in appendix B:

$$\frac{y}{l_{BU_\infty}} = C_{b5}\left(\frac{x}{l_{M_eU_\infty}}\right)^{4/3} \tag{5.3.5}$$

Further we have

$$\frac{z}{l_{M_eU_\infty}} = 0 \tag{5.3.6}$$

The variation of C_{b4} as found from Ayoub's data is shown in fig. 5.14. C_{b4} is an inconsistent function of $l_{QMe}/l_{MeU\infty}$ but a reasonably consistent function of $l_{MeU\infty}/l_{MeBU\infty}$. The data may be inaccurate as they were almost all in the transition region between MDNF and MDFF.

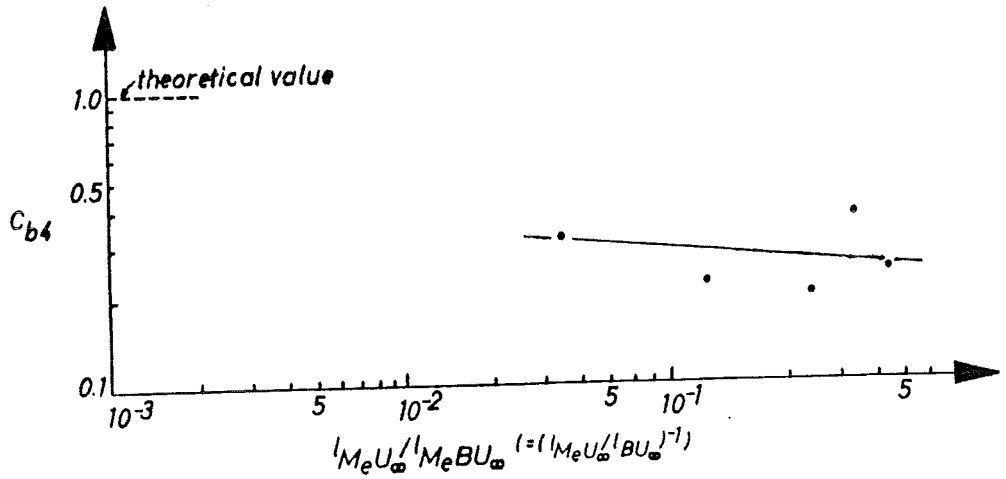

Fig. 5.14. The coefficient C_{b4} as a function of $l_{MeU\infty}/l_{MeBU\infty}$.

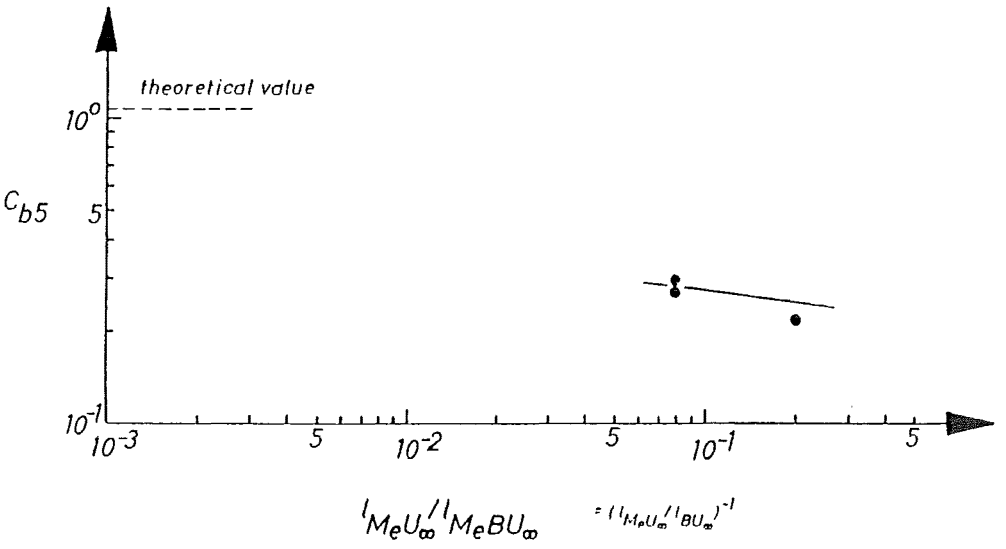

Fig. 5.15. The coefficient C_{b5} as a function of $l_{MeU\infty}/l_{MeBU\infty}$.

From a set of experiments for pure jets in a coflow by the author C_{b4}=0.7-0.9 was found. (Because of buoyancy effects it was not possible to obtain sufficient data in the MDFF region). The theoretical value is 1.00.

None of Ayoub's data could serve to determine C_{b5}. However, the author recorded the trajectory of a number of buoyant jets in coflows. From these recordings C_{b5} could be found. The result is shown in fig. 5.15. Only three values were available. The theoretical value of C_{b4}=1.08 is also shown.

5.3.3. Buoyancy dominated near field in coflowing jets.

The buoyancy dominated near field in a coflowing jet can be located by using figs. 5.5 or 5.6. There is not always a BDNF in a jet, but if there is and $U_\infty \neq 0$ then it is followed by a BDFF. This transition corresponds to the length scale l_{BU_∞} which will be used in the following analysis in this section.

The coordinates of the trajectory will be non-dimensionalised by division by l_{MeU_∞}.

The dilution S_{CL} will be 'non-dimensionalised' by using the length scale l_{BU_∞}, B, Q and U_∞ in the same manner as for the momentum dominated flows: $S_{CL}\, Q/(U_\infty\, l_{BU_\infty}{}^2)$.

Buoyancy is the dominating parameter. The jet behaves like a pure plume being advected by the ambient flow. Since the initial excess momentum M_e is negligible then its angle with $\underline{U}_\infty$ is also negligible. The dilution and trajectory equations would therefore be expected to be the same for co-, cross- and counterflow (with 'x' in coflows replaced by 'z' in crossflows and '-x' in MDFF,BDNF and BDFF of counterflows). This will be discussed in more detail later.

It was logical to use x as the variable coordinate in the dilution equation for the momentum dominated flows because x is the coordinate in the direction of the initial momentum.

Similarly it is logical to use y as the variable coordinate in the dilution equation for the buoyancy dominated flows because y goes in the direction of the buoyant forces.

For the BDNF in a coflowing jet the dilution equation, eq. (4.3.11) applies. However, l_{BU_∞} is chosen as the appropriate length scale and then it becomes

$$\frac{S_{CL}\, Q}{U_\infty\, l_{BU_\infty}^2} = C_{b7}\left(\frac{y}{l_{BU_\infty}}\right)^{5/3} \qquad (5.3.7)$$

The trajectory in the xy-plane is found from eq. (4.3.8) using $u_{em} = dy/dt$ and $dx/dt = U_\infty$: (see appendix B)

$$\frac{y}{l_{BU_\infty}} = C_{b8}\left(\frac{x}{l_{BU_\infty}}\right)^{3/4} \tag{5.3.8}$$

and

$$\frac{z}{l_{BU_\infty}} = 0 \tag{5.3.9}$$

None of Ayoub's coflow data are in the BDNF. The author's and Brown's [1984] concentration measurements have given values which are plotted in fig. 5.16. There seems to be a dependency on l_{MeB}/l_{BU_∞}. The theoretical value of C_{b7} as derived in appendix D is 0.102.

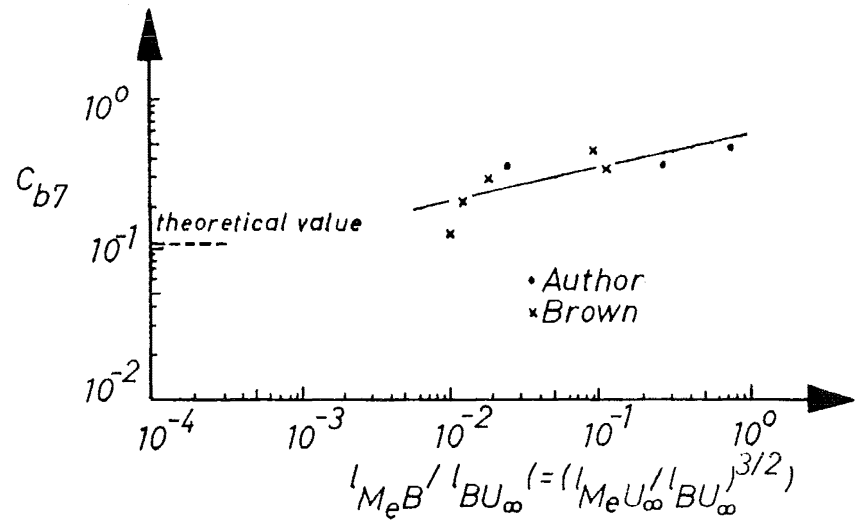

Fig. 5.16. The variation of the coefficient C_{b7} as a function of l_{MeB}/l_{BU_∞}.

The author's and Brown's data are not available over a sufficiently large range to find the value of C_{b8}.

No trajectory data are available for BDNF in coflows so C_{b8} has not been assessed. However, the theoretical value is 0.341.

5.3.4. Buoyancy dominated far field in coflowing jets.

The buoyancy dominated far field in a coflowing jet can be located by using figs. 5.5 and 5.6.
When B≠0 then the buoyant jet in a coflow will always eventually become BDFF.
Because the length scale $l_{BU\infty}$ was chosen for the analysis of BDNF in previous section it will also be used here.
Momentum is not important in this region and the jet is behaving like a buoyant line thermal advected by the ambient flow.
For the same reasons as in the BDNF the dimensionless parameters $S_{CL}\, Q/(U_\infty\, l_{BU\infty}{}^2)$, $x/l_{BU\infty}$, $y/l_{BU\infty}$ and $z/l_{BU\infty}$ are chosen.

Because of the similarity with the flow in an advected line thermal from a continous source the equations which were derived for that type of flow must therefore apply to this case (cfr. eqs. (4.4.18) and (4.4.20)):

The equation for the BDFF in a coflowing jet then become

$$\frac{S_{CL}\, Q}{U_\infty\, l_{BU_\infty}^2} = C_{b9}\left(\frac{y}{l_{BU_\infty}}\right)^2 \tag{5.3.10}$$

$$\frac{y}{l_{BU_\infty}} = C_{b10}\left(\frac{x}{l_{BU_\infty}}\right)^{2/3} \tag{5.3.11}$$

$$\frac{z}{l_{BU_\infty}} = 0 \tag{5.3.12}$$

Ayoub's coflow data indicate $C_{b9} = 0.3 - 0.6$ but do not go far enough to be accurate.
The author's coflow data with $l_{MeU\infty}/l_{BU\infty} = 0$ gave $C_{b9} = 0.41$ and Brown's coflow data have great scatter but have an average of $C_{b9} = 0.45$. There does not appear to be any dependency on $l_{QMe}/l_{BU\infty}$ or $l_{MeB}/l_{BU\infty}$. The theoretical value of C_{b9} as derived in appendix D is 0.41.
As for the value of C_{b10} Ayoub's data do not go far enough.
The author's experiments with $l_{MeB}/l_{BU\infty} = 0$ yield $C_{b10} = 1.39$. Video recordings of a number of jets yield $C_{b10} = 1.1$, see fig. 5.17. Wright found in his experiments with vertical jets that the value of trajectory coefficients like C_{b10} depended on whether they had been

found from concentration measurements or photographs. For small values of $l_{QMe}/l_{BU\infty}$ the coefficients found from concentration measurements were higher than those found from photographs. The single point in fig. 5.17 determined from concentration measurements is indeed somewhat higher than the other points in the figure.

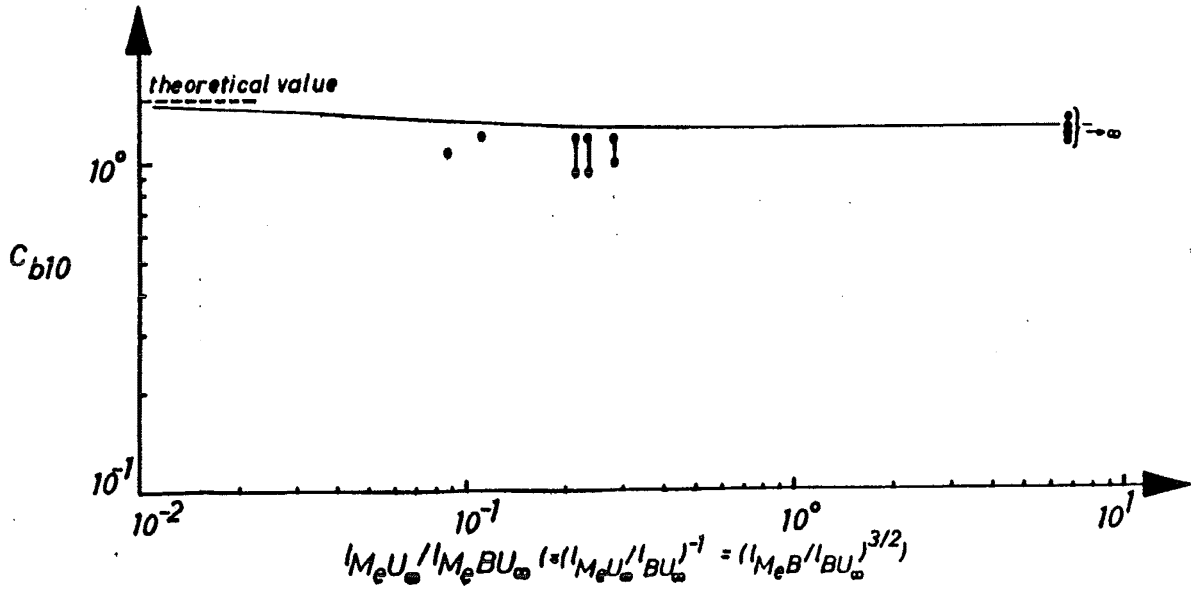

Fig. 5.17. The variation of C_{b10} as a function of $l_{MeU\infty}/l_{MeBU\infty}$.

5.4. Flow regions in crossflowing jets.

5.4.1. Momentum dominated near field in cross flowing jets.

For the MDNF in a crossflowing jet the same type of equations as for a coflowing jet would be expected except that z no longer is constantly equal to 0. The coefficients might be somewhat different from the coflowing case and have therefore been given subscripts 'c' rather than 'b ':

$$\frac{S_{CL}\,Q}{U_\infty\, l_{M_eU_\infty}^2} = C_{c1}\left(\frac{x}{l_{M_eU_\infty}}\right) \tag{5.4.1}$$

$$\frac{y}{l_{BU_\infty}} = C_{c2}\left(\frac{x}{l_{M_eU_\infty}}\right)^3 \tag{5.4.2}$$

Wright's trajectory equation for the MDNF in a vertical jet in a crossflow applies to the case of the trajectory in the XZ-plane for a horizontal jet in a crossflow.

$$\frac{x}{l_{M_e U_\infty}} = C_{c3}\left(\frac{z}{l_{M_e U_\infty}}\right)^{1/2} \tag{5.4.3}$$

The value of C_{c1} as found from Ayoub's [1971] crossflow data are shown as a function of $l_{QMe}/l_{MeU\infty}$ in fig. 5.18.

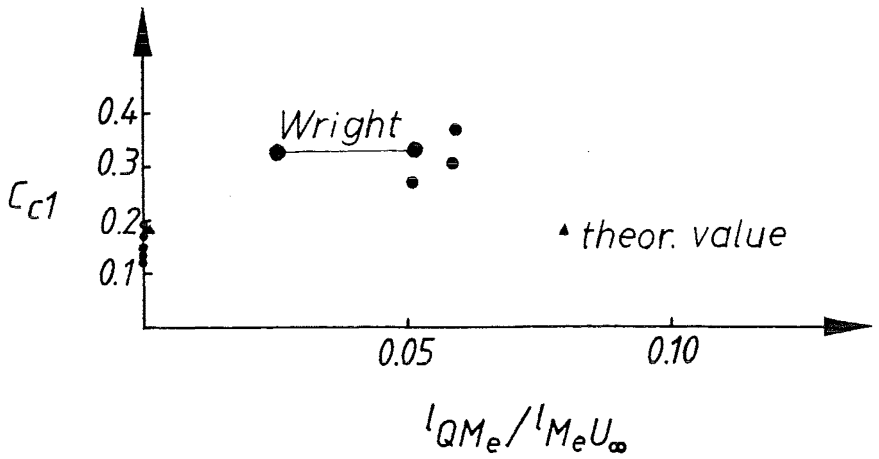

Fig. 5.18. The coefficient C_{c1} as a function of $l_{QMe}/l_{MeU\infty}$.

C_{c1} can be seen to possibly be a function of $l_{QMe}/l_{MeU\infty}$ varying between 0.15 and 0.35 for $0<l_{QMe}/l_{MeU\infty}<0.05$. There were too few points to see if there was any dependence on the values of $l_{MeB}/l_{MeU\infty}$. The theoretical value of C_{c1} as found in appendix D is also shown. Wright found the equivalent coefficient to C_{c1} for vertical jets to bé 0.42 for $0.027<l_{QM}/l_{MB}<0.051$. (NB! His figure 5.20 indicates $C_{c1}\approx0.38$! That value is also given in his 1977 article.) His value is somewhat inaccurate because his data may have been in the transition between MDNF and MDFF ($x/l_{MeU\infty} > 0.5$). The same applies to Ayoub's data. It then seems most reasonable to set C_{c1} constantly equal to 0.185.

The trajectory coefficient C_{c2} was determined from Ayoub's data. There was much scatter and the data were of a poor quality, but a value of $C_{c2} = 0.050$ was indicated. There were not enough data to see whether C_{c2} was a function of $l_{QMe}/l_{MeU\infty}$ or $l_{MeB}/l_{MeU\infty}$. It seems most reasonable to choose the **theoretical value** of C_{c2} which is 0.048. Bühler & Hauenstein found $C_{c2} = 0.05$.

Ayoub's data indicated a value of $C_{c3} = 2.6$. For comparison, Wright's results for the equivalent of C_{c3} for vertical jets in a crossflow, which would be expected to be applicable to

horizontal jets in crossflows also, are shown in fig. 5.19. In the figure both Wright's photographic and concentration measurement data are shown along with Pratte & Baines' [1967] data. The theoretical value of C_{c3} is 3.8. A curve has been drawn through all the data in fig. 5.19.

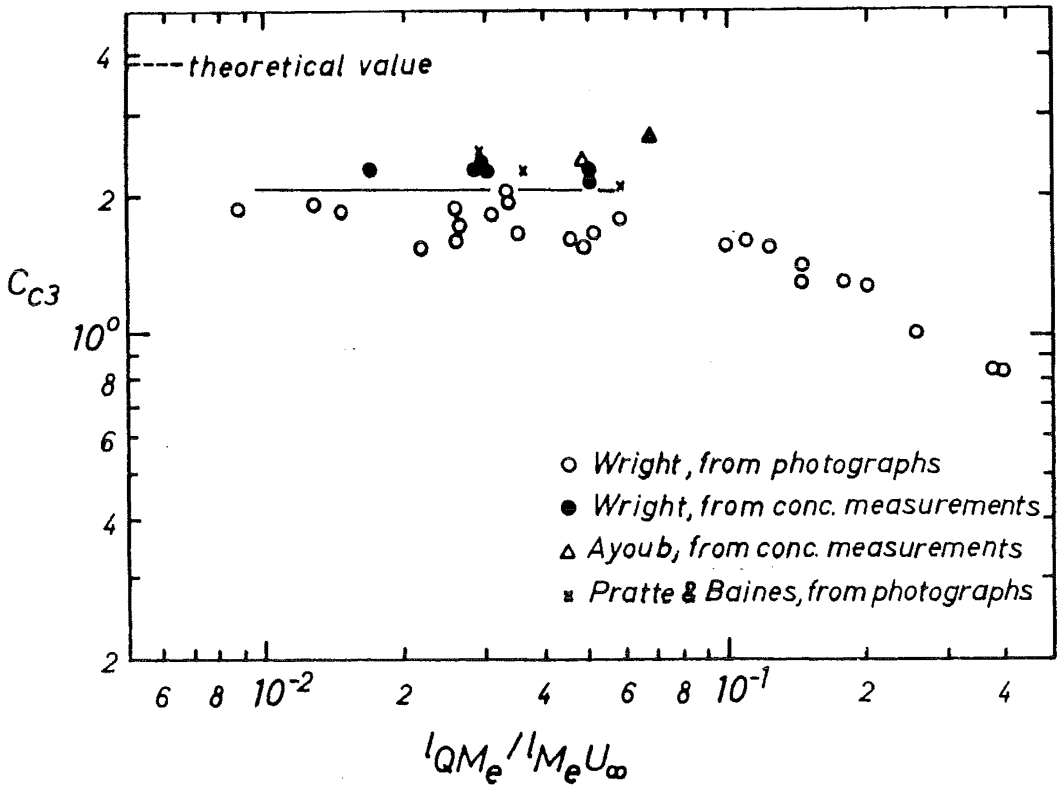

Fig. 5.19. Wright's equivalent to the coefficient C_{c3} with other data.

5.4.2. Momentum dominated far field in crossflowing jets.

For the MDFF region in a crossflowing jet eq. (4.5.18) becomes:

$$\frac{S_{CL}\,Q}{U_\infty\, l^2_{M_eU_\infty}} = C_{c4}\left(\frac{x}{l_{M_eU_\infty}}\right)^2 \qquad (5.4.4)$$

Bühler & Hauenstein found for the trajectory in the YZ-plane (note that y is non-dimensionalised with l_{BU_∞}):

(This has also been derived in appendix B)

$$\frac{y}{l_{BU_\infty}} = C_{c5}\left(\frac{z}{l_{M_eU_\infty}}\right)^{4/3} \tag{5.4.5}$$

And (4.5.19) becomes

$$\frac{x}{l_{M_eU_\infty}} = C_{c6}\left(\frac{z}{l_{M_eU_\infty}}\right)^{1/3} \tag{5.4.6}$$

The variation of C_{c4} as found from Ayoub's data is shown in fig. 5.20. There seems to be a slight dependency on $l_{QMe}/l_{MeU\infty}$. Wright found for vertical jets that the coefficient corresponding to C_{c4} was equal to 0.38 independent of $l_{QMe}/l_{MeU\infty}$ within the range of his data ($0.027 < l_{QM}/l_{MU\infty} < 0.25$). (NB! His figure 5.20 indicates C_{c4}=0.14! This value was also given in his 1977 article.) The theoretical value of C_{c4} is 0.41. Both the value of C_{c4} based on Ayoub's and Wright's data may be inaccurate as there are only data at small distances from the transition from MDNF to MDFF in both cases (0.5 $l_{MeU\infty}$ to 3 $l_{MeU\infty}$).

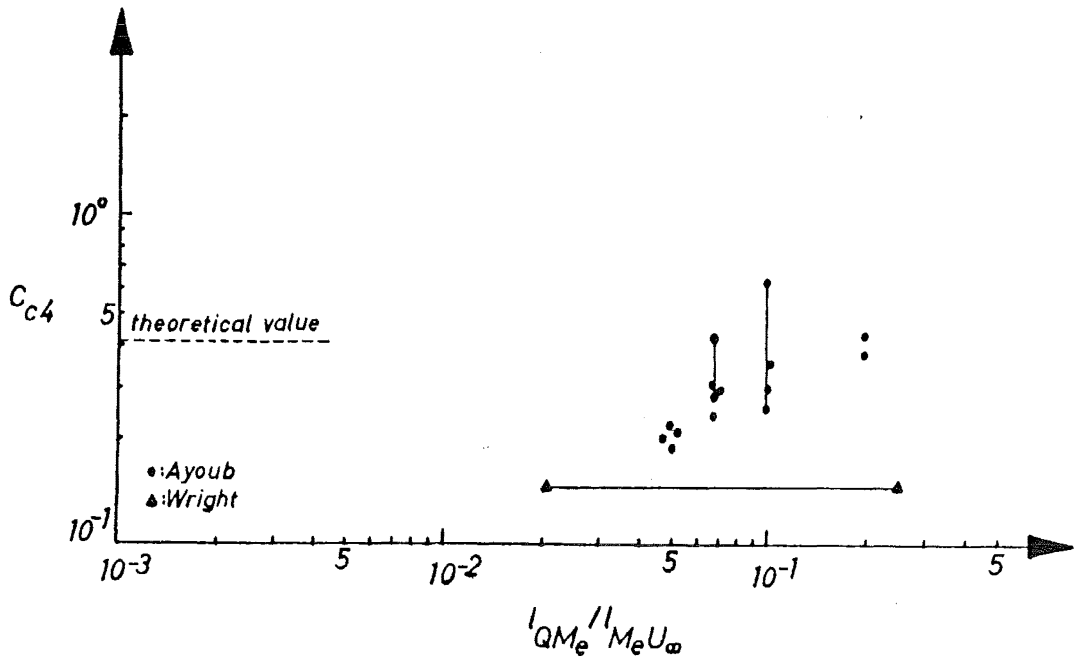

Fig. 5.20 The coefficient C_{c4} as a function of $l_{QMe}/l_{MeU\infty}$.

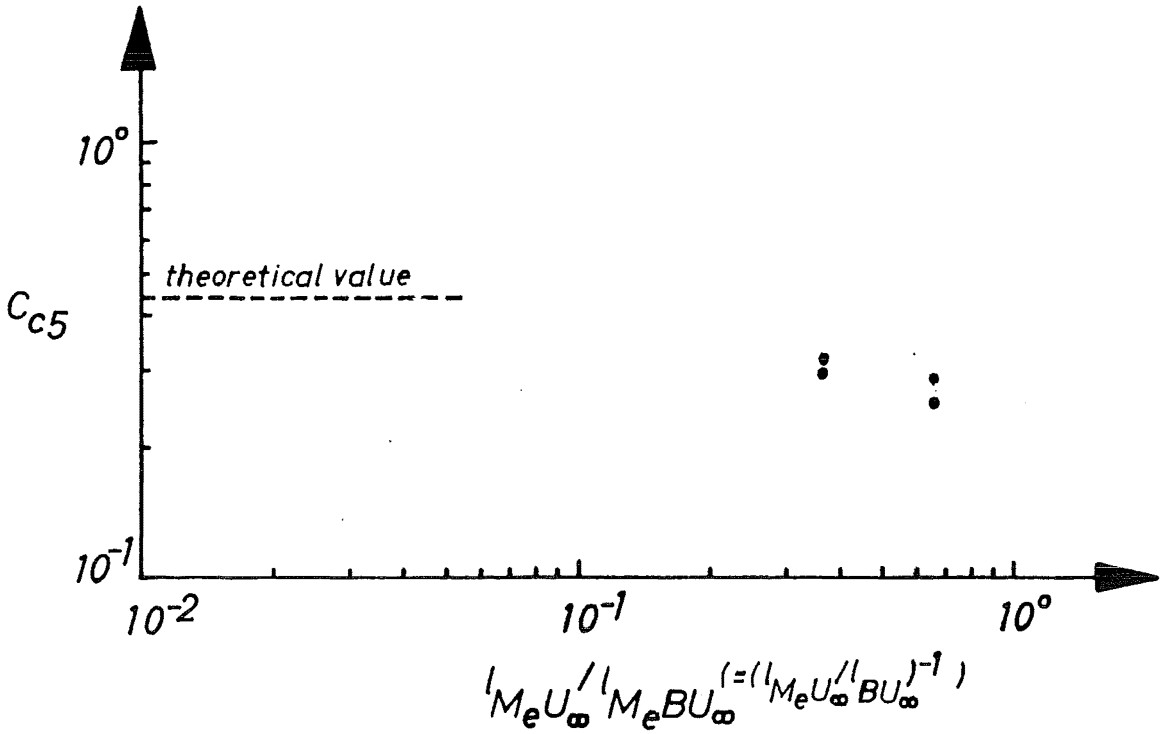

Fig. 5.21. The variation of C_{c5} as a function of $l_{MeU\infty}/l_{MeBU\infty}$.

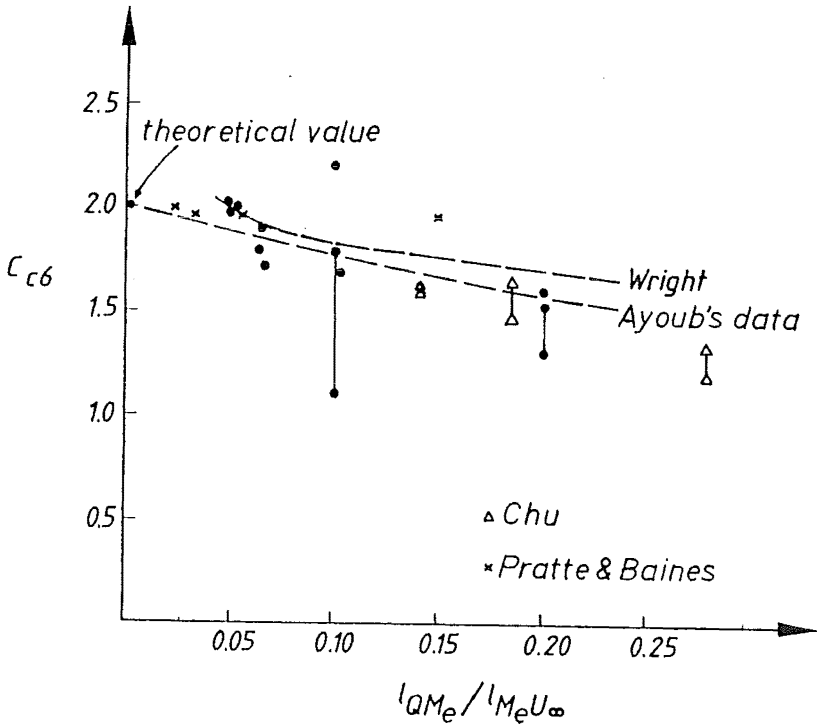

Fig. 5.22. The coefficient C_{c6} as a function of $l_{QMe}/l_{MeU\infty}$ and compared with Wright's equivalent coefficient and other data.

Bühler & Hauenstein used $C_{c5} \approx 0.26$. Ayoub's data were too inaccurate to determine C_{c5}

from. The variation of C_{c5} as found from Chu's [1975] data is shown in fig. 5.21. The theoretical value of C_{c5} is 0.44.

The values of C_{c6} as found from Ayoub's data are shown in fig. 5.22. Wright's , Pratte & Baines' [1967] and Chu's [1975] values have been shown for comparison and as expected there is very little difference. A theoretically derived value of C_{c6}=2.0 has also been included and the curves have been extended to include this point.

5.4.3.Buoyancy dominated near field in crossflowing jets.

For the BDNF in a crossflow the equations are similar to the equations for the BDNF in coflows just with a change from x to z and z is no longer equal to zero:

$$\frac{S_{CL}\,Q}{U_\infty l_{BU_\infty}^2} = C_{c7}\left(\frac{y}{l_{BU_\infty}}\right)^{5/3} \tag{5.4.7}$$

Equation (5.3.8) also applies, just with a change from x to z:

$$\frac{y}{l_{BU_\infty}} = C_{c8}\left(\frac{z}{l_{BU_\infty}}\right)^{3/4} \tag{5.4.8}$$

The similarity with a pure plume finally gives us:

$$\frac{x}{l_{BU_\infty}} = \frac{x_{max}}{l_{BU_\infty}} \tag{5.4.9}$$

(Cfr. also section 5.2).

Ayoub's data for crossflows are only in the momentum dominated regimes.

The data compiled by Lee & Neville-Jones [1987] give a value of 0.31 for C_{c7}. The data are from in situ measurements above ocean outfalls in a crossflow. There was therefore ambient turbulence present. They did not find C_{c7} to depend on l_{MB}/l_{QM} but they did not investigate

any dependence on $l_{MB}/l_{BU\infty}$. Wright [1977] found that for vertical buoyant jets in a crossflow the coefficient corresponding to C_{c7} was independent of $l_{QM}/l_{BU\infty}$ and $l_{MB}/l_{BU\infty}$ within the range of his parameters, $0.003<l_{QM}/l_{BU\infty}<0.014$, and was equal to 0.42. (NB! His figure 5.46 5.21 rather indicates a value of 0.22 and this value has also been used in his 1977 article). In fig. 5.23 Wright's value has been compared with Lee & Neville-Jones' value. The theoretical value of C_{c7} as derived in appendix D is also shown.

Ayoub had no data in the BDNF region of a crossflow.

Wright found for vertical jets that the coefficient equivalent to C_{c8} was a function of $l_{QM}/l_{BU\infty}$ with an average value of 1.3-1.8. His data have been re-plotted in fig. 5.24 as a function of l_{QMe}/l_{MeB}. In this figure the theoretical value of C_{c8} is also shown.

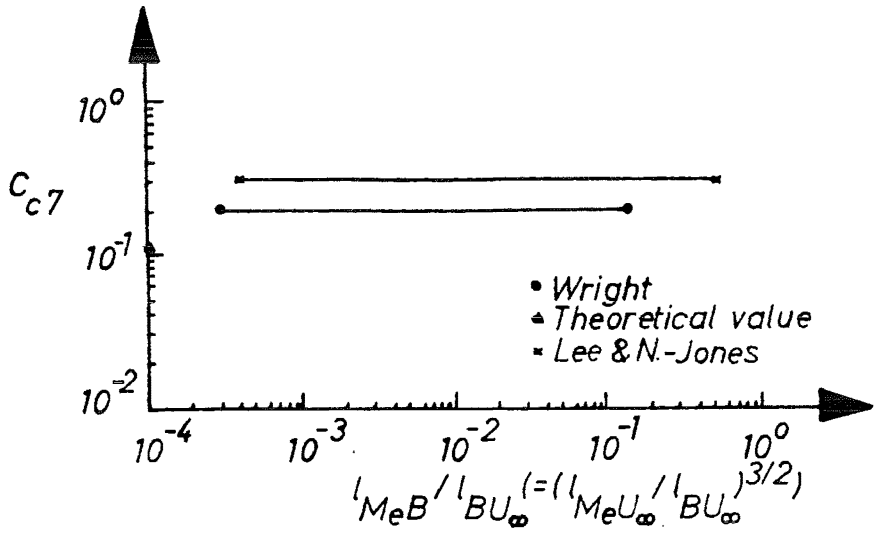

Fig. 5.23. The variation of C_{c7} as a function of $l_{MeB}/l_{BU\infty}$.

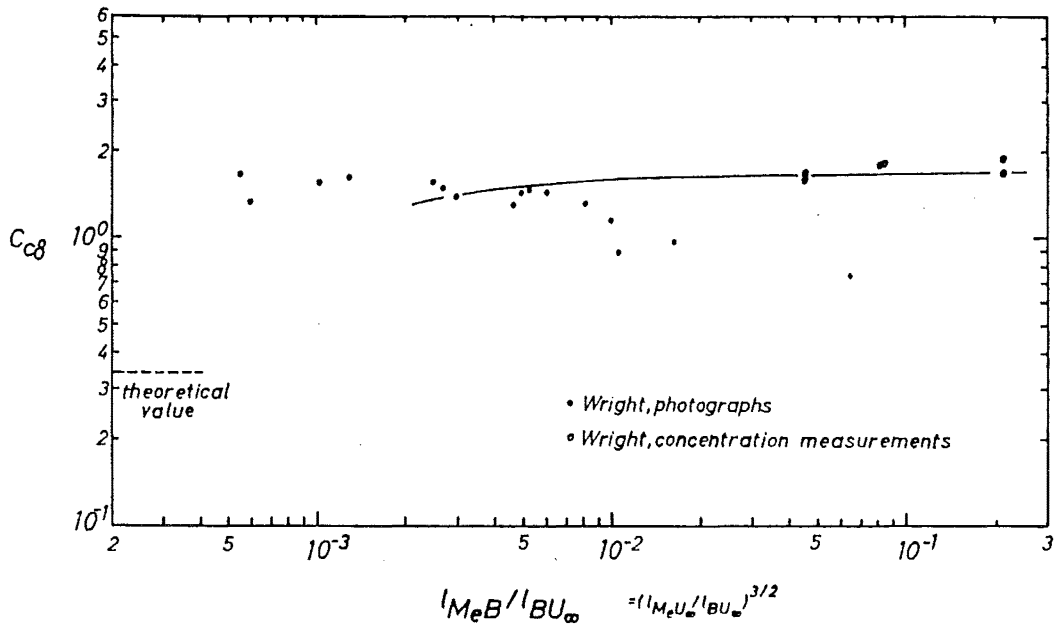

Fig. 5.24. Wright's equivalent coefficient to C_{c8}.

It seems reasonable to assume that x_{max} has approximately the same value as for a buoyant jet in still ambient, i.e. ≈ 8.4 l_{MeB}.

5.4.4. Buoyancy dominated far field in crossflowing jets.

For a jet in a crossflow we will expect equations similar to eqs. (5.3.10) and (5.3.11) because the initial momentum is negligible (however, x in eq. (5.3.11) is exchanged with z) :

$$\frac{S_{CL}\,Q}{U_\infty l_{BU_\infty}^2} = C_{c9}\left(\frac{y}{l_{BU_\infty}}\right)^2 \tag{5.4.10}$$

$$\frac{y}{l_{BU_\infty}} = C_{c10}\left(\frac{z}{l_{BU_\infty}}\right)^{2/3} \tag{5.4.11}$$

Further, just like for the BDNF in a crossflow we must have

$$\frac{x}{l_{BU_\infty}} = \frac{x_{max}}{l_{BU_\infty}} \tag{5.4.12}$$

The reason for x being limited is that the initial momentum is negligible in this region (cfr. also section 5.2).

Ayoub's data do not go into the BDFF regime.

Lee & Neville-Jones used data from real ocean outfalls plus laboratory data from Wallingford Hydraulic Research Station (HRS [1977]) to assess the value of C_{c9} and C_{c10}. Ambient turbulence may have affected the results. They found $C_{c9} \approx 0.32$ for all data except one outfall and the laboratory results which gave as a result $C_{c9} \approx 1.12$. It is suggested that the difference between the results may be caused by the different measuring methods and that C_{c9}=0.32 probably is better. They found that within the experimental range (1<Fr<10) there was no dependence of C_{c9} on l_{MB}/l_{QM}.

Wright found for his experiments with vertical jets in BDFF that the equivalent coefficient to C_{c9} had a value of 0.41 and did not seem to depend on l_{QM}/l_{BU_∞}, at least within his

experimental range ($0.03<l_{QM}/l_{BU\infty}<28.0$, $0.5<l_{MU\infty}/l_{BU\infty}<112$). In his 1977 article he gives the value $3.3^{-1} = 0.30$. The theoretical value of C_{c9} is 0.41.

Ayoub's crossflow data do not go far enough to determine C_{c10}. Lee & Neville-Jones found $C_{c10} = 0.94$. Wright's coefficient equivalent to C_{c10} is shown in fig. 5.25. Bühler found $C_{c10} = 1.01$. The theoretical value of C_{c10} is 1.59.

No data were available to determine x_{max} but it seems reasonable to assume $x_{max}\approx 8.4\ l_{MeB}$ like for the still ambient case.

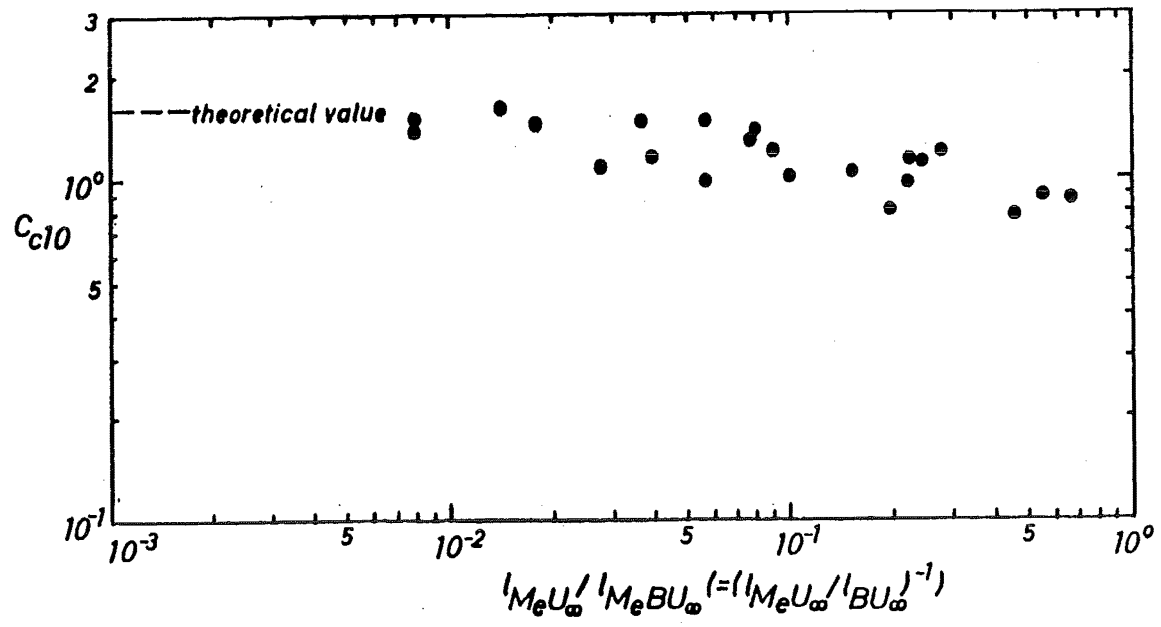

Fig. 5.25. Wright's equivalent to the coefficient C_{c10}.

5.5. Flow regions in counterflowing jets.

5.5.1. Momentum dominated near field in counterflowing jets.

Similar equations to (5.3.1)-(5.3.2) would be expected for the MDNF in counterflowing jets. The coefficients have been given the subscript 'd ' :

$$\frac{s_{CL}\,Q}{U_\infty\, l^2_{M_eU_\infty}} = C_{d1}\left(\frac{x}{l_{M_eU_\infty}}\right)$$

(5.5.1)

$$\frac{y}{l_{BU_\infty}} = C_{d2}\left(\frac{x}{l_{M_eU_\infty}}\right)^3 \qquad (5.5.2)$$

$$\frac{z}{l_{M_eU_\infty}} = 0 \qquad (5.5.3)$$

No data are available for the MDNF in a counterflowing jet so the values of C_{d1} and C_{d2} can not be assessed. However, the theoretical values as derived in appendix D are 0.105 and 0.048 respectively.

5.5.2. Momentum dominated far field in counterflowing jets.

Equations (5.3.4) - (5.3.5) for the MDFF in a coflow also apply to the MDFF in counterflow if x is replaced by -x:

$$\frac{S_{CL}Q}{U_\infty l^2_{M_eU_\infty}} = C_{d4}\left(\frac{-x}{l_{M_eU_\infty}}\right)^{2/3} \qquad (5.5.4)$$

$$\frac{y}{l_{BU_\infty}} = C_{d5}\left(\frac{-x}{l_{M_eU_\infty}}\right)^{4/3} \qquad (5.5.5)$$

$$\frac{z}{l_{M_eU_\infty}} = 0 \qquad (5.5.6)$$

No data are available for the MDFF in a counterflowing jet and the coefficients C_{d4} and C_{d5} can therefore not be determined. However, the theoretical values as derived in appendix D are 1.00 and 1.08 respectively.

5.5.3. Buoyancy dominated near field in counterflowing jets.

In the buoyancy dominated regions the behaviour of the jets does not depend on the initial

direction of discharge. Eqs. (5.3.7)-(5.3.9) for BDNF in coflows can therefore be expected to apply with a change of sign for x:

$$\frac{S_{CL}\,Q}{U_\infty l_{BU_\infty}^2} = C_{d7}\left(\frac{y}{l_{BU_\infty}}\right)^{5/3} \tag{5.5.7}$$

$$\frac{y}{l_{BU_\infty}} = C_{d8}\left(\frac{-x}{l_{BU_\infty}}\right)^{3/4} \tag{5.5.8}$$

$$\frac{z}{l_{BU_\infty}} = 0 \tag{5.5.9}$$

Brown's [1984] dilution data for counterflowing jets produced values of C_{d7} as shown in fig. 5.26. There was only one point per experiment so in order to assess C_{d7} in each case it was necessary to fit a line on log/log paper with slope 5/3 through each point and the intersection of the line with $y/l_{BU_\infty} = 1$ was the value of C_{d7}. This approach could not be expected to be very accurate and there is much scatter in fig. 5.26. The average value was $C_{d7} \approx 0.45$. The theoretical value was 0.102. It was decided to let C_{d7} vary like C_{b7}.

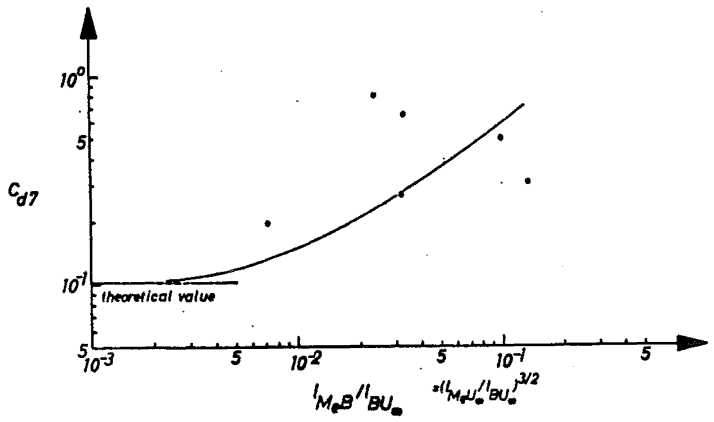

Fig. 5.26. The coefficient C_{d7} as a function of l_{MeB}/l_{BU_∞} .

There are not trajectory data available for a sufficiently long range to assess the value of the coefficient C_{d8}. The theoretical value of C_{d8} is 0.341.

5.5.4. Buoyancy dominated far field in counterflowing jets.

For the BDFF in counterflows, similar equations to eqs. (5.3.10)-(5.3.12) can be expected, just with a change of sign for x:

$$\frac{S_{CL}\,Q}{U_\infty l_{BU_\infty}^2} = C_{d9}\left(\frac{y}{l_{BU_\infty}}\right)^2 \tag{5.5.10}$$

$$\frac{y}{l_{BU_\infty}} = C_{d10}\left(\frac{x}{l_{BU_\infty}}\right)^{2/3} \tag{5.5.11}$$

$$\frac{z}{l_{BU_\infty}} = 0 \tag{5.5.12}$$

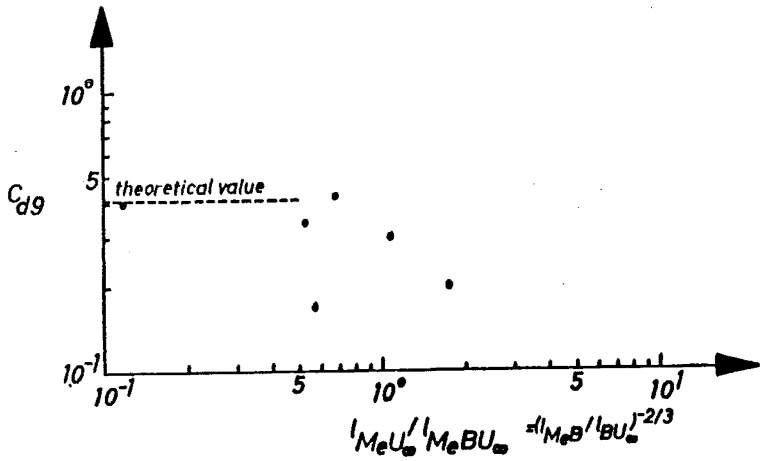

Fig. 5.27. The coefficient C_{d9} as a function of l_{MeB}/l_{BU_∞} as found from Brown's data.

Brown's counterflow data suggest a value C_{d9}=0.31 independent of l_{QMe}/l_{BU_∞} and l_{MeB}/l_{BU_∞}, see fig. 5.27. The theoretical value of C_{d9} is 0.41. Because of the great scatter it is decided to let C_{d9} have the constant theoretical value.

No data are available to assess the value of C_{d10}. The theoretical value of C_{d10} is 1.59.

5.6. Summary of dimensional analysis.

To round off the dimensional analysis in this and previous chapter all the results are summarised in fig. 5.28 below.

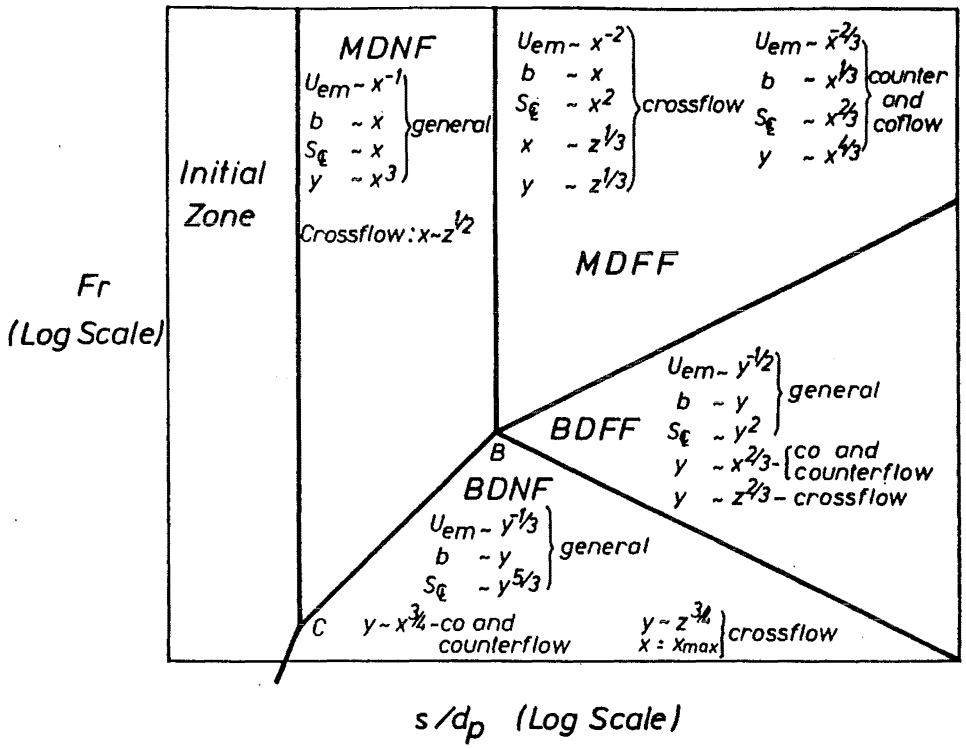

Fig. 5.28. A summary of all results from the dimensional analysis in chapters 4 and 5.

5.7. Summary of the values of various coefficients.

Below in table 5.3 is given a summary of the equations that have been presented in this chapter.

In table 5.4 the theoretical values of the coefficients as calculated in appendix D are listed. These values correspond to infinitely long regions. The corresponding experimentally determined values are given in brackets.

	Still ambient	Coflow	Crossflow	Counterflow
MDNF	$\frac{S_{CL}Q}{M^{1/2}l_{MB}} = C_{a1}\frac{x}{l_{MB}}$ $\frac{y}{l_{MB}} = C_{a2}\left(\frac{x}{l_{MB}}\right)^3$	$\frac{S_{CL}Q}{U_\infty^2 l_{M_eU_\infty}} = C_{b1}\left(\frac{x}{l_{M_eU_\infty}}\right)$ $\frac{y}{l_{BU_\infty}} = C_{b2}\left(\frac{x}{l_{M_eU_\infty}}\right)^3$ $\frac{z}{l_{M_eU_\infty}} = 0$	$\frac{S_{CL}Q}{U_\infty^2 l_{M_eU_\infty}} = C_{c1}\left(\frac{x}{l_{M_eU_\infty}}\right)$ $\frac{y}{l_{BU_\infty}} = C_{c2}\left(\frac{x}{l_{M_eU_\infty}}\right)^3$ $\frac{x}{l_{M_eU_\infty}} = C_{c3}\left(\frac{z}{l_{M_eU_\infty}}\right)^{1/2}$	$\frac{S_{CL}Q}{U_\infty^2 l_{M_eU_\infty}} = C_{d1}\left(\frac{x}{l_{M_eU_\infty}}\right)$ $\frac{y}{l_{BU_\infty}} = C_{d2}\left(\frac{x}{l_{M_eU_\infty}}\right)^3$ $\frac{z}{l_{M_eU_\infty}} = 0$
MDFF		$\frac{S_{CL}Q}{U_\infty^2 l_{M_eU_\infty}} = C_{b4}\left(\frac{x}{l_{M_eU_\infty}}\right)^{2/3}$ $\frac{y}{l_{BU_\infty}} = C_{b5}\left(\frac{x}{l_{M_eU_\infty}}\right)^{4/3}$ $\frac{z}{l_{M_eU_\infty}} = 0$	$\frac{S_{CL}Q}{U_\infty^2 l_{M_eU_\infty}} = C_{c4}\left(\frac{x}{l_{M_eU_\infty}}\right)^2$ $\frac{y}{l_{BU_\infty}} = C_{c5}\left(\frac{z}{l_{M_eU_\infty}}\right)^{4/3}$ $\frac{x}{l_{M_eU_\infty}} = C_{c6}\left(\frac{z}{l_{M_eU_\infty}}\right)^{1/3}$	$\frac{S_{CL}Q}{U_\infty^2 l_{M_eU_\infty}} = C_{d4}\left(\frac{-x}{l_{M_eU_\infty}}\right)^{2/3}$ $\frac{y}{l_{BU_\infty}} = C_{d5}\left(\frac{-x}{l_{M_eU_\infty}}\right)^{4/3}$ $\frac{z}{l_{M_eU_\infty}} = 0$
BDNF	$\frac{S_{CL}Q}{l_{MB}M^{1/2}} = C_{a7}\left(\frac{y}{l_{MB}}\right)^{5/3}$ $\frac{x}{l_{MB}} \rightarrow \frac{x_{max}}{l_{MB}}$	$\frac{S_{CL}Q}{U_\infty^2 l_{BU_\infty}^2} = C_{b7}\left(\frac{y}{l_{BU_\infty}}\right)^{5/3}$ $\frac{y}{l_{BU_\infty}} = C_{b8}\left(\frac{x}{l_{BU_\infty}}\right)^{3/4}$ $\frac{z}{l_{BU_\infty}} = 0$	$\frac{S_{CL}Q}{U_\infty^2 l_{BU_\infty}^2} = C_{c7}\left(\frac{y}{l_{BU_\infty}}\right)^{5/3}$ $\frac{y}{l_{BU_\infty}} = C_{c8}\left(\frac{z}{l_{BU_\infty}}\right)^{3/4}$ $\frac{x}{l_{BU_\infty}} = \frac{x_{max}}{l_{BU_\infty}}$	$\frac{S_{CL}Q}{U_\infty^2 l_{BU_\infty}^2} = C_{d7}\left(\frac{y}{l_{BU_\infty}}\right)^{5/3}$ $\frac{y}{l_{BU_\infty}} = C_{d8}\left(\frac{-x}{l_{BU_\infty}}\right)^{3/4}$ $\frac{z}{l_{BU_\infty}} = 0$
BDFF		$\frac{S_{CL}Q}{U_\infty^2 l_{BU_\infty}^2} = C_{b9}\left(\frac{y}{l_{BU_\infty}}\right)^2$ $\frac{y}{l_{BU_\infty}} = C_{b10}\left(\frac{x}{l_{BU_\infty}}\right)^{2/3}$ $\frac{z}{l_{BU_\infty}} = 0$	$\frac{S_{CL}Q}{U_\infty^2 l_{BU_\infty}^2} = C_{c9}\left(\frac{y}{l_{BU_\infty}}\right)^2$ $\frac{y}{l_{BU_\infty}} = C_{c10}\left(\frac{z}{l_{BU_\infty}}\right)^{2/3}$ $\frac{x}{l_{BU_\infty}} = \frac{x_{max}}{l_{BU_\infty}}$	$\frac{S_{CL}Q}{U_\infty^2 l_{BU_\infty}^2} = C_{d9}\left(\frac{y}{l_{BU_\infty}}\right)^2$ $\frac{y}{l_{BU_\infty}} = C_{d10}\left(\frac{-x}{l_{BU_\infty}}\right)^{2/3}$ $\frac{z}{l_{BU_\infty}} = 0$

Table 5.4

	Still ambient	Coflow	Crossflow	Counterflow
	C_{a1}=0.185 [0.14-0.17]	C_{b1}=0.185 [0.18]	C_{c1}=0.185 [0.18?]	C_{d1}=0.185 [?]
MDNF	C_{a2}=0.048 [0.05?]	C_{b2}=0.048 [?]	C_{c2}=0.048 [0.05?]	C_{d2}=0.048 [?]
			C_{c3}=3.83 [2.4]	
		C_{b4}=1.00 [0.6-0.9]	C_{c4}=0.41 [0.15]	C_{d4}=1.00 [?]
MDFF		C_{b5}=1.08 [?]	C_{c5}^{*}=0.44 [?]	C_{d5}=1.08 [?]
			C_{c6}^{*}=2.0 [2.4]	
	C_{a7}=0.102 [0.091]	C_{b7}=0.102 [?]	C_{c7}=0.102 [?]	C_{d7}=0.102 [?]
BDNF		C_{b8}=0.341 [?]	C_{c8}=0.341 [2.3]	C_{d8}=0.341 [?]
		C_{b9}=0.411 [0.41]	C_{c9}=0.41 [0.41?]	C_{d9}=0.41 [?]
BDFF		C_{b10}^{*}=1.59 [1.37]	C_{c10}^{*}=1.59 [1.5]	C_{d10}^{*}=1.59 [?]

Note: the unknown cross sectional constant I_v was found by fitting the experimental values of the constants C_{c6} , C_{b9} and C_{b10} which were all of good quality. The theoretical value of the constants marked with an asterix was found using the value of I_v=4.2.

Table 5.4.

5.8. General plots.

The data that have been analysed in the previous sections have produced results which can now be used to produce charts which describe the dilution and trajectory for the general case of a horizontal buoyant jet in a still ambient , a co-, cross- or counterflow.

These charts are in principle similar to those presented by Wright for vertical jets in perpendicular crossflow and by Bühler & Hauenstein for the trajectories for horizontal jets in a perpendicular crossflow.

As it can be seen from table **5.3** the dilution equations are given either as a function of $x/l_{MeU\infty}$ or $y/l_{BU\infty}$ as the overall variable.

It is most practical to choose $y/l_{BU\infty}$ because $x/l_{MeU\infty}$ is upwards limited in the buoyancy dominated part of the crossflows.

The MDNF and MDFF dilution equations then have to be rewritten as function of $y/l_{BU\infty}$ by using the trajectory equations:

Momentum dominated still ambient : $$\frac{S_{CL}\,Q}{l_{MB}\,M^{1/2}} = C_{a1}\,C_{a2}^{-1/3}\left(\frac{y}{l_{MB}}\right)^{1/3}$$

MDNF coflow : $$\frac{S_{CL}\,Q}{U_\infty\,l_{BU_\infty}^2} = \left(\frac{l_{BU_\infty}}{l_{M_eU_\infty}}\right)^{-2} C_{b1}\,C_{b2}^{-1/3}\left(\frac{y}{l_{BU_\infty}}\right)^{1/3}$$

MDNF crossflow : $$\frac{S_{CL}\,Q}{U_\infty\,l_{BU_\infty}^2} = \left(\frac{l_{BU_\infty}}{l_{M_eU_\infty}}\right)^{-2} C_{c1}\,C_{c2}^{-1/3}\left(\frac{y}{l_{BU_\infty}}\right)^{1/3}$$

MDNF counterflow : $$\frac{S_{CL}\,Q}{U_\infty\,l_{BU_\infty}^2} = \left(\frac{l_{BU_\infty}}{l_{M_eU_\infty}}\right)^{-2} C_{d1}\,C_{d2}^{-1/3}\left(\frac{y}{l_{BU_\infty}}\right)^{1/3}$$

MDFF coflow : $$\frac{S_{CL}\,Q}{U_\infty\,l_{BU_\infty}^2} = \left(\frac{l_{BU_\infty}}{l_{M_eU_\infty}}\right)^{-2} C_{b4}\,C_{b5}^{-1/2}\left(\frac{y}{l_{BU_\infty}}\right)^{1/2}$$

MDFF crossflow : $$\frac{S_{CL}\,Q}{U_\infty\,l_{BU_\infty}^2} = \left(\frac{l_{BU_\infty}}{l_{M_eU_\infty}}\right)^{-2} \frac{C_{c4}\,C_{c6}^2}{C_{c5}^{1/2}}\left(\frac{y}{l_{BU_\infty}}\right)^{1/2}$$

MDFF counterflow : $$\frac{S_{CL}\,Q}{U_\infty\,l_{BU_\infty}^2} = \left(\frac{l_{BU_\infty}}{l_{M_eU_\infty}}\right)^{-2} C_{d4}\,C_{d5}^{-1/2}\left(\frac{y}{l_{BU_\infty}}\right)^{1/2}$$

In the following pages charts are presented for dilution and trajectories for horizontal buoyant jets in still ambient, coflows, crossflows and counterflows , figs. 5.30-5.34.

Note that it is not necessary to know what regions exist in a given jet before using the charts. The charts automatically show where the transitions occour in a jet.
The trajectory charts show the flow as going directly from one region to another. As mentioned earlier the transition from one region to another takes place over a certain distance and the length scales are only an indication of the order of magnitude from the port in which the transition is occurring.

The following values of the constants have been used: (cfr. table 5.3 and table 5.4.)

$C_{a1} = C_{b1} = C_{c1} = C_{d1} = 0.185$

$C_{a2} = C_{b2} = C_{c2} = C_{d2} = 0.048$

C_{c3} : function of l_{QMe}/l_{MeB} , see fig. 5.19

$C_{b4} = C_{d4}$: function of $l_{MeU\infty}/l_{MeBU\infty}$, see fig. 5.14

C_{c4} : function of $l_{QMe}/l_{MeU\infty}$, see fig. 5.20

$C_{b5} = C_{d5}$: a function of $l_{MeU\infty}/l_{MeBU\infty}$, see fig. 5.15

C_{c5} : a function of $l_{MeU\infty}/l_{MeBU\infty}$, see fig. 5.21

C_{c6} : function of $l_{QMe}/l_{MeU\infty}$, see fig. 5.22

$C_{a7} = 0.102$

$C_{b7} = C_{d7}$: function of $l_{MeB}/l_{BU\infty}$, see fig. 5.16.

C_{c7} : function of $l_{MeB}/l_{BU\infty}$, see fig. 5.23 and 5.16.

$x_{max}/l_{MeB} = 8.4$

$C_{b8} = C_{c8} = C_{d8}$: function of $l_{MeB}/l_{BU\infty}$, see fig. 5.24.

$C_{b9} = C_{c9} = C_{d9} = 0.41$

$C_{b10} = C_{c10} = C_{d10}$: function of $l_{MeU\infty}/l_{MeBU\infty}$, see fig. 5.17.

A discussion of the theoretical values is given in appendix D. Some of the theoretical values of the constants can not be calculated because they depend on cross sectional constants from the equations in chapter 6, which are not known. The experimental values for the coefficients which have been determined in this chapter have instead been used to determine the values of these cross sectional constants.
The values of the constants as chosen above could have been further adjusted: in appendix D the relationships beween some of the constants as derived theoretically are given. Furthermore, the condition that for $l_{MeU\infty}/l_{BU\infty} \approx 1$
a MDNF goes directly into a BDFF (see e.g. fig. 5.5)could have been used to derive further

relationships between the experimentally found constants . However, it was judged that this would not increase the accuracy of the charts noticeably and it was therefore not done.
The charts which have been produced in this chapter give good predictions of dilutions and trajectories for jets which are within a region (i.e. not in a transition between two regions).

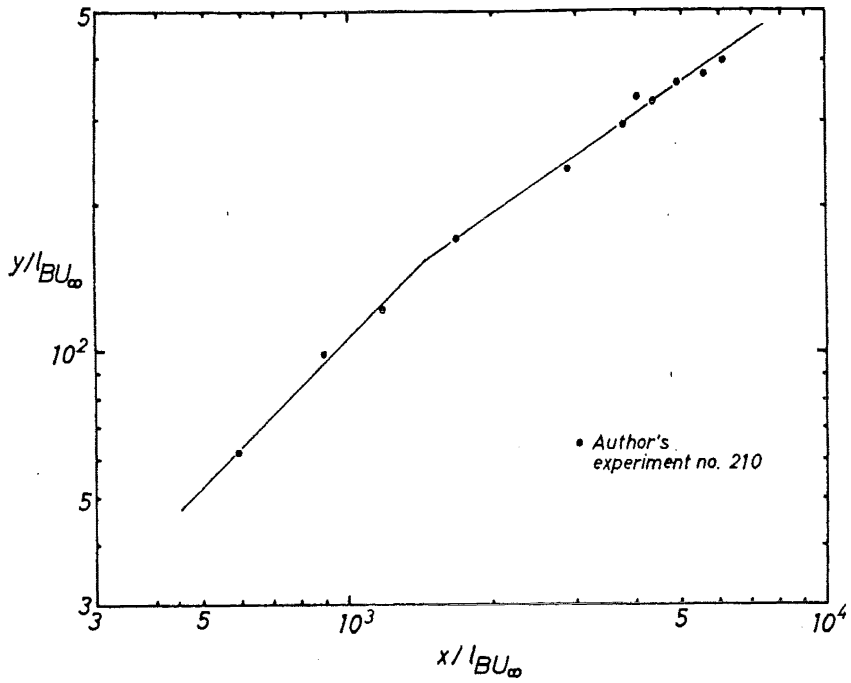

Fig. 5.29. The transition region MDFF-BDFF for a trajectory in a coflow.

Fig. 5.29 is a figure which shows a transition region MDFF-BDFF in a coflowing jet. The data follow the asymptotic lines of the MDFF and BDFF closely even in the transition. In contrast fig. 6.10 shows the dilution curve for a transition MDNF-MDFF (coflow) where the data deviate up to 25% from the asymptotic solution in the transition. In figs. 6.13 and 6.14 trajectory and dilution data for a jet in still ambient can be seen to deviate up to 100% from the asymtotic solutions in the transition. It can thus be concluded that the asymptotic solutions in some cases describe even the flow in the transitions well whereas they in other cases deviate considerably from data in the transition regions.

To get a better understanding of the transitions it is necessary to formulate a mathematical model and study the solutions in the transitions. An attempt to do this has been made in next chapter.

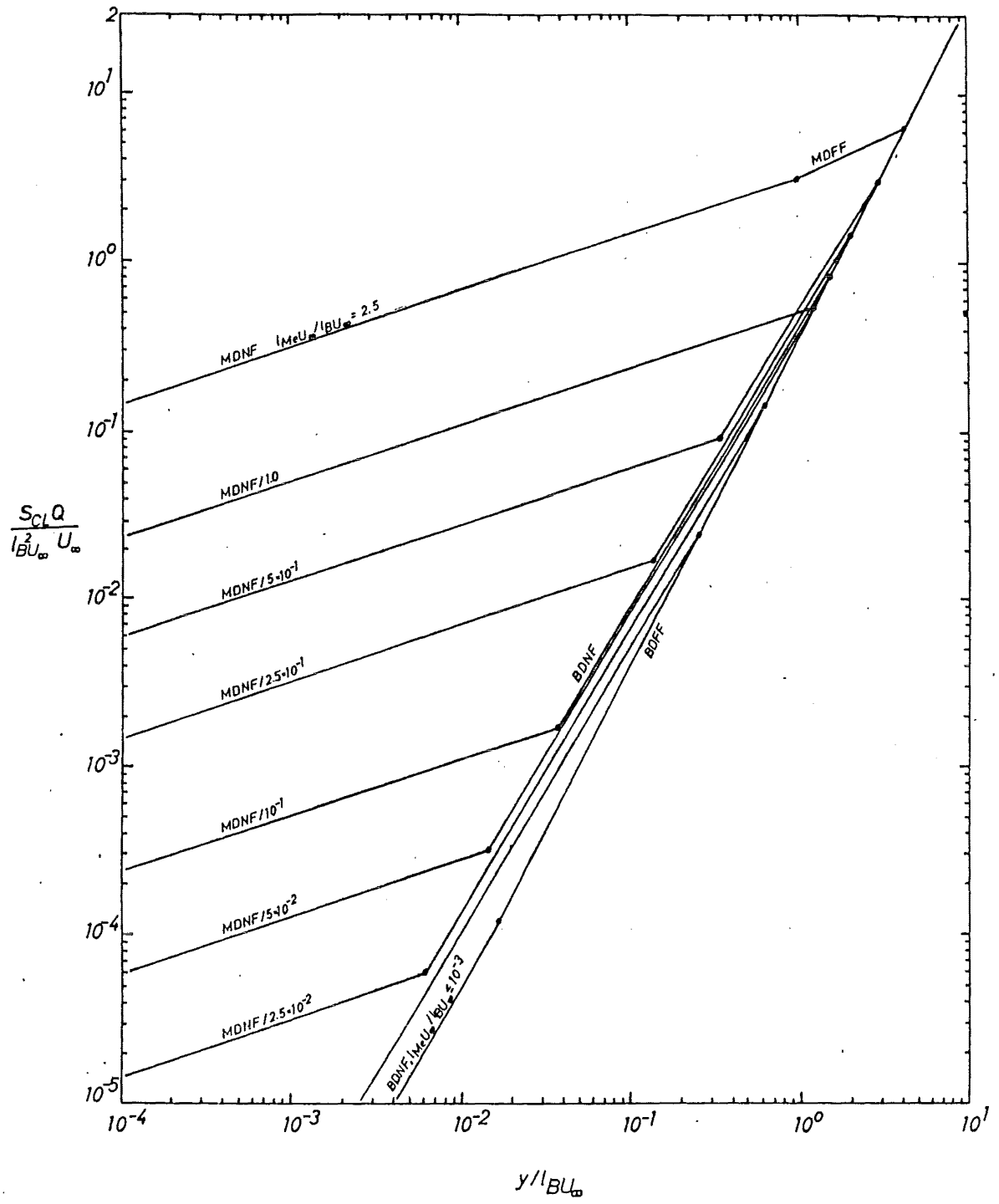

Fig. 5.30. Dilution chart for coflow.

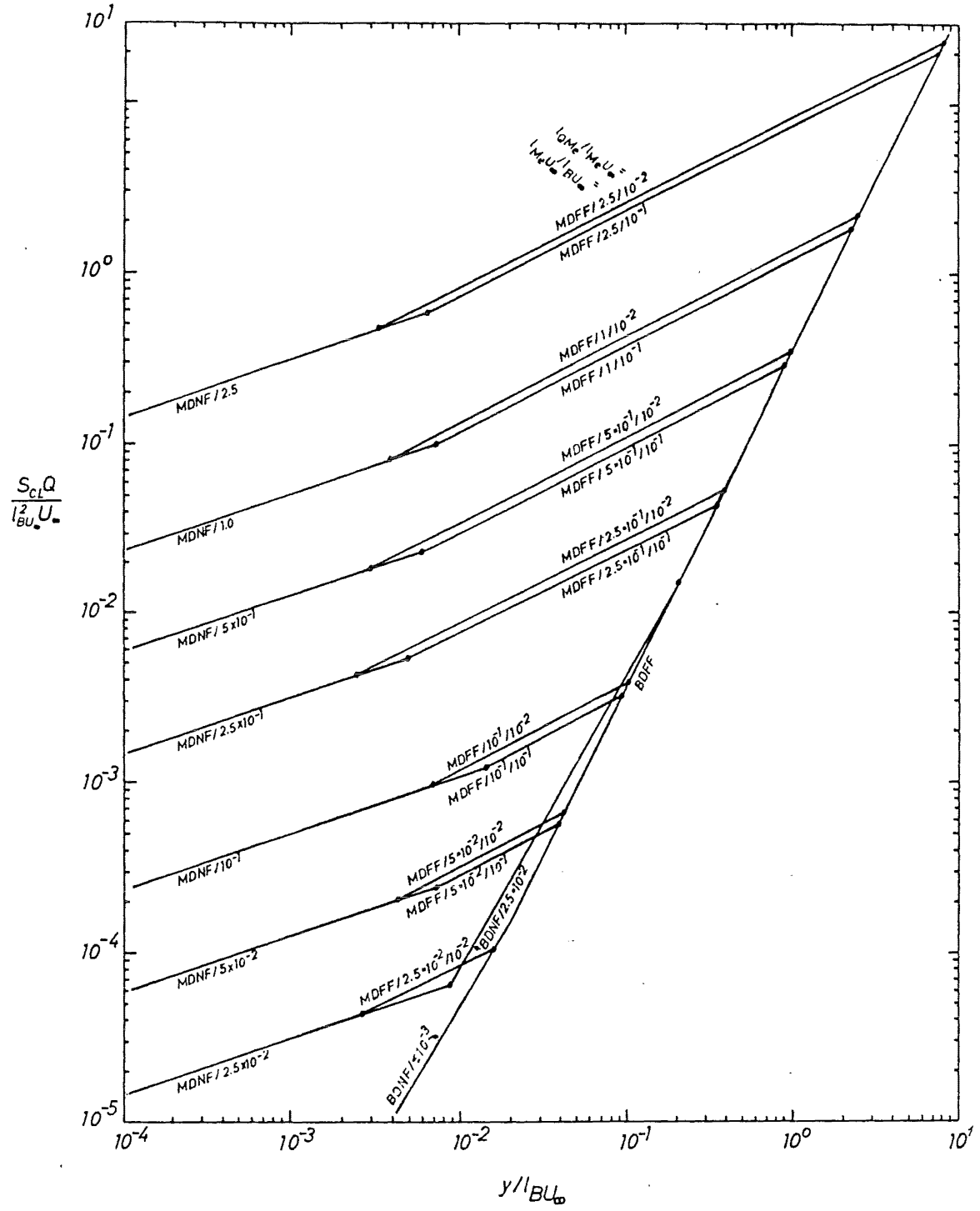

Fig. 5.31. Dilution chart for crossflow.

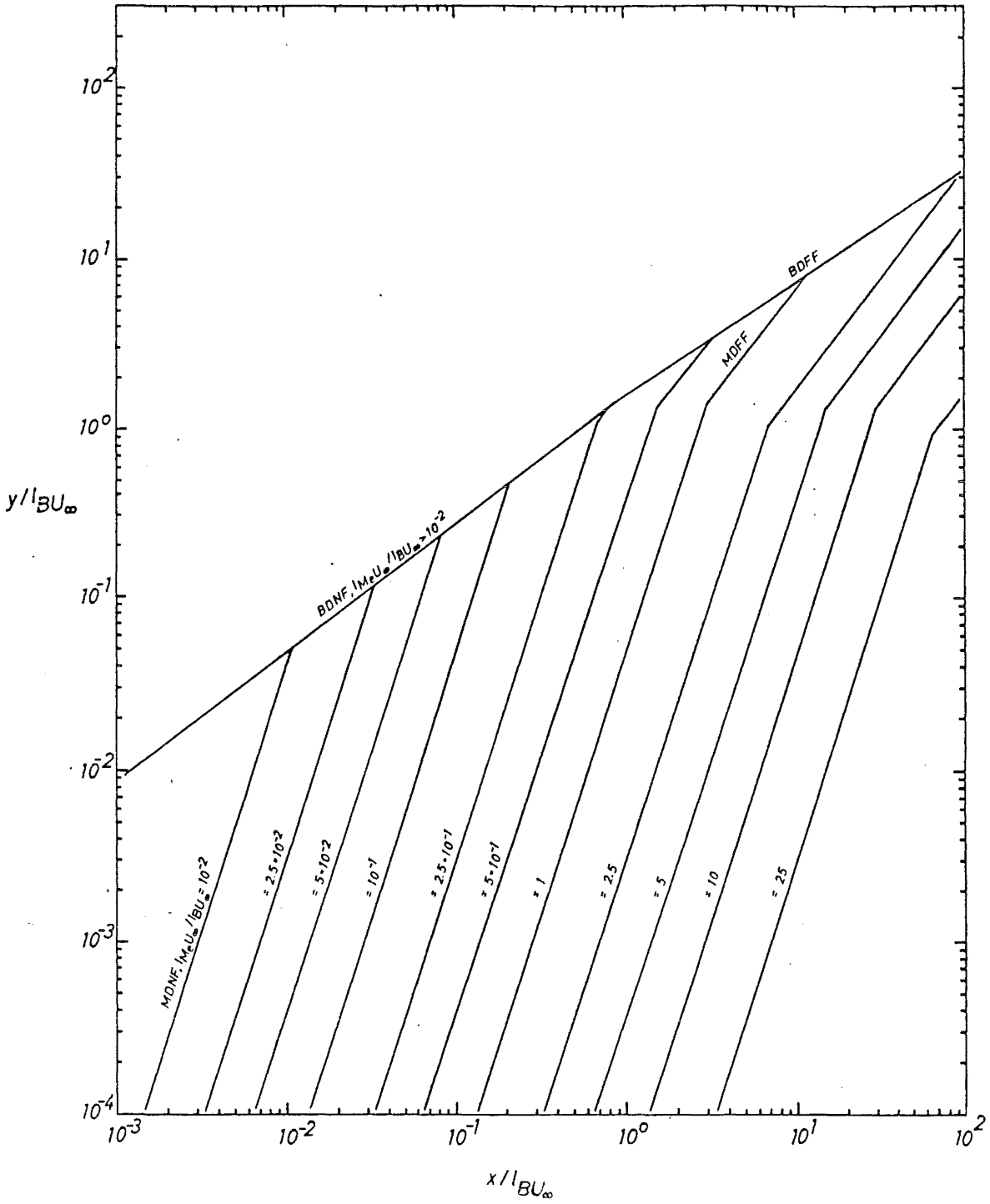

Fig. 5.32. Trajectory chart (xy) for coflow.

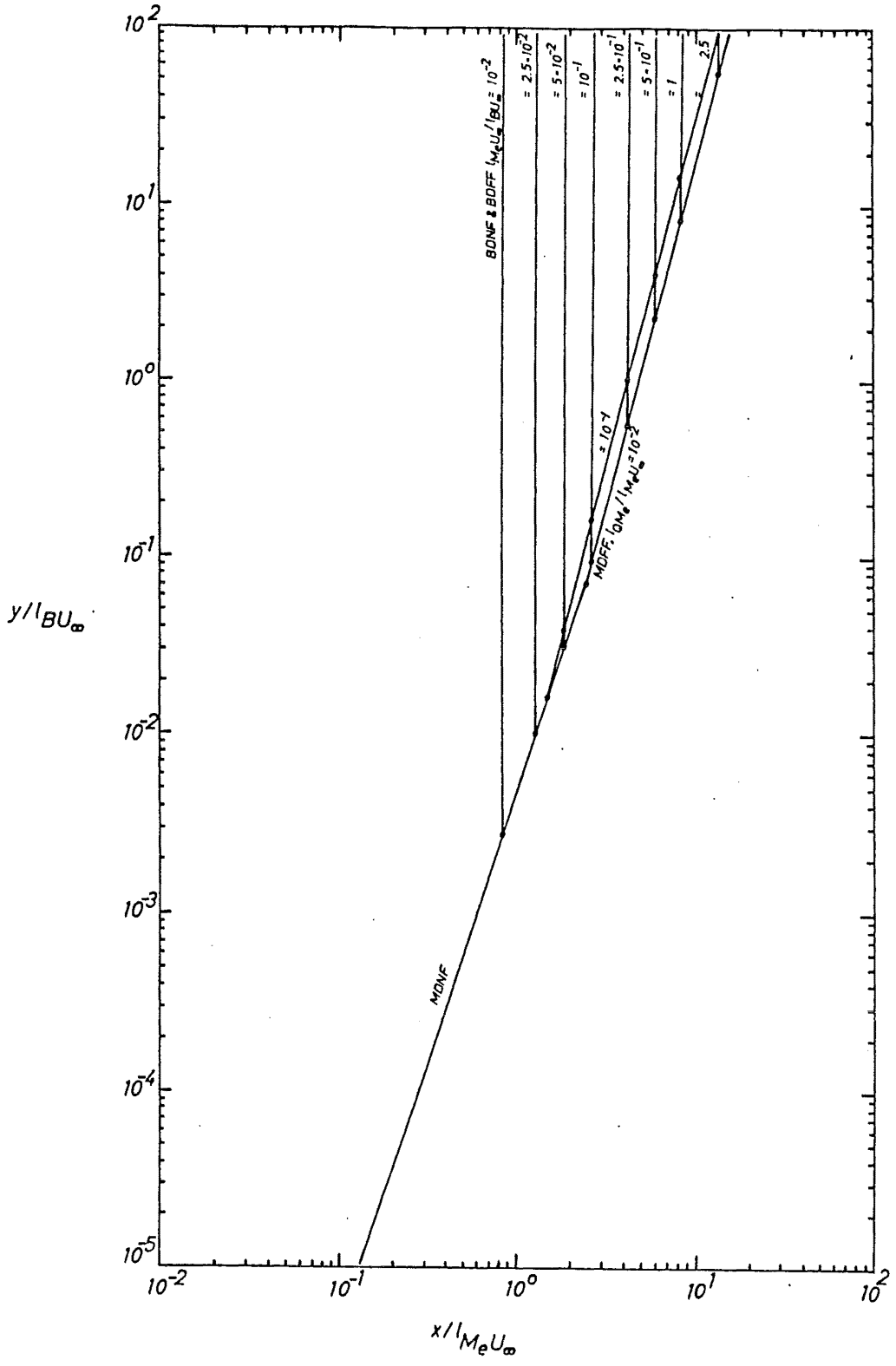

Fig. 5.33. Trajectory chart (xy) for crossflow.

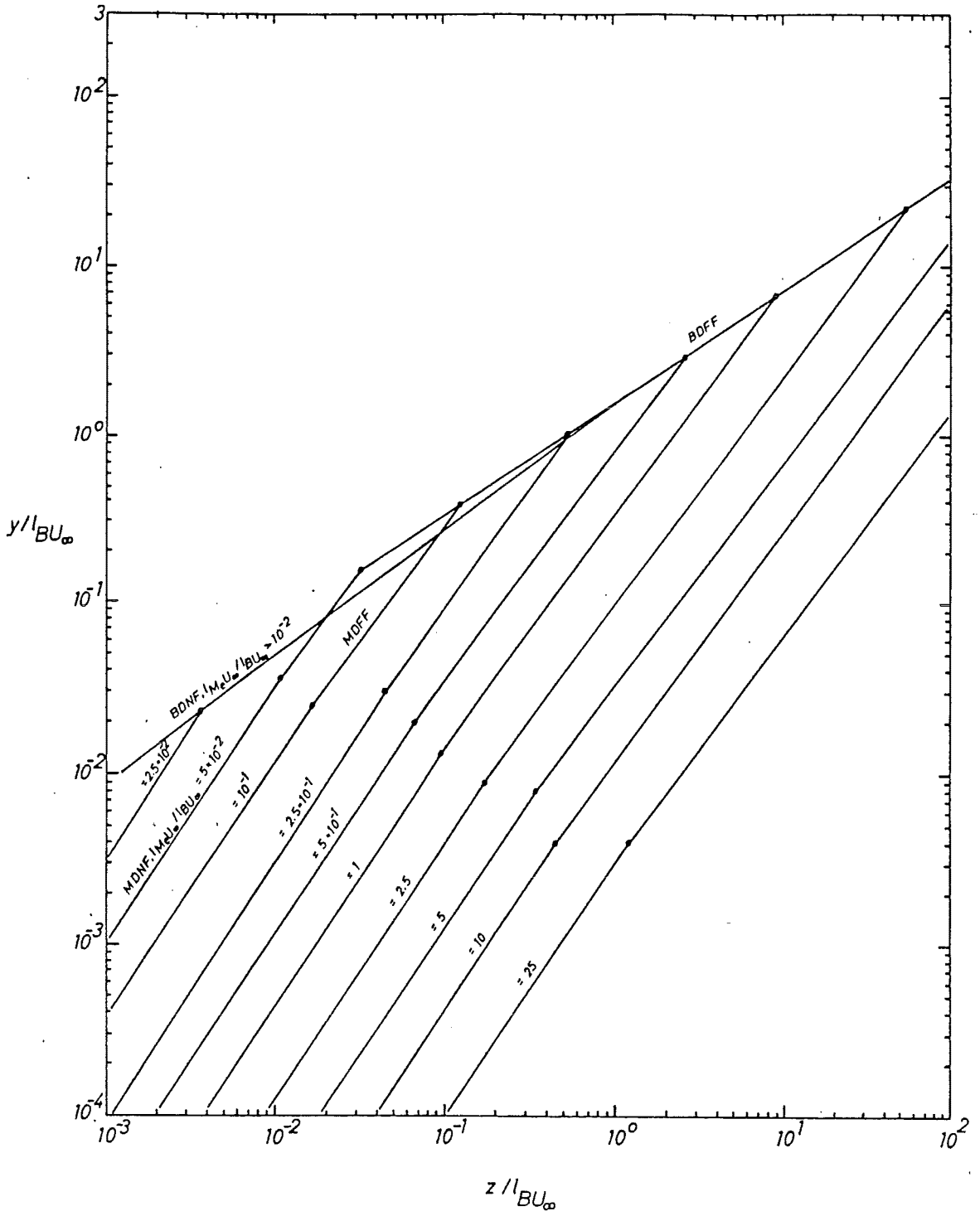

Fig. 5.34. Trajectory chart (yz) for crossflow.

CHAPTER 6

BASIC EQUATIONS AND ANALYSIS OF BASIC CASES.

6.1. Introduction

In the dimensional analysis in the previous chapters the equations of motion have been referred to when additional information, which could not be derived from simple dimensional arguments alone, was required.

The traditional approach to deriving the equations consists of deriving the four equations below

conservation of x-excess momentum
y-momentum balance
conservation of buoyancy flux
geometric relationship(s)

and assuming that the flow is self similar in cross sections perpendicular to the center line. These equations contain 5 variables so an additional equation, a closure equation, is also required . The most commonly used closure is the so-called entrainment hypothesis, which will be discussed in more detail in next section.

However, choosing cross sections perpendicular to the center line does not necessarily give the correct self similar direction in e.g. advected thermals where the proper direction of the cross sections must be vertical (cfr. chapter 4). Furthermore, in the transition between e.g. the BDNF (with Gaussian distribution) and the BDFF (with vortex pair distribution) there is clearly not self similarity in cross sections perpendicular to the center line.
In the present work it has therefore been found necessary to use cross sections which form a variable angle with the center line.
It is assumed that the velocity field in a jet can be considered as consisting of a Gaussian component and a vortex pair component. The two components are perpendicular to each other. Each component is self similar throughout the flow. The Gaussian component is perpendicular to the cross section and the vortex pair component is parallel to the cross section.
The above four equations have consequently been derived using this concept. This introduces an additional variable (an angle) in the four equations so that two closures are now required.

In this chapter a number of simple composite cases in which the self similar directions of the cross sections are known will be studied. The equations then only have 5 variables and in those cases only one closure is required.

Further work will be required to derive the second closure in order to obtain a closed system of equations for the general case of a buoyant jet in an ambient flow.

In the following section the four basic equations will be derived for a coflowing, crossflowing and a counterflowing jet.
Then a discussion will be given of various closure equations (including the entrainment hypothesis) suggested by different researchers. This leads to the suggestion of the type of closure that will be used in the present work.
By using the results from the analysis in the two previous chapters the form of the closure in the regions MDNF, MDFF, BDNF and BDFF and in some of the transitions can be found. The form of the closure is not known for all the transitions between these regions.
However, it is hoped that the present discussion will serve as a useful basis for further development of the first closure.

A closed system of equations has then been obtained for the simple cases . The dimensional analysis as applied in previous chapter gives information about the flow within regions but not about the transitions between these. It is therefore of interest with the help of the equations of motion and the chosen closure to find information about flows in which transitions occur. The equations are applicable to two types of composite flows: horizontal bouyant jet in still ambient and pure jet in a coflow. The equations will be solved analytically or numerically for these two cases and the results will be compared with data.

6.2. Basic equations.

In the discussion of the basic jets in chapter 4 it was shown that the flows fell in two categories:
in the first category which we will call category I the excess velocity was parallel with the center line of the jet and with the ambient flow if there was any. The cross sections were circular with a Gaussian velocity/buoyancy/tracer distribution and had a maximum value at the center line.
To this category belonged pure jets in still ambient (MDNF), pure plumes in still ambient(BDNF), weak jets (MDFF coflow and counterflow). From this it follows that buoyant jets in still ambient and pure jets in coflows also belong to this category.
In the second category which we will call category II the excess velocity formed a right angle with the ambient velocity and was almost perpendicular to the center line of the jet.
A counter rotating vortex pair existed in all cross sections. The velocity/buoyancy/tracer

concentration distribution was not Gaussian but had two maximum points, each in the center of a vortex.
To this category belonged advected line thermal from a continuous source (BDFF) and advected momentum line puff from a continuous source (MDFF in crossflow)

For the first category, category I, the flow was self similar in cross sections perpendicular to the excess velocity.
In the second category, category II, the flow was self similar in cross sections parallel with the excess velocity.

In the general case of a buoyant jet in an ambient flow it is assumed that both categories are present.
Throughout the flow the category I component of u_{em}, which will be called u_{sm}, see fig. 6.1, will be self similar in cross sections perpendicular to it.
Similarly, the category II component of u_{em}, which will be called v_{vm},see fig. 6.1, will be self similar in cross sections parallel with it.
Assuming u_{sm} perpendicular to v_{vm} this leads to the two components being self-similar with respect to the same direction of the cross section.

The angle from u_{sm} to u_{em} is called δ and the angle from the X-axis to u_{sm} is called β, see fig. 6.1. Note that with the given orientation of the X and Y axis the positive direction of ratation in fig. 6.1 will be clockwise.
The control volumes are cylinders with the end pieces parallel with the direction of the cross section and thickness ds'.
ds' is therefore measured in a direction parallel with u_{sm} and should not be confused with ds, the step length along the center line.

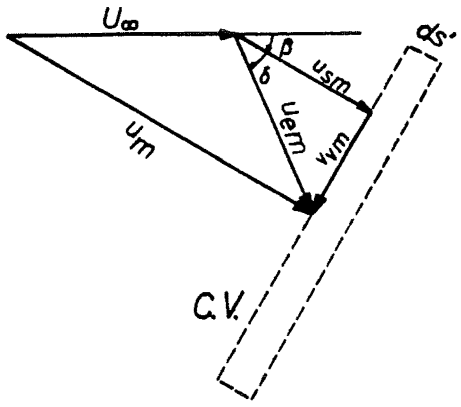

Fig. 6.1. Definition sketch of velocity components in a coflow.

The above assumptions about the decomposition of u_{em} and the subsequent choice of direction

of the cross sections have been used in the following calculations.

To obtain a simple form of the equations of motion it has been necessary to make a number of simplifying assumptions about the character of the jet flows which are studied here. Some of them are implicitly others explicitly stated in the following. In appendix C a comprehensive list of assumptions is given.
The coordinate system which will be used is as defined in chapter 4.

The basic equations can now be derived for a jet in a coflow:
The difference in volume flux between the two ends of the control surface must equal the amount of fluid that has flown in through the sides of the control volume, q_{inflow}:

$$\frac{d}{ds'}\int_0^R (U_\infty \cos\beta + u_s)\, 2\pi r\, dr = q_{inflow} \tag{6.2.1}$$

where R is some large value of r.

The change in x-momentum flux between the two ends of the control surface must equal the x-momentum of the entrained fluid, $q_{inflow}U_\infty$:

$$\frac{d}{ds'}\int_0^R (U_\infty \cos\beta + u_s)(U_\infty + u_s \cos\beta - v_v \sin\beta)\, 2\pi r\, dr - q_{inflow}U_\infty = 0 \tag{6.2.2}$$

Inserting (6.2.1) in (6.2.2) yields:

$$\frac{d}{ds'}\int_0^R (u_s \cos\beta - v_v \sin\beta)(U_\infty \cos\beta + u_s)\, 2\pi r\, dr = 0$$

or:

$$\frac{d}{ds'}\int_0^R (u_s^2 + U_\infty u_s \cos\beta)\cos\beta\, 2\pi r\, dr - \frac{d}{ds'}\int_0^R (u_s v_v + v_v U_\infty \cos\beta)\sin\beta\, 2\pi r\, dr = 0 \tag{6.2.3}$$

Some researchers include a drag term in the momentum equations. They explain this by assuming that the ambient flow conceives the jet as a solid body on which it will exert a drag

force . The drag force will affect the momentum flux through the control volume. However, in the present work no such drag forces have been assumed.

The equation for the vertical momentum becomes:

$$\frac{d}{ds'}\int_0^R (U_\infty \cos\beta + u_s)(u_s \sin\beta + v_v \cos\beta)\, 2\pi r\, dr = \int_0^R \Delta\, 2\pi r\, dr$$

Or:

$$\frac{d}{ds'}\int_0^R (u_s^2 + u_s U_\infty \cos\beta)\sin\beta\, 2\pi r\, dr$$
$$+\frac{d}{ds'}\int_0^R (u_s v_v + U_\infty v_v \cos\beta)\cos\beta\, 2\pi r\, dr = \int_0^R \Delta\, 2\pi r\, dr \qquad (6.2.4)$$

The equation for the continuity of buoyancy flux is

$$\frac{d}{ds'}\int_0^R (U_\infty \cos\beta + u_s)\Delta\, 2\pi r\, dr = 0 \qquad (6.2.5)$$

Now define

$$u_s/u_{sm} = \Phi(r/b) = \Phi(\zeta) \qquad (6.2.6)$$

$$v_v/v_{vm} = h(r/b) = h(\zeta) \qquad (6.2.7)$$

$$\Delta/\Delta_m = f(r/b) = f(\zeta) \qquad (6.2.8)$$

Substituting into (6.2.3), (6.2.4) and (6.2.5) and letting $R \to \infty$ yields:

Horizontal momentum:

$$\frac{d}{ds'}[(I_m u_{sm}^2 + I_q U_\infty u_{sm}\cos\beta)\cos\beta\, b^2]$$

$$-\frac{d}{ds'}[(I_{mv}\,u_{sm}\,v_{vm}+I_v\,U_\infty\,v_{vm}\cos\beta)\sin\beta\,b^2] = 0 \qquad (6.2.9)$$

Vertical momentum:

$$\frac{d}{ds'}[(I_m\,u_{sm}^2+I_q\,U_\infty\,u_{sm}\cos\beta)\sin\beta\,b^2]$$
$$+\frac{d}{ds'}[(I_{mv}\,u_{sm}\,v_{vm}+I_v\,U_\infty\,v_{vm}\cos\beta)\cos\beta\,b^2] = I_\Delta\,\Delta_m\,b^2 \qquad (6.2.10)$$

Buoyancy flux conservation:

$$\frac{d}{ds'}(I_{q\Delta}\,\Delta_m\,b^2\,u_{sm}+I_\Delta\,U_\infty\,b^2\,\Delta_m\cos\beta) = 0 \qquad (6.2.11)$$

In non-buoyant jets a tracer conservation equation is relevant. It is similar to the buoyancy conservation equation but with Δ_m, $I_{q\Delta}$ and I_Δ replaced by c_m, I_{qc} and I_c.

Where

$$I_m = \int_0^\infty \Phi^2\,2\pi\eta\,d\eta \qquad (6.2.12)$$

$$I_q = \int_0^\infty \Phi\,2\pi\eta\,d\eta \qquad (6.2.13)$$

$$I_{mv} = \int_0^\infty \Phi h\,2\pi\eta\,d\eta \qquad (6.2.14)$$

$$I_v = \int_0^\infty h\,2\pi\eta\,d\eta \qquad (6.2.15)$$

$$I_\Delta = \int_0^\infty f\,2\pi\eta\,d\eta \qquad (6.2.16)$$

$$I_{q\Delta} = \int_0^\infty \Phi f 2\pi\eta \, d\eta \tag{6.2.17}$$

Note that although we can assume I_m, I_q, I_{mv} and I_v constant because of the assumption about splitting up the flow in two independent components, I_Δ will vary because of the varying distribution of Δ.
The values of the cross sectional constants are discussed in appendix D.

We also have two geometric relationships:

$$\frac{dx}{ds'} = \frac{u_{sm}\cos\beta - v_{vm}\sin\beta + U_\infty}{U_\infty\cos\beta + u_{sm}} \tag{6.2.18}$$

$$\frac{dy}{ds'} = \frac{u_{sm}\sin\beta + v_{vm}\cos\beta}{U_\infty\cos\beta + u_{sm}} \tag{6.2.19}$$

u_{sm} and v_{vm} can be written as:

$$u_{sm} = u_{em}\cos\delta \tag{6.2.20}$$

$$v_{vm} = u_{em}\sin\delta \tag{6.2.21}$$

There are now 5 equations and 7 unknowns (u_{em}, δ, β, b, x, y, Δ_m).

To obtain a closed system of equations two closure equations are required.
In the category I and II flows δ is known ($\delta = 0^o$ in category I and $\delta=90^o$ in category II)
In those cases only one closure is required.
A further closure is required in flows where a transition from category I to category II takes place. Only category I and category II flows will be studied and for that purpose one closure suffices. The closure equation will be discussed in next section.

A definition sketch for a jet in a crossflow is shown in fig. 6.2.
u_{em} is entirely in the xy-plane and as before β is the angle from the x-axis to u_{sm} and δ is the angle from u_{sm} to u_{em}. The angle from the X-axis to u_{em} is called γ. The velocity

components u_{sm} and v_{vm} are assumed to be in the plane defined by U_∞, u_m and u_{em}. (see figs. 6.2 and 6.3). The direction of positive rotation in this triangle is chosen as the shortest way U_∞ has to be rotated to go in the direction of u_{em}.

It can be shown that $\cos\gamma = \cos\beta/\cos\delta$.

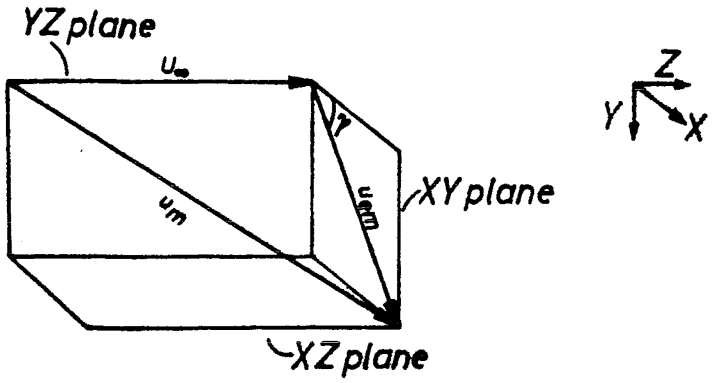

Fig. 6.2. Definition sketch for a jet in a crossflow.

The conservation of volume flux equation becomes in a similar way as (6.2.1):

$$\frac{d}{ds'}\int_0^R (U_\infty \sin\delta + u_s)\, 2\pi r\, dr \;-\; q_{inflow} \;=\; 0 \qquad (6.2.22)$$

The horizontal momentum equation becomes:

$$\frac{d}{ds'}\int_0^R (U_\infty \sin\delta + u_s)(u_s \cos\delta + v_v \sin\delta)\cos\gamma\, 2\pi r\, dr \;=\; 0 \qquad (6.2.23)$$

Note that the entraining fluid does not change the momentum in the x-direction.
The vertical momentum equation becomes:

$$\frac{d}{ds'}\int_0^R (U_\infty \sin\delta + u_s)(u_s \cos\delta + v_v \sin\delta)\sin\gamma\, 2\pi r\, dr \;=\; \int_0^R \Delta\, 2\pi r\, dr \qquad (6.2.24)$$

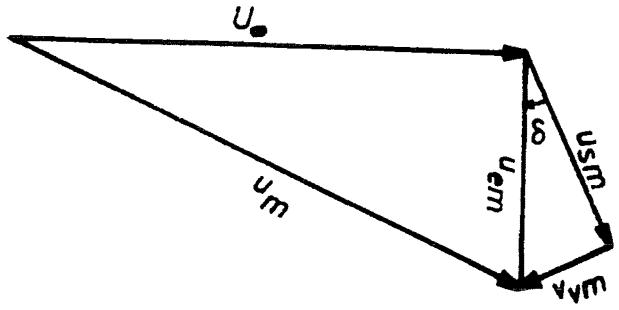

Fig. 6.3. The velocities in a jet in a crossflow.

And the buoyancy flux conservation equation becomes:

$$\frac{d}{ds'}\int_0^R (U_\infty \sin\delta + u_s)\Delta\, 2\pi r\, dr = 0 \tag{6.2.25}$$

Again by assuming Gaussian distribution for u_s and vortex pair distribution for v_v, letting $R \rightarrow \infty$ and introducing the cross sectional constants defined in equations (6.2.12) - (6.2.17) into equation (6.2.23) it becomes:

$$\frac{d}{ds'}[(I_q U_\infty u_{sm} \sin\delta + I_m u_{sm}^2)\cos\delta \cos\gamma b^2] + \frac{d}{ds'}[(I_v U_\infty v_{vm} \sin\delta + I_{mv} u_{sm} v_{vm})\sin\delta \cos\gamma b^2] = 0 \tag{6.2.26}$$

and equation (6.2.24) becomes:

$$\frac{d}{ds'}[(I_q U_\infty u_{sm} \sin\delta + I_m u_{sm}^2)\cos\delta \sin\beta b^2] + \frac{d}{ds'}[(I_v U_\infty v_{vm} \sin\delta + I_{mv} u_{sm} v_{vm})\sin\delta \sin\beta b^2] = I_\Delta \Delta_m b^2 \tag{6.2.27}$$

and equation (6.2.25) finally becomes:

$$\frac{d}{ds'}[I_\Delta U_\infty \Delta_m \sin\delta\, b^2 + I_{q\Delta} u_{sm} \Delta_m b^2] = 0 \tag{6.2.28}$$

In non-buoyant jets a tracer conservation equation is relevant. It is similar to the buoyancy conservation equation but with Δ_m, $I_{q\Delta}$ and I_Δ replaced by c_m, I_{qc} and I_c.

Three geometric relationships can be derived: (cfr. fig. 6.3).

$$\frac{dx}{ds'} = \frac{(u_{sm}\cos\delta + v_{vm}\sin\delta)\cos\gamma}{U_\infty \sin\delta + u_{sm}} \tag{6.2.29}$$

$$\frac{dy}{ds'} = \frac{(u_{sm}\cos\delta + v_{vm}\sin\delta)\sin\gamma}{U_\infty \sin\delta + u_{sm}} \tag{6.2.30}$$

$$\frac{dz}{ds'} = \frac{U_\infty}{U_\infty \sin\delta + u_{sm}} \tag{6.2.31}$$

Like for coflows two closure equations are required for the system of equations to be closed.

A definition sketch for a jet in a counterflow is shown in fig. 6.4. The triangle of the velocities U_∞, u_{em} and u_m looks different in the two cases $s<<l_{MeU_\infty}$ (before the stagnation point) and $s>>l_{MeU_\infty}$ (after the stagnation point). β is defined as the angle from the X-axis to u_{sm}. δ is the angle from u_{sm} to u_{em}. Now $U_\infty<0$ since this is a counterflow.

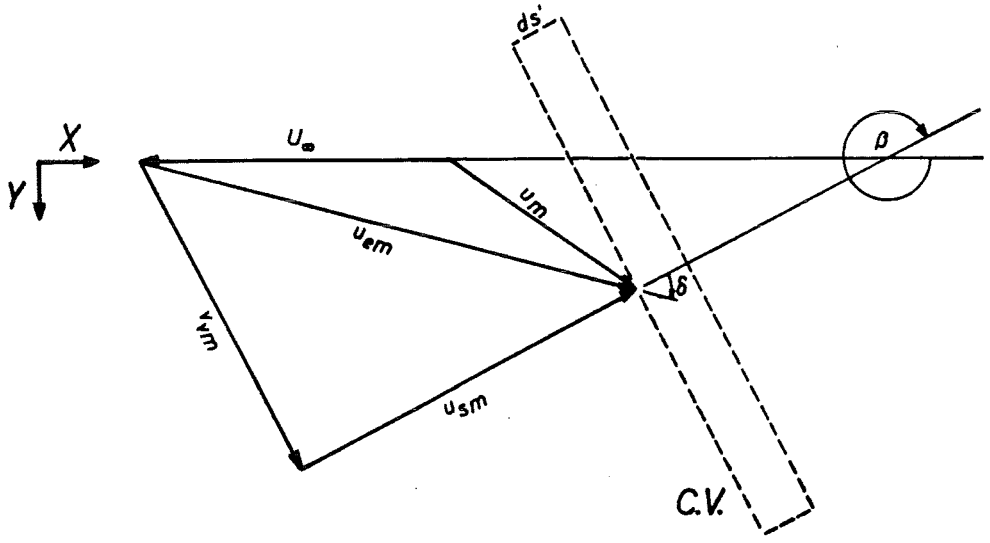

Fig. 6.4. Definition sketch for a jet in a counterflow.

The volume flux balance equation becomes:

$$\frac{d}{ds'}\int_0^R (U_\infty \cos\beta + u_s)\, 2\pi r\, dr = q_{inflow} \tag{6.2.32}$$

The horizontal momentum flux equation becomes

$$\frac{d}{ds'}\int_0^R (U_\infty \cos\beta + u_s)(U_\infty + u_s \cos\beta - v_v \sin\beta)\, 2\pi r\, dr - q_{inflow} U_\infty = 0 \tag{6.2.33}$$

The vertical momentum flux equation becomes

$$\frac{d}{ds'}\int_0^R (U_\infty \cos\beta + u_s)(u_s \sin\beta + v_v \cos\beta)\, 2\pi r\, dr = \int_0^R \Delta\, 2\pi r\, dr \tag{6.2.34}$$

The buoyancy flux conservation equation becomes

$$\frac{d}{ds'}\int_0^R (U_\infty \cos\beta + u_s)\, \Delta\, 2\pi r\, dr = 0 \tag{6.2.35}$$

Equations (6.2.32)-(6.2.35) can be transformed in a similar way as to how the equations for coflow and crossflow were transformed.
Then equation (6.2.33) becomes

$$\frac{d}{ds'}[(I_m u_{sm}^2 + I_q U_\infty u_{sm} \cos\beta)\cos\beta\, b^2] - \frac{d}{ds'}[(I_{mv} u_{sm} v_{vm} + I_v U_\infty v_{vm} \cos\beta)\sin\beta\, b^2] = 0 \tag{6.2.36}$$

Equation (6.2.34) becomes

$$\frac{d}{ds'}[(I_v U_\infty \cos\beta\, v_{vm} + I_{mv} u_{sm} v_{vm})\cos\beta\, b^2] + \frac{d}{ds'}[(I_{mv} u_{sm} v_{vm} + I_v U_\infty v_{vm} \cos\beta)\cos\beta\, b^2] = I_\Delta \Delta_m b^2 \tag{6.2.37}$$

And equation (6.2.35) becomes

$$\frac{d}{ds'}[I_\Delta U_\infty \Delta_m \cos\beta\, b^2 + I_{q\Delta}\, u_{sm} \Delta_m b^2] = 0 \qquad (6.2.38)$$

In non-buoyant jets a tracer conservation equation is relevant. It is similar to the buoyancy conservation equation but with Δ_m, $I_{q\Delta}$ and I_Δ replaced by c_m, I_{qc} and I_c.

Two geometric relationships can be derived

$$\frac{dx}{ds'} = \frac{u_{sm}\cos\beta - v_{vm}\sin\beta + U_\infty}{U_\infty \cos\beta + u_{sm}} \qquad (6.2.39)$$

$$\frac{dy}{ds'} = \frac{u_{sm}\sin\beta + v_{vm}\cos\beta}{U_\infty \cos\beta + u_{sm}} \qquad (6.2.40)$$

The equations of motion have now been derived for the three cases of a jet in a coflow, a crossflow and a counterflow.

Ayoub [1984] also derived equations of motion for horizontal buoyant jets in a coflow and in a crossflow. However, he also had a drag term in his momentum equations.
Furthermore, he chose $R=\sqrt{2}\ b$ and fully integrated his volume flux balance equations (equivalent to eqs. (6.2.1) and (6.2.22)) to that limit before inserting it into the x- and y-momentum equations. This practice was also used by Fan and as pointed out by Schatzmann [1979] this leads to incorrect equations.

6.3. Closure equations.

The most commonly used closure is the so-called entrainment hypothesis which was first presented by Morton, Taylor & Taylor [1956] . The entrainment hypothesis was subsequently used in modelling (with modifications) by Abraham [1963] , Fan [1968] , Schatzmann [1976] and many others.

The entrainment hypothesis can be derived in the following way:
In order to find the entrainment into the jet per unit length of the centerline (which was called q_{inflow} in previous section) we have to determine the entraining velocity, u_{entr}, see fig. 6.5. The entraining velocity is defined as the inward velocity at the distance b from the center line.

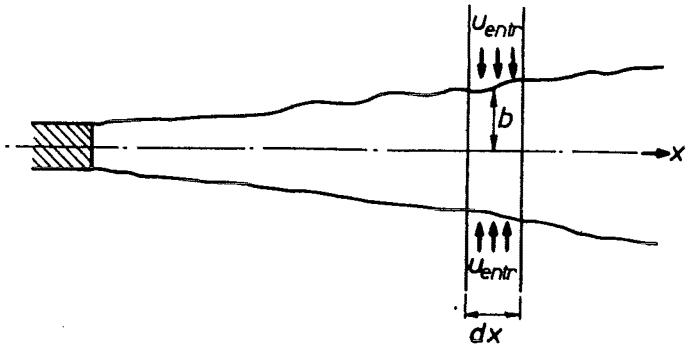

Fig. 6.5. Definition sketch of the entraining velocity u_{entr}.

The form of u_{entr} can be derived by using dimensional analysis. u_{entr} will first be derived for the case of a pure jet in still ambient. For $s >> l_{QM} = Q/M^{1/2}$ u_{entr} must be a function of M and s alone. The only possible solution is that

$$u_{entr} \sim u_{em} \tag{6.3.1}$$

Studying other basic jets and thus regions like MDNF, MDFF, BDNF and BDFF would have led to the same conclusion as (6.3.1) because u_{em} is the only local velocity scale.

The entrainment per unit length of the center line in one of the above mentioned regions of a jet can then be written as

$$\frac{dq}{ds} = u_{entr} 2\pi b \sim u_{em} 2\pi b \tag{6.3.2}$$

where q is the local volume flux in the jet.

Eq. (6.3.2) can also be written as

$$\frac{dq}{ds} = \alpha u_{em} 2\pi b \tag{6.3.3}$$

where α is called the entrainment coefficient.

α must be a constant in MDNF, MDFF , BDNF and BDFF but it does not necessarily have the same value in each of these regions. Furthermore, the reasoning leading to (6.3.1) does not hold in transitions between two different regions because in those parts of the flow there are two length scales and two velocity scales. Equation (6.3.3) does therefore not hold in transitions between two regions.

Because of this researchers have had to determine the variation of α by fitting the theory to data.

Thus the resulting models have only applied strictly within the limits of the data that were used to find the α - function.

As well as finding an α - function in this manner Ayoub [1971] also fitted a spreading factor function , λ , and a drag coefficient C_D to the data . In this and Fan's case data-fitting concealed the fact that some of the basic equations were incorrect.

From the above discussion it is clear that α must be a constant in MDNF , MDFF, BDNF and BDFF . α has been found to be constantly equal to 0.054 in pure jets in still ambient (MDNF) and constantly eqaual to 0.083 in pure plumes in still ambient(BDNF). Abraham [1972] found α to be equal to 0.50 in thermals (BDFF). No value of α is available for MDFF like flows.

Taylor originally derived the entrainment hypothesis from a combination of the balance laws of mass, momentum and kinetic energy and using an assumption as to the similarity of the Reynold's stresses. Similarity can only be assumed in one of the regions MDNF , MDFF, BDNF and BDFF. In the transitions between these regions self similarity can not be assumed.

Hutter [1978] used a higher moment of the kinetic energy euation as a closure and found that the entire spectrum of the plume/jet behaviour could be described satisfactorily.

Schatzmann [1976] used the kinetic energy equation to derive the form of the entrainment function. The resulting model predicted a wide range of non-buoyant and bouyant jet in still and moving ambient well.

Antonia & Bilger [1974] compared three different closure equations for the case of a pure jet in a coflow. The first closure was a growth of width equation (a spreading equation) which was inspired by a growth of width equation suggested by Patel [1971] for plane jets in a coflow. Antonia & Bilger's equation was

$$\frac{db}{ds} = k\frac{u_{em}}{u_{em}+U_\infty} \qquad (6.3.4)$$

where k is the value of db/ds for pure jets, cfr. (4.2.1).

The second closure they examined was the turbulent energy equation.
The third closure was a two-parameter model of turbulence by Rodi & Spalding [1970] based on the turbulent energy equation. Antonia & Bilger found the two parameter model of turbulence the most promising of the three closures. However, they discarded the growth of width closure on the basis that it did not fit one set of data only.

The growth of width equation will be used as the closure in the calculations in this work.
It will be shown in the following that the spreading equation is very simple in the basic cases. Because db/ds = 0.109 in both the momentum dominated and the buoyancy dominated part of a buoyant jet in still ambient, one will expect db/ds = 0.109 also to be true in the transition between the two regions.

$$\frac{db}{ds} = 0.109 \tag{6.3.5}$$

Eq. (6.3.5) therefore can be used as the closure in any jet flow in still ambient.
For comparison, using the entrainment assumption as closure would require one to let α vary between initially the value 0.054 (like in pure jets) to 0.083 (like in pure plumes).
For the still ambient cases (6.3.5) then is the simplest possible closure.
Noutsopoulos & Yannopoulos [1986] used this concept to satisfactorily predict the behaviour of a vertical buoyant jet in still ambient. However, they used a semi-emperical formula for db/ds where it varied from initially 0.12 to finally 0.10.

For the MDFF in coflows (6.3.4) should be used. It will be shown that (6.3.4) gives a correct variation of α from initially 0.054 to 0 for great distances from the port.
It is worth noting that in a coordinate system moving with the speed U_∞ along the X-axis the growth of width appears to be db/ds = k.

All of the above types of jets have had axisymmetric profiles and the excess velocity has been parallel with the center line.
In the remaining types of flows : MDFF in crossflow and BDFF the flow is characterised by having a counterrotating vortex pair in the cross sections. This greatly increases entrainment.
Fig. 6.6 shows a plot of the width b versus distance in the x -direction in the MDFF of a jet in a crossflow. From that it can be seen that

$$\frac{db}{dx} \approx 0.3 \tag{6.3.6}$$

Since we for this type of flows have $u_{sm} \approx 0$, $v_{vm} \approx u_{em}$, $dx/dz = u_{em}/U_\infty$ then (6.3.6) can also be written as

$$\frac{db}{ds} \approx 0.3 \frac{u_{em}}{U_\infty} \tag{6.3.7}$$

Fig. 6.7 is a similar plot for BDFF flows (the author's data) and it shows that

$$\frac{db}{dy} \approx 0.3 \tag{6.3.8}$$

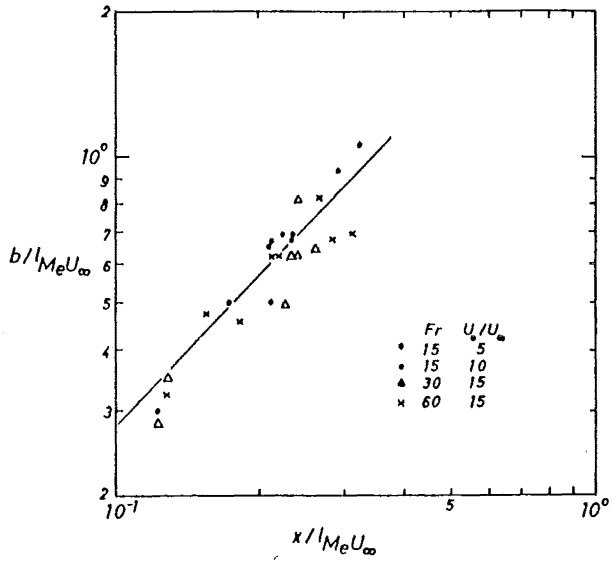

Fig. 6.6 MDFF width vs. distance

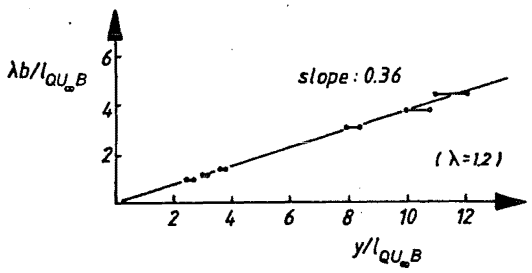

Fig. 6.7 BDFF width vs. distance

Since we for this type of flow have $u_{sm} \approx 0$, $v_{vm} \approx u_{em}$, $dy/dz = u_{em}/U_\infty$ then (6.3.8) can be written as

$$\frac{db}{ds} = 0.3 \frac{u_{em}}{U_\infty} \tag{6.3.9}$$

It can now be summarised that for jets where u_{em} is parallel with the center line we have

$$\frac{db}{ds} = 0.109 \frac{u_{em}}{U_\infty + u_{em}} \tag{6.3.10}$$

and for jets where u_{em} in the far field goes either in the y-direction or in the z-direction (which most likely can be expanded to cases where u_{em} is comtained in the YZ-plane) we have

$$\frac{db}{ds} = 0.3\frac{u_{em}}{U_\infty} \tag{6.3.11}$$

Equations (6.3.10) and (6.3.11) will be used as closures.

The expressions for db/ds given above for the basic cases can be generalised to a formula which is suggested below.

Coflow (cfr. fig. 6.1) :

(Note that ds' goes in the direction of u_{sm} whereas ds goes in the direction of u_m.)

$$\frac{db}{ds'} = \frac{k u_{sm} + m v_{vm}}{U_\infty \cos\beta + u_{sm}} \tag{6.3.12}$$

Crossflow (cfr. fig. 6.2)

$$\frac{db}{ds'} = \frac{k u_{sm} + m v_{vm}}{U_\infty \sin\delta + u_{sm}} \tag{6.3.13}$$

Counterflow (cfr. fig. 6.4)

$$\frac{db}{ds'} = \frac{k u_{sm} + m v_{vm}}{U_\infty \cos\beta + u_{sm}}$$

6.4. Pure jets in a coflow (compound jets).

The control volume is as for the pure jet in still ambient a cylinder with thickness ds'=ds=dx and radius r.

In this type of flow B =0, $\delta = 0^o$and $\beta = 0^o$ and s =s'= x. This implies $u_{sm}=u_{em}$ and $v_{vm}=0$. The equations of motion eqs. (6.2.9) and (6.2.11) (with Δ_m replaced by tracer concentration c_m) become:

$$\frac{d}{dx}\left[I_m u_{em}^2 b^2 + I_q u_{em} U_\infty b^2\right] = 0 \tag{6.4.1}$$

$$I_c U_\infty c_m b^2 + I_{qc} u_{em} c_m b^2 = C_o Q \tag{6.4.2}$$

and the closure equation is(cfr. (6.3.4))

$$\frac{db}{dx} = k\frac{u_{em}}{U_\infty + u_{em}} \tag{6.4.3}$$

Note that the closure (6.4.3) confirms the findings in chapter 4:
when $u_{em}>>U_\infty$ then the jet behaves like a pure jet in still ambient and $b \sim s$, cfr. (4.2.7) i.e. db/ds is constant. When $u_{em} >>U_\infty$ then the jet behaves like a weak jet and $b\sim s^{1/3}$ cfr. (4.5.32), i.e. $db/ds \sim s^{-2/3} \sim u_{em}$. Both are confirmed by (6.7.3).

When eqs. (6.4.1) - (6.4.3) are solved the following solutions are found, cfr. appendix E for details:

$$\left(\frac{1}{2}\left(\frac{u_{em}}{U_\infty}\right)^2 + \left(\frac{u_{em}}{U_\infty}\right)\right)^{-1/2}\left[\frac{8k}{3\sqrt{\pi}}\left(\frac{u_{em}}{U_\infty}+1\right) - \frac{2k}{3\sqrt{\pi}}\left(\frac{u_{em}}{U_\infty}\right)^{-1} + \frac{2k}{\sqrt{\pi}}\frac{u_{em}}{U_\infty}\right] = \frac{x}{l_{M_e}U_\infty} + c_4 \tag{6.4.4}$$

$$k^{-1}\left\{\frac{b}{l_{M_e}U_\infty} + \frac{\pi}{6}\left(\frac{b}{l_{M_e}U_\infty}\right)^3 + \frac{1}{6\sqrt{\pi}}\left[\left(\frac{b}{l_{M_e}U_\infty}\right)^2 + 2\right]^{3/2}\right\} = \frac{x}{l_{M_e}U_\infty} + c_5 \tag{6.4.5}$$

$$\frac{S_{CL}Q}{U_\infty l_{M_e}^2 U_\infty} = \left(I_c + I_{qc}\frac{u_{em}}{U_\infty}\right)\left(\frac{b}{l_{M_e}^2 U_\infty}\right)^2 \tag{6.4.6}$$

where c_4 and c_5 are integration constants which are chosen such that $x/l_{MeU\infty} \rightarrow 0$ when

$b/l_{MeU\infty} \rightarrow 0$ and $u_{em}/U_\infty \rightarrow 0$, i.e. $c_4 = -2k\sqrt{2}/(3\sqrt{\pi})$ and $c_5 = 2\sqrt{2}/(6k\sqrt{\pi})$.

Velocity and width measurements have been made by Landis & Shapiro [1951] (velocity only), Smith & Hughes [1977], Biringen [1975], Antonia & Bilger [1974] and Challen [1968] (velocity only).
Measurements of width and tracer dilution have been made by the author in order to extend the range of values of $x/l_{MeU\infty}$ for which there were data available.

In fig. 6.8 the measured and calculated widths have been compared. In fig. 6.9 the measured and calculated velocities have been compared. The velocity data for the author's experiments have been found indirectly by inserting the experimentally found width-values in the excess momentum conservation equation. Finally in fig. 6.10 the measured and calculated dilutions are compared. In all cases the model predicts the data well.

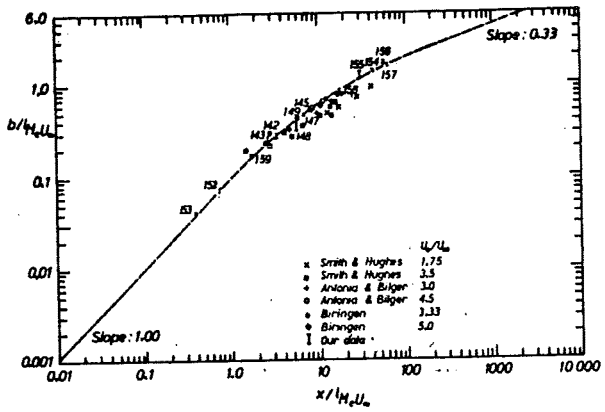

Fig. 6.8 Width vs horizontal distance

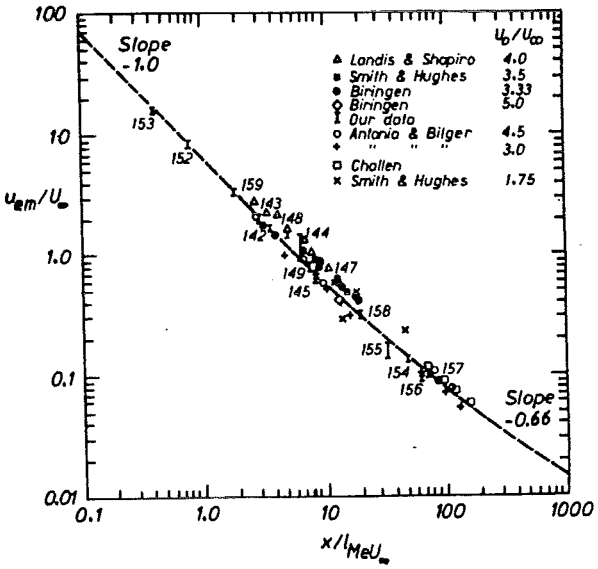

Fig. 6.9 Velocity vs horizontal distance

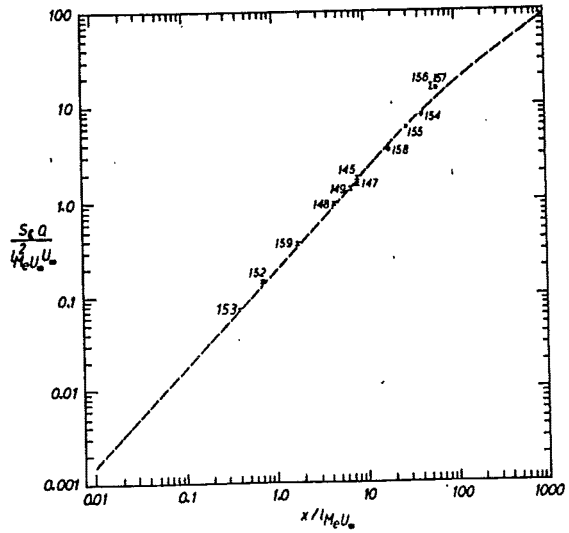

Fig. 6.10. Dilution versus horizontal distance.

The entrainment coefficient α can be calculated using the results from the above analysis.

To distinguish this variable entrainment coefficient from the constant α it will be called E and it is defined by

$$\frac{d}{dx}[I_q u_{em} b^2] = E 2\pi u_{em} b \tag{6.4.7}$$

By inserting the functions for u_{em} and b that have already been found above we find

$$E = k \frac{\left(\frac{u_{em}}{U_\infty}\right)^2}{2\left(1+\frac{u_{em}}{U_\infty}\right)^2} \tag{6.4.8}$$

If k/2 is called E_0 then (6.7.8) can also be written

$$\frac{E}{E_0} = \frac{\left(\frac{u_{em}}{U_\infty}\right)^2}{\left(1+\frac{u_{em}}{U_\infty}\right)^2} \tag{6.4.9}$$

Equation (6.4.8) has been plotted in fig. 6.11 as a function of $x/l_{MeU\infty}$.

It can be seen that the function exhibits the right behaviour; it starts with an E value which corresponds to the entrainment coefficient in a pure jet in still ambient. The value of E decreases towards 0 in the weak jet region.

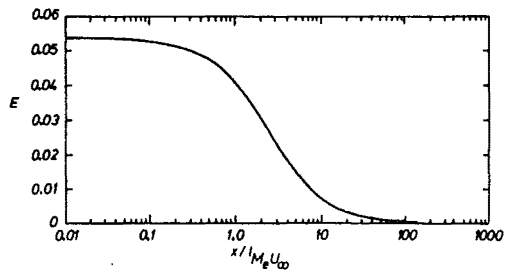

Fig. 6.11. Variation of entrainment function.

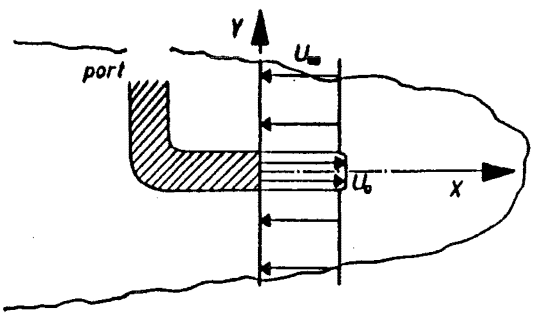

Fig. 6.12. Sketch of jet in counterflow.

It is interesting that with a single constant k-value in the growth of width equation a qualitatively correct variation of the entrainment coefficient is obtained.

The results that have been found in this section can also be applied to counterflows with some modification.

In a counterflow there will be a flow reversal where $u_{em} = -U_\infty$, see fig. 6.12. After this point the downstream fluid will mix with upstream fluid. The above model can therefore not be expected to apply in the initial part of the flow. However, for $|x|$ large, i.e. far downstream, the weak jet equations would be expected to apply when the sign of x is changed, i.e. x is replaced by -x in equations (6.4.4) - (6.4.6).

6.5. Buoyant jet in still ambient.

The control volume is a cylinder with thickness ds'=ds and radius r. $\delta=0^o$ and β is variable. $U_\infty = 0$, $u_{sm} = u_{em}$ and $v_{vm} = 0$. The equations of motion, eqs. (6.2.9) - (6.2.11) and (6.3.5) become:

$$I_m u_{em}^2 \cos\beta b^2 = M = \text{constant} \tag{6.5.1}$$

$$\frac{d}{ds}[I_m u_{em}^2 \sin\beta b^2] = I_\Delta \Delta_m b^2 \tag{6.5.2}$$

$$I_{q\Delta} \Delta_m u_{em} b^2 = B \tag{6.5.3}$$

$$\frac{db}{ds} = k \tag{6.5.4}$$

The geometric relationships eqs. (6.2.18) and (6.2.19) are

$$\frac{dx}{ds} = \cos\beta \tag{6.5.5}$$

$$\frac{dy}{ds} = \sin\beta \tag{6.5.6}$$

Eqs. (6.5.1) - (6.5.4) can be rearranged into:

$$(1+\tan^2\beta)^{1/4}\frac{d(\tan\beta)}{d(s/l_{MB})^2} = \frac{I_\Delta I_m^{1/2} k}{2 I_{q\Delta}} \tag{6.5.7}$$

Equation (6.5.7) has been solved numerically with the assumption of a virtual origin. By using the solution with eqs. (6.5.5) and (6.5.6) the trajectory was found. Eq. (6.5.3) could be rewritten as:

$$\frac{S_{CL} Q}{l_{MB} M^{1/2}} = \frac{I_{q\Delta} k}{I_m^{1/2}} (1+\tan^2\beta)^{1/4}\left(\frac{s}{l_{MB}}\right) \tag{6.5.8}$$

The solution for the trajectory has been shown in fig. 6.13. The asymptotic lines corresponding to the solutions for the buoyancy dominated and the momentum dominated part of the flow as found in section 5.2 are also shown. Data from Ayoub [1973] and the author are also included. The solution for the dilution corresponding to eq. (6.5.8) is shown in fig. 6.14. The asymptotic solutions and data from Ayoub and the author are also included.

It can be seen that in the transition regions of the solutions the calculated values and the data deviated more than 100 % from the asymptotic solutions.

It was found numerically that the upper limit for x/l_{MB} in theory is 8.4. Bühler & Hauenstein [1979] gave a value of 5.0 based on experimental data but they used trajectory data which did not go sufficiently far into the buoyancy dominated part of the flow. Indeed, it can be seen from fig. 6.13 that in theory the trajectory approaches the vertical tangent very slowly.

Also in the still ambient case the variation of the entrainment coefficient E can be found:

$$E = \frac{I_q k}{2\pi}\left(\frac{S_{CL} Q}{M^{1/2} l_{MB}}\right)^{-1} \frac{s}{l_{MB}} \frac{d}{d(s/l_{MB})}\left(\frac{S_{CL} Q}{M^{1/2} l_{MB}}\right) \tag{6.5.9}$$

The result is shown in fig. 6.15. The value of E varies from the value 0.0545 = k/2 which corresponds to the entrainment coefficient in pure jets to the value 0.091 = 5/3 x k/2 which corresponds to the entrainment coefficient in a pure plume. That is somewhat above the value 0.082 as suggested by Rouse, Yih & Humphreys [1952]. Like in the case of compound jets it has been demonstrated that an expansion closure with one constant value of k produces a qualitatively correct variation of the entrainment coefficient between the correct limits.

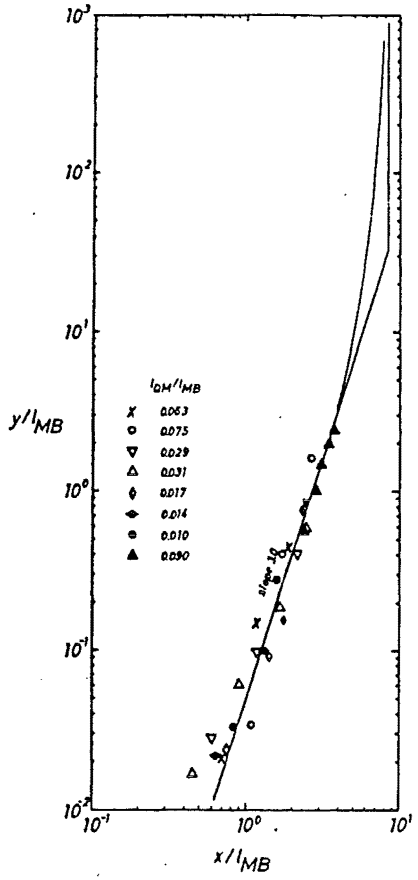

Fig. 6.13. Trajectory for buoyant jet in still amb.

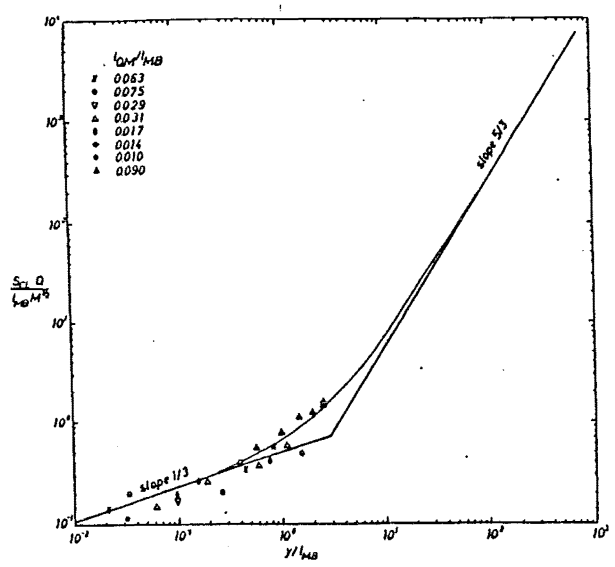

Fig. 6.14. Dilution for buoyant jet in still amb.

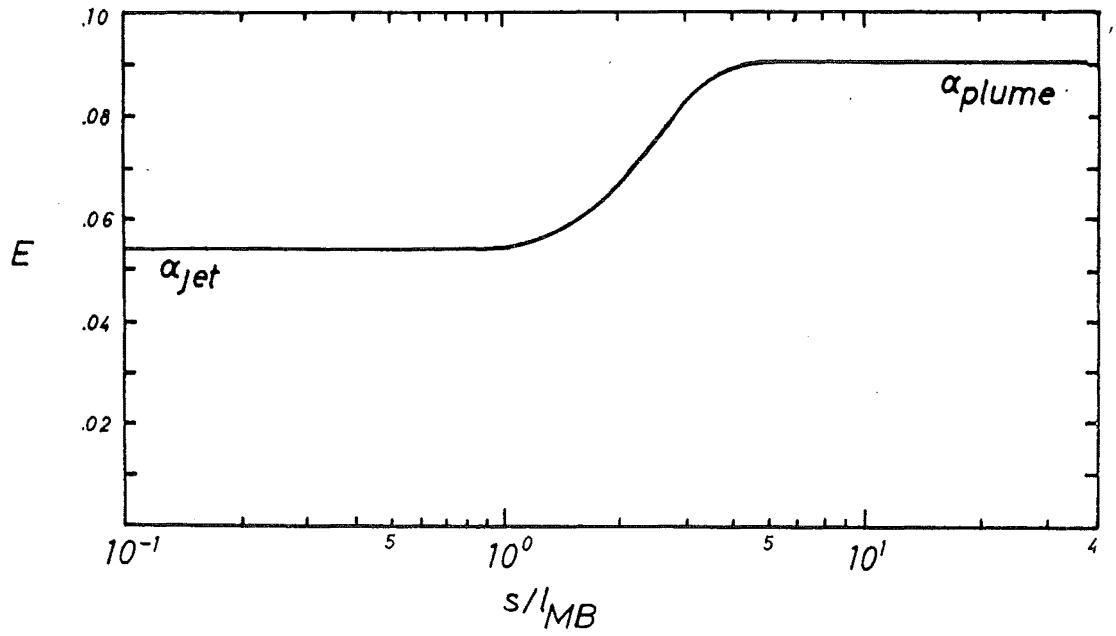

Fig. 6.15. The variation of the entrainment coefficient in a buoyant jet in still ambient.

CHAPTER 7
INSTABILITY PHENOMENA IN COUNTERFLOWS.

7.1. Introduction.

The flow in a jet discharging into a coflow or into a still ambient is stable. The position and shape of the trajectory does not change with time and small deviations of the direction of discharge are damped.

In contrast, the case of a jet discharging into a counterflow is inherently unstable with deviations in the flow direction being amplified. For this case the jets are unstable for large Froude numbers but become stable as the Froude number decreases.

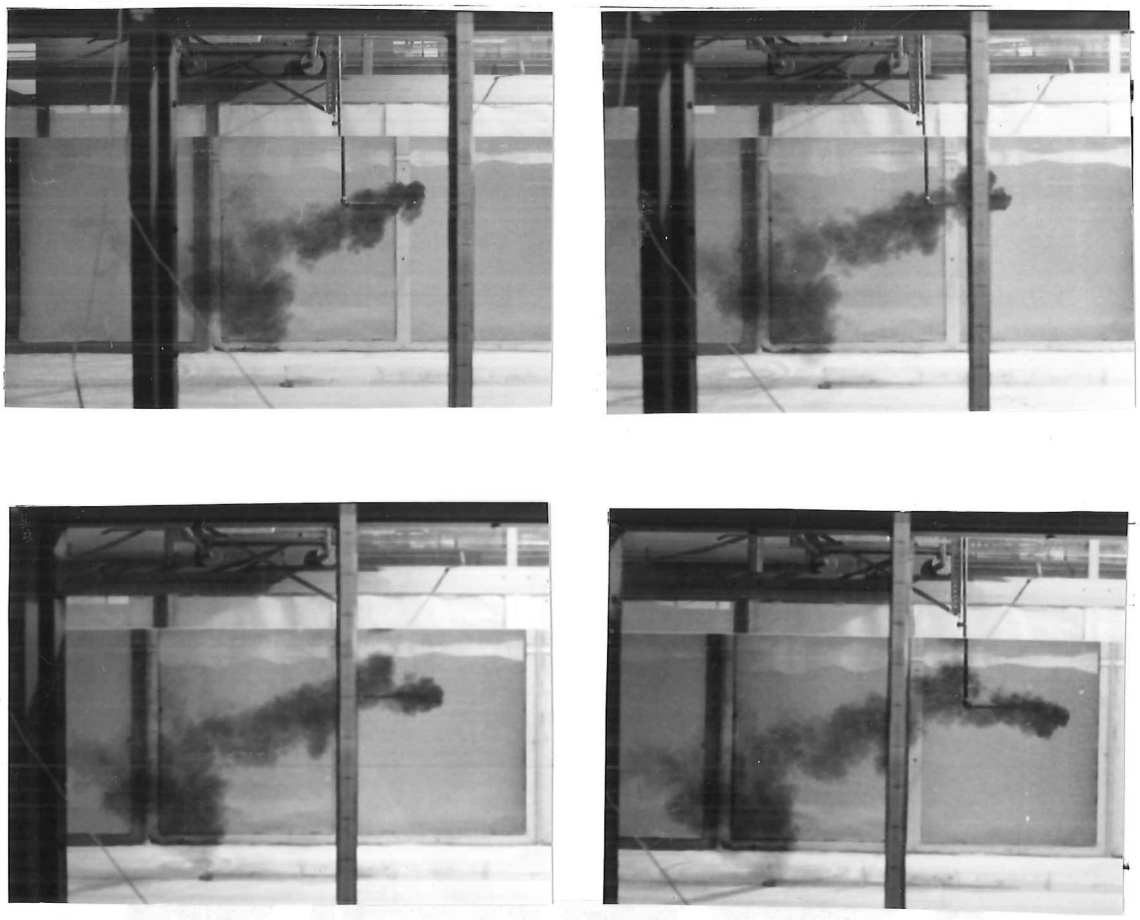

Fig. 7.1. The author's experiments with a buoyant jet in a counterflow.

All sketches and arguments in this chapter deal with negatively buoyant jets. These are the jets that were used in the experiments. Similar types of behaviour would have been found with positively buoyant jets. "Downwards" would then have to be replaced by "upwards" and vice versa, "free surface" replaced by "bottom" etc.

The unstable behaviour appears as more or less periodic irregular changes in the direction of discharge in the first 5-15 port diameters of the jet. These changes take place in the vertical as well as in the transverse direction. The movements can be described as 3-dimensional oscillations. Fig. 7.1 is a photograph showing a typical oscillating counterflow. To the knowledge of the author the instability phenomena in axisymmetric, buoyant jets in counterflows have not previously been described.

However, a somewhat similar phenomenon was described by Robillard [1971] and Robillard and Ramamurthy [1974] for plane pure jets discharging into a counterflow. The jets seemed to bend over close to the slot and be swept downstream.

The oscillations were regular and showed no sideways motion. A series of photographs of one of Robillard's experiments is shown in fig. 7.2. Notice how the jet sweeps up and down from above and underneath the outlet device.

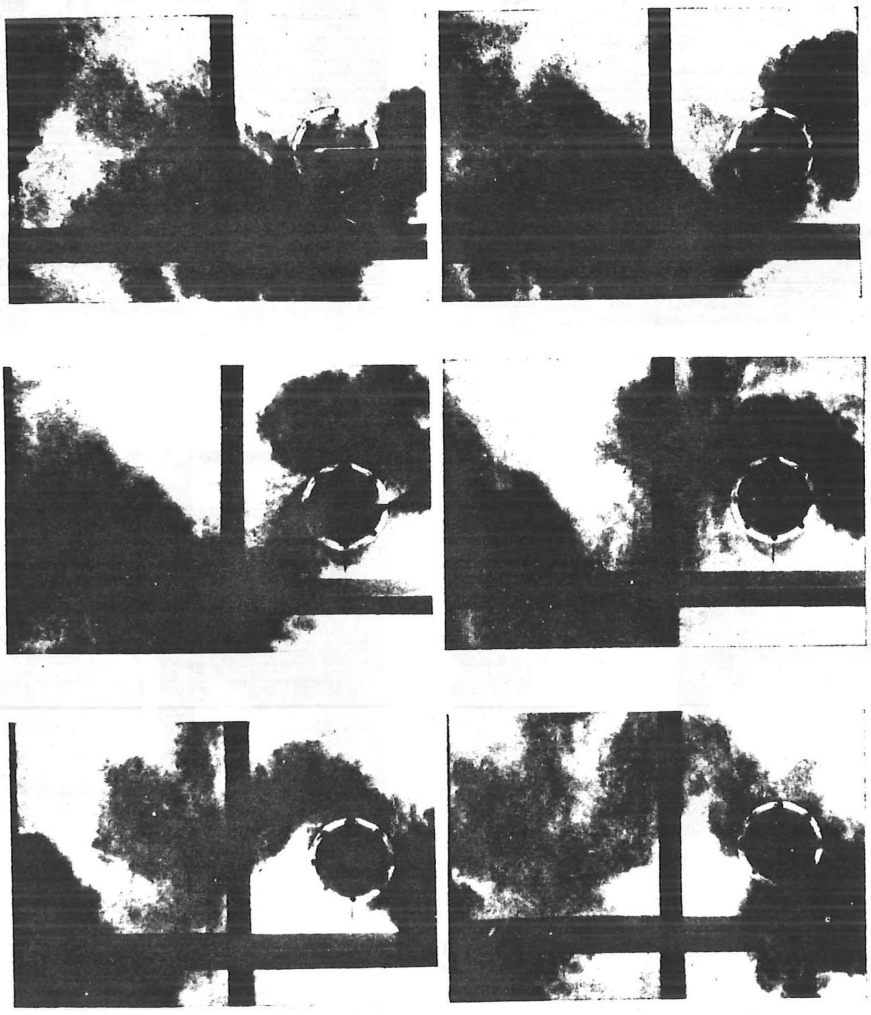

Fig. 7.2. Robillard's experiments with a plane non-buoyant jet in a counterflow.

Robillard described the formation of the oscillations in the following way:

the jet behaves in the counterflow as if it were a solid solid body behind which vortices similar to von Kármán vortices are formed from alternating sides. The Strouhal number was defined as

$$\frac{f d_p}{U_\infty}\left(\frac{U_o}{U_\infty}\right)^2$$

where f is the frequency of the oscillations

In accordeance with Robillard's description the Strouhal number of the oscillations was found to be a function of the specific Reynold's number defined as

$$R = \frac{\rho U_\infty d_p}{\mu}\left(\frac{U_o}{U_\infty}\right)^2 = \frac{\rho U_o d_p}{\mu}\left(\frac{U_o}{U_\infty}\right)$$

In Robillard's experiments R was varied between $7.9\text{x}10^3$ and $8.6\text{x}10^4$ and U_o/U_∞ was varied between -0.08 and -0.31. (U_∞ is negative in counterflows) . Thus the flow was well within the fully turbulent regime.

It is not known how the perturbations in the jet outline are created. However, they can be described as the jet outline being intermittent or 'wobbly'. Kotsovinos [1975] measured the intermittency and crossing of hot/cold interfaces in plane (almost) pure jets and in plane pure plumes in still ambient and from his data it can be seen that the frequency in a given pure jet decreases downstream.

A second phenomenon was observed in jets in counterflow, coflow and still ambient; when the port was sufficiently close to the free surface and/or the Froude number was sufficiently large then the jet tended to 'cling' to the free surface in a manner similar to the Coanda effect for solid surfaces. (See fig. 7.3.b (jet in still ambient), fig. 7.4.b (jet in a coflow) and fig. 7.5.b (jet in a counterflow)).

The Coanda effect can be explained as follows:

The free surface is a surface through which there can be no flow. To satisfy this entrainment condition the flow field induced by the jet below the free surface can be viewed as being balanced by an image flow field of equal strength from an image jet above the free surface. This image field draws the trajectory of the lower jet to the surface and vice versa for the image jet.

In counterflows, where both the oscillation phenomenon and the clinging phenomenon can occur, it was found in the experiments that they could interact in a variety of ways.

In the following a qualitative description and classification of the occurrence of these two phenomena is given. Dimensional analysis has been performed to determine suitable parameters to describe the occurence of oscillations or clinging behaviour in jets. From this a

stability criterion has also been found. Based on this an experimentally determined flow regime chart is presented.
Frequency measurements of the oscillating instabilities are presented and are also plotted according to the results from a dimensional analysis.

7.2. Types of behaviour - classification.

Jets in still ambient.

For buoyant jets in still ambient two types of behaviour were observed. These two types are shown in figs. 7.3.a and 7.3.b.

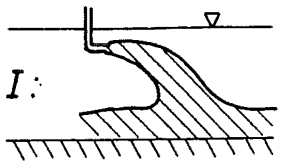

Fig. 7.3.a Type I jet in still ambient.

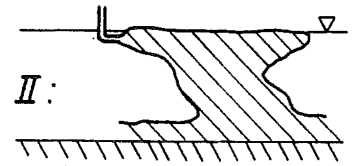

Fig. 7.3.b. Type II jet in still ambient.

The flow in figure 7.3.a which we will denote type I is characterised by the trajectory moving in the direction of the buoyancyand with no interaction with the surface. When the Froude number is increased and/or the port is moved closer to the free surface a flow like the one shown in fig. 7.3.b results. It is called type II flow and ressembles a surface jet. However, gravity eventually forces the jet from the free surface.

Jets in a coflow.

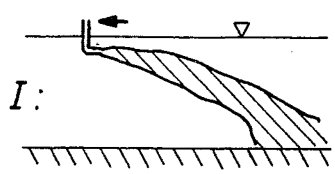

Fig. 7.4.a. Type I jet in a coflow.

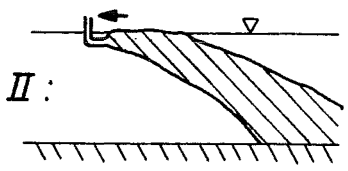

Fig. 7.4.b. Type II jet in a coflow.

For jets in coflow there is either no-clinging or clinging behaviour as shown in figs. 7.4.a and 7.4.b. The situation shown in fig. 7.4.a where there is no interaction with the free surface is denoted type I and the situation in fig. 7.4.b where there is contact with the free surface before gravity forces the jet downwards is called type II.

Jets in counterflow.

For jets in counterflow both the clinging phenomena and the instability phenomena can occur and they can interact in the ways as illustrated in figs. 7.5.a-7.5.d.
Five different types of behaviour were observed.
In type I (fig. 7.5.a) the jet behaves in principle like a jet in still ambient type I or a jet in coflow type I.
Type II which is shown in fig. 7.5.b is also equivalent to type II for jets in still ambient and in a coflow.
Type I and II are the only stable configurations in counterflow.
Type III is shown in fig. 7.5.c. It is an oscillating flow where the direction of discharge changes periodically in the vertical direction, and at times it changes in the transverse direction as well. However, the majority of the recordings were done from the side only. The amplitude of the periodic motion is not large enough for the effluent to reach the free surface.

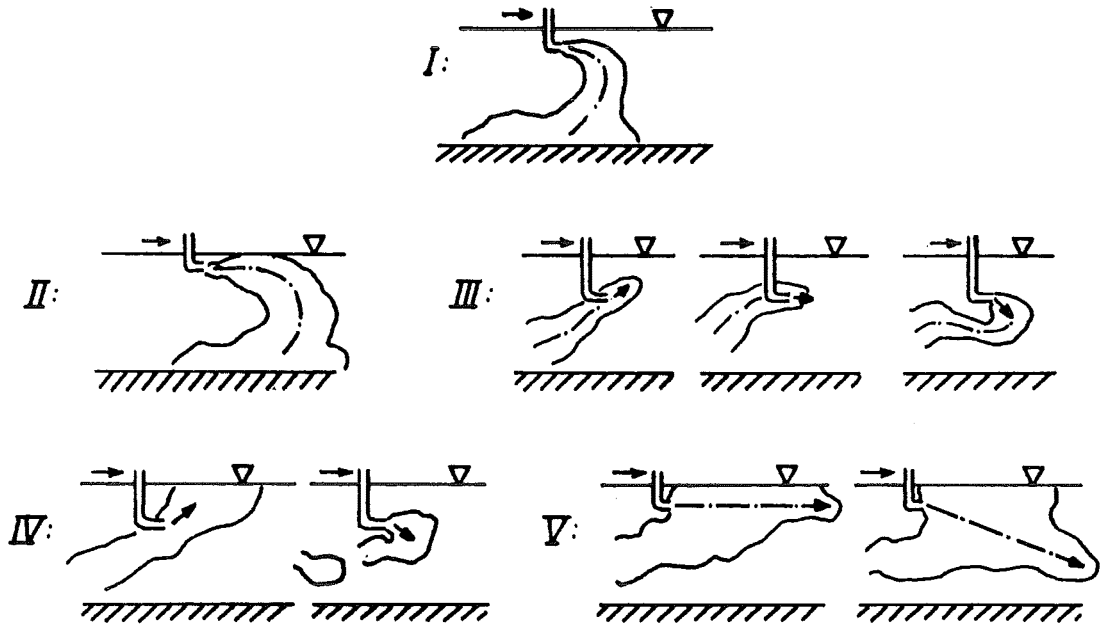

Fig. 7.5a-e. Types of behaviour in a buoyant jet in a counterflow.

Type IV as shown in fig. 7.5.d is characterised by the oscillatory motion of type III. Here the amplitude of the oscillations is so large that the effluent reaches the free surface and clings to it before breaking off in a large cloud. This leads to the diluted effluent reaching the bottom (which corresponds to the surface in the sea) in large intermittent clouds. This phenomenon has been observed at some ocean outfalls.

Type V is shown in fig. 7.5.e In this case the jet is in constant contact with the surface like in type II (fig. 7.5.b) but it also shows the oscillatory motion of types III and IV.

7.3. Qualitative experiments.

Experiments with port diameters d_p=0.89 cm, 0.58 cm and 0.33 cm and port to surface distances d'=4.5, 10 and 20 d_p were carried out with negatively buoyant jets to explore the extent of each flow regime.
Experiments were made for coflow ($U_\infty/U_0>0$), still ambient ($U_\infty/U_0=0$) and counterflow ($U_\infty/U_0<0$).
The following three parameters were varied: the densimetric Froude number Fr, the velocity ratio U_∞/U_0, and the distance from the port to the free surface relative to the port diameter d'/d_p.

The data suggested that the oscillation phenomenon is linked to the parameters U_∞/U_0 and Fr and the clinging phenomenon is linked to some combination of the parameters U_∞/U_0, Fr and d'/d_p.

A jet in a counterflow is shown in fig. 7.6. The point where the flow reverses is called T. The outline of any jet is not completely fixed but exhibits some unevenness which varies with time (intermittency). It is assumed that the amplitude of these perturbations is proportional to the local width which is the only local length scale. It is further assumed that point T is the critical point in the flow; if the amplitude of the perturbations at T exceeds the depth of T below the port, L_{VT}, by a certain factor then an oscillation will develop. From the discussion in chapter 5 it can be seen directly that the horizontal part of the jet is a MDNF region and this means that the local width b grows linearly with the distance from the port (cfr. (4.2.7)).
The amplitude of the perturbations at T are therefore proportional to L_{HT}, the horizontal

distance of the point T from the port.

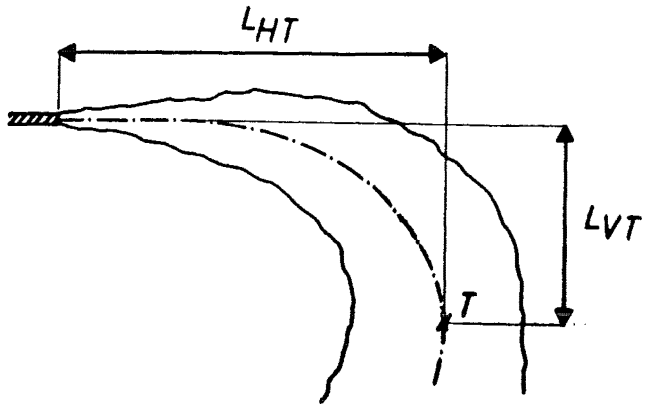

Fig. 7.6. Sketch of a buoyant jet in a counterflow.

This has to be compared against the distance L_{VT}, cfr. the assumption above.

It is then assumed that an instability will occur if the ratio L_{HT}/L_{VT} exceeds a certain critical value C:

$$\frac{L_{HT}}{L_{VT}} > C \tag{7.3.1}$$

Simple dimensional analysis gives

$$\frac{L_{HT}}{L_{VT}} = \Phi\left(\frac{M_e^{1/2}\, U_\infty^2}{B}\right) = \Phi\left(Fr^2\left(\frac{U_\infty}{U_o}\right)^2\right) = \Phi^*\left(Fr\,\frac{U_\infty}{U_o}\right)$$

where Φ and Φ^* are unknown functions.

Thus (7.3.1) becomes

$$\Phi^*\left(Fr\frac{U_\infty}{U_o}\right) > C \tag{7.3.2}$$

If we assume that Φ^* is a monotonically decreasing function then (7.3.2) can be expressed as

$$Fr\left|\frac{U_\infty}{U_o}\right| > C^* \tag{7.3.3}$$

where C^* is a constant .

The available data have been plotted in fig. 7.7. The data suggest a value of $C^* = 0.6$. We then have

$$Fr > 0.6\left(\left|\frac{U_\infty}{U_o}\right|\right)^{-1} \quad : \text{unstable flow} \tag{7.3.4}$$

$$Fr < 0.6\left(\left|\frac{U_\infty}{U_o}\right|\right)^{-1} \quad : \text{stable flow} \tag{7.3.5}$$

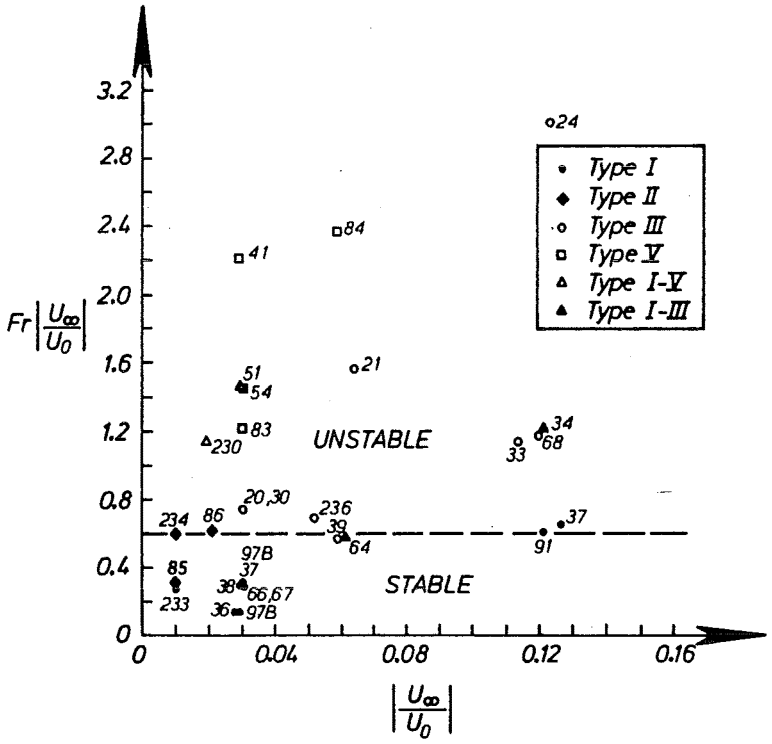

Fig. 7.7. Plot of stable/unstable regimes in a counterflow.

[Eq. (7.2.3) could also be written as $l_{MeB} > l_{MeU\infty}$ (cfr. the definitions of l_{MeB} and $l_{MeU\infty}$). This condition means there is no BDNF region in an unstable jet cfr. chapter 4. In a similar way it can be shown that a stable jet always has a BDNF region.]

In order to find a criterion for when clinging takes place it is necessary to distinguish between two types of clinging:

The clinging mechanism we choose to call 'passive clinging' occurs when the upper boundary of the otherwise stable jet gets so close to the free surface that it necessarily will interact with it (~ clings to it). This type of clinging is therefore the mechanism that transforms a type I jet into a type II or V jet in counterflows.

If Fr $(U_\infty/U_0) < 0.6$ (i.e. no oscillations) but the clinging condition (which we are going to derive) is satisfied, then it will be a type II jet.

If Fr $(U_\infty/U_0) > 0.6$ and the clinging condition is satisfied, then the jet will be a type V jet.

The second clinging mechanism is where the trajectory of the jet varies considerably with time. It will be called intermittent clinging. It occurs when the amplitude of the oscillations in a type III flow become so large that the jet during the upwards part of the motion gets sufficiently close to the free surface to cling to it. Then a type III flow becomes a type IV flow (see fig. 7.8.b).

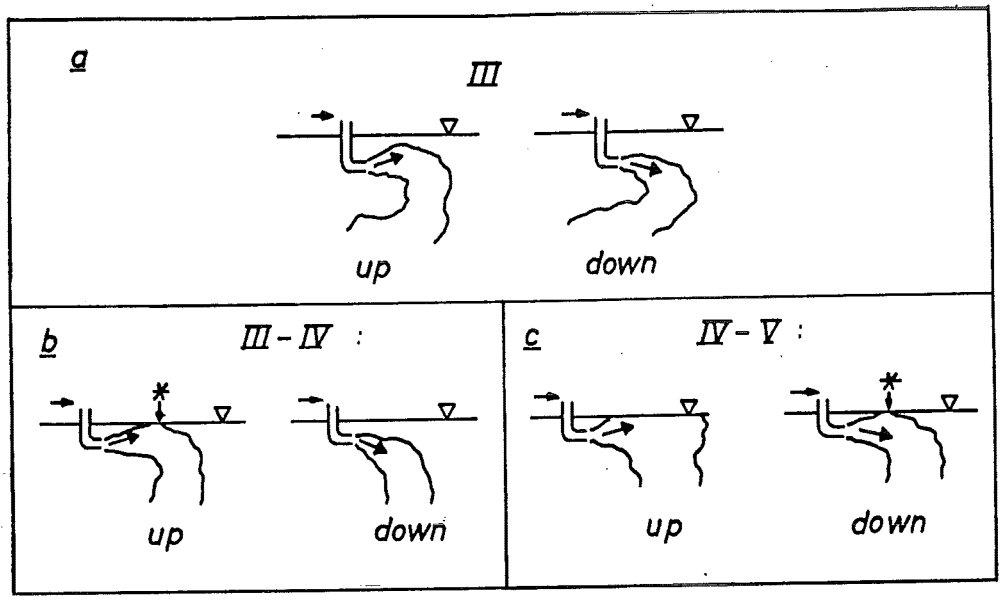

Fig. 7.8. Transformations between different types of flow.

When the jet is in contact with the free surface when it is in its lowest position (discharging downwards) (see fig. 7.8.c) then the type IV flow has become a type V flow.

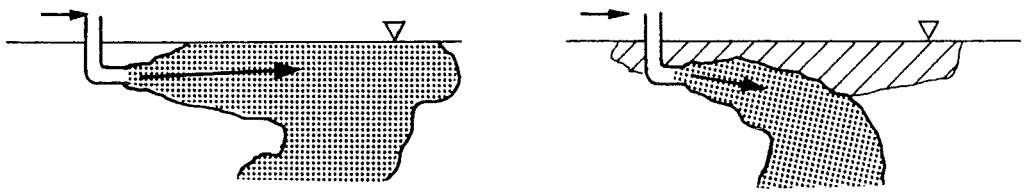

Fig. 7.9. A 'false' type V flow.

Some runs showed that although the lowest postion of the jet was well below the free surface the jet still appeared to be constantly in contact with the surface. For this case the

frequency of the oscillations was so high and the ambient velocity so low that effluent, which had been discharged under the free surface during the previous upwards movement of the discharge, had not had time to fall or be convected away (see fig. 7.9).

The form of criterion for passive clinging can also be derived if it is assumed that passive clinging occurs when the upper boundary of the jet gets sufficiently close to the free surface. (We are here looking at stable jets and according to the comments in the discussion of a stability criterion earlier in this section this means that the jet has a MDNF region followed by a BDNF region).

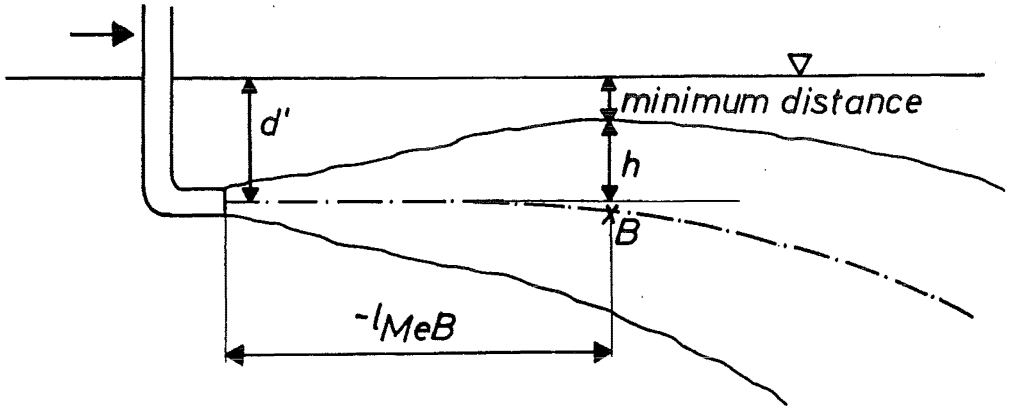

Fig. 7.10. Sketch of a buoyant jet in a counterflow.

In the momentum dominated initial part of the jet (MDNF) the trajectory is almost horizontal and because of the growth of width of the jet its upper boundary gets increasingly closer to the free surface (see fig. 7.10). It is at its closest to the free surface in point B where the effect of buoyancy is just being felt (transformation from MDNF to BDNF) and the trajectory starts moving considerably downwards. From the discussion of length scales in chapter 4 we know that the effect of buoyancy starts being felt at a distance from the port of an order of magnitude of l_{MeB}. The region up to point B is momentum dominated and therefore

$$db/ds = k \tag{7.3.6}$$

That means that the distance from the highest point of the upper jet boundary to the port, y, (see fig. 7.10) is given by

$$y \sim k\, l_{MeB} \tag{7.3.7}$$

We now assume that if the ratio of y to d', the distance from the port to the free surface,

exceeds a certain value C_1 then passive clinging will occur, i.e. $y/d' > C_1$ means clinging.

$$\frac{y}{d'} \sim \frac{{}^{l}M_e B}{d'} \sim \frac{Fr\, d_p}{d'} = \frac{Fr}{d'/d_p} > C_1^* \tag{7.3.8}$$

where C_1^* is a constant.

Experiments give a value of C_1^* of 5.3, see fig. 7.11. The stability criteria (7.3.4) and (7.3.5) have also been shown in fig. 7.11.

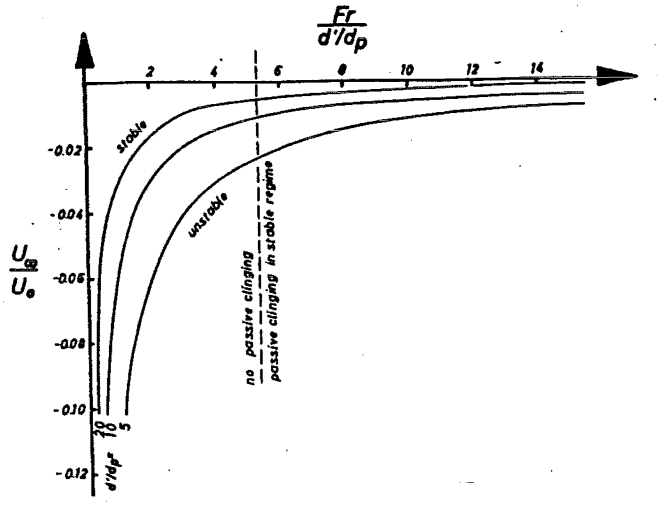

Fig. 7.11. Diagram of stable vs. unstable flow.

The intermittent clinging mechanism is more complex than the passive clinging because it takes place in an unstable flow and depends on the amplitude of the oscillations.
The conditions for the transformations type III to type IV and type IV to type V have therefore not been derived here. It has been found that if the data are plotted versus U_∞/U_0 and $Fr/(d'/d_p)$ then they form distinct regimes, see fig. 7.12. The boundary between types I and the remaining types is actually a number of curves, depending on the value of d'/d_p, cfr. fig. 7.11. As mentioned above, the boundaries between type III and type IV and between type IV and type V have not been derived theoretically and are therefore represented as straight lines.
The values for $U_\infty/U_0=0$ correspond to jets in still ambient and for $U_\infty/U_0 > 0$ to coflow.
A few experiments were performed in a flume in which a positively buoyant jet was discharged horizontally into a moving fluid. These experiments confirmed what had been found in the experiments with a negatively buoyant jet near a free surface.
However, as there is little friction at the water surface, the length of the attached part of the jet will be greater than the case where the surface is solid.

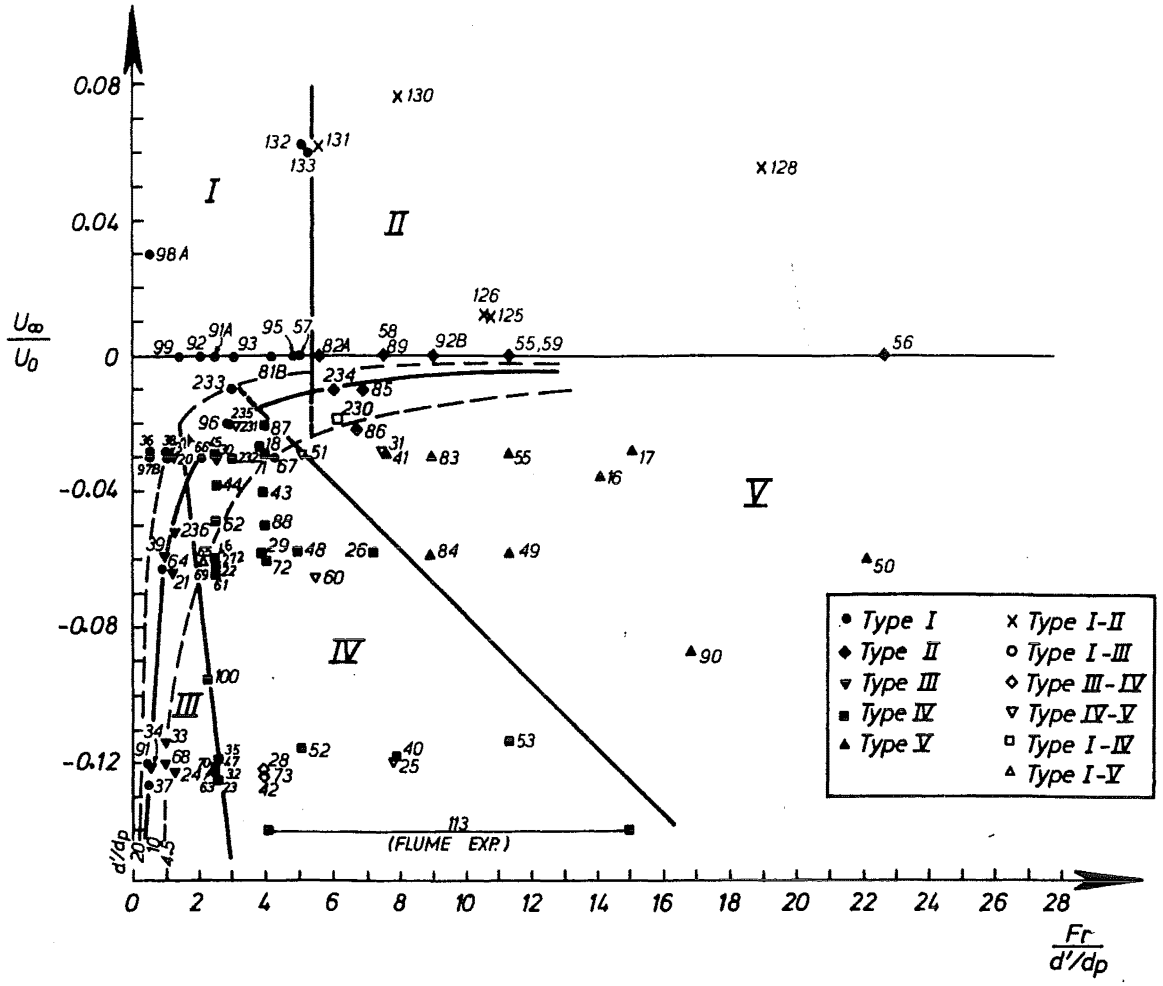

Fig. 7.12. Regime chart for buoyant jets in coflow, still ambient and counterflow.

7.4. Frequencies of the oscillations.

For the type III flows the frequencies of the oscillations could be found from photographs or video recordings of the runs.

No attempt was made to determine the frequency of the oscillations for types IV and V.

The quantities that govern the flow are

$$Q \sim U_0 d_p \tag{7.4.1}$$

$$M_e \sim U_0^2(1 - U_\infty/U_0)d_p \tag{7.4.2}$$

$$B \sim U_0 A_0 d_p \tag{7.4.3}$$

U_∞ (7.4.4)

Observations show that the oscillations take place in the momentum dominated part of the jet.

This suggests that although the initial buoyancy flux B plays a role in determining whether a jet is unstable or not, it is not an important parameter in unstable (oscillating, type III) flows. Then the important parameters must be Q, M_e and U_∞.

We want to find the frequency of the oscillations as a function of Q , M_e and U_∞.

We can write $f = h(Q , M_e, U_\infty)$ where h is an unknown function.

Buckingham's π theorem gives us that there can be formed 2 non-dimensional parameters. If Q and M_e are chosen as the repeating variables then

$$\frac{f}{Q^2/M_e^{3/2}} = h^*\left(\frac{U_\infty Q}{M_e}\right) \qquad (7.4.5)$$

which can be written as

$$\frac{d_p f}{U_o} = h^*\left(\frac{U_\infty}{U_o}\right) \qquad (7.4.6)$$

where h^* is an unknown function.

In fig. 7.13 the available data have been plotted as $d_p f/U_\infty$ versus U_∞/U_0.

There are no data for values of $U_\infty/U_0 > -0.045$, cfr. fig. 7.12. Also, there are only data for $U_\infty/U_0 > -0.20$. It was judged that for U_∞/U_0 values any smaller than -0.20 the flow would change character and the jet would become more like a wake where the dimensional arguments applied earlier no longer would hold.

The oscillations that were observed in the flows were very irregular and of varying size. Often oscillations occurred in pairs and triplets. Now if pairs and triplets of large oscillations were considered as only one oscillation and all small oscillations were ignored then a value of f was found which was about 1/3 - 1/2 of the value that was found when all oscillations were counted. This explains the large error bars in fig. 7.13.

The results in fig. 7.13 indicate that the Strouhal number fd_p/U_∞ is a constant independent of U_∞/U_0 and equal to approximately 0.02.

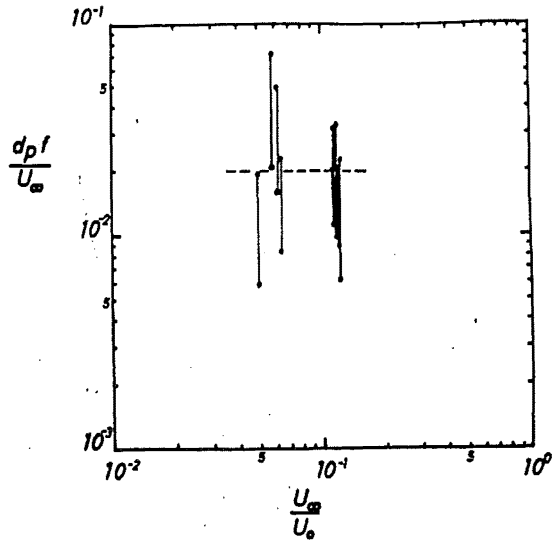

Fig. 7.13. Strouhal number versus velocity ratio for type III counterflows.

It should also be noted that photographs were taken of the early runs whereas video recordings were available of later runs. Since video recordings show a flow in much greater detail than a series of photographs it would be expected that the frequencies which are found from photographs would be lower than if they had been found from a video recording. There does not seem to be any dependency of the Strouhal number on the relative distance between the port and the free surface, d'/d_p.

Unlike Robillard's experiments, the present oscillations were very irregular.

Fig. 7.13 has confirmed the present dimensional analysis. This shows that the mechanism which generates oscillations in axisymmetric jets in a mild counterflow ($-0.04 > U_\infty/U_0 > -0.12$) is generated by perturbations in the initial part of the flow before it has become fully developed.

CHAPTER 8
CONCLUSIONS

In the present work progress has been made in 3 areas:
Firstly, a comprehensive dimensional analysis has been performed on the flow in horizontal buoyant jets in a co-, cross- or counterflow. As a result, charts have been obtained which enable the flow regions MDNF, MDFF, BDNF and BDFF to be determined as a function of the traditional engineering variables Fr, U_∞/U_0 and the dimensionless distance from the port. The transitions between the regions are determined only approximately and further experimental data are required to define them precisely.
Formulae for trajectories and dilution in these regions have been obtained. The coefficients in the formulae have been determined by analysing all available relevant data. On the basis of this charts for dilution and trajectory have been produced (figs. 5.30 - 5.34). From these charts it is possible to predict the trajectory and dilution in any horizontal jet in a co-, cross- and counterflow. In the transitions between regions in a jet the charts only give approximate values in some cases. Additional experiments are required to accurately determine the variation of the coefficients. The available data were usually not sampled over a sufficiently long region.

In most ocean outfalls the densimetric Froude number of the jets is between 1 and 10. Because of this , the jets are almost entirely buoyancy dominated. It was shown in chapter 5 that in the BDNF and BDFF regions the initial direction of discharge does not affect the flow. Thus the results found for the BDNF and BDFF can be applied to jets discharging at any angle between 0^o and 360^o to the ambient flow. However, it may be beneficial to design outfalls which discharge at higher Foude numbers than 10. For those cases the present analysis of jets in the MDNF and MDFF regions show that the dilution has the same functional relationship with respect to the depth whether the jet is co-, cross- or counterflowing or in still ambient but the coefficients are ~~0~~ 100% greater than those for coflows in MDFF ~~i.e. the dilutions are, all else equal, approximately 50% greater~~.
There were no dilution data available for counterflowing jets in the momentum dominated regions, but they would be expected to be similar to the dilutions in co-flowing jets. Cameron & Ho [1985] compared dilutions in co- and counterflowing jets and found them to be of an equal order of magnifude. Dilutions in jets in still ambient are considerably below the dilutions in similar jet in a moving ambient.
The best dilution over a certain depth in a momentum dominated jet is then obtained in a strong crossflow . For buoyancy dominated jets the best dilution is obtained in any strong ambient flow.

The least dilution is obtained in a jet in still ambient.

In an attempt to obtain a more detailed understanding of the jet behaviour particularly in transition regions general equations have been derived. In the derivation it has been assumed that the flow field in a jet can be considered as composed of a flow with circular cross sections and Gaussian distribution (category I flow) and a flow with a vortex pair distribution (category II flow). Accordingly, the excess velocity is resolved in two components corresponding to these two types of flow. The equations reduce to give correct solutions for the limiting cases and some progress has been made in obtaining a closure equation which adequately describes the transitions from the MDNF to the BDNF , the MDNF to the MDFF in coflows and from the MDFF to the BDFF.
A further closure equaiton is required to describe the general flows which involve a transition from category I flow to category II flow.
Further work in this area is necessary.
Indeed it seems to the author that completion of this problem will be necessary before the complex problem of the merging of buoyant jets can be understood.

The third area in which progress has been made is the study of instability of counterflowing jets. Although dilutions in a counterflowing stable jet are comparable to the dilutions in similar coflowing jets this can not be expected in unstable counterflowing jets in which case the effluent tends to form big 'clouds'. This is therefore a situation that should be avoided.
The jets were found to be stable when $Fr\,|\,U_\infty/U_0\,| < 0.6$.
An effect similar to the Coanda effect for solid surfaces was observed and has been described. A stable jet was found not to cling to the surface when $Fr/(d'/d_p) < 5.3$. [The surface in the present experiments corresponds to the sea bed in prototypes].
Clinging would probably improve the dilution (Sharp [1975] found surface dilutions in circular wall jets to be up to two times the surface dilutions in similar non-clinging jets).
The behaviour of counterflowing jets was classified and a flow regime chart produced on the basis of extensive experiments, fig. 7.12.
Dimensional analysis was also used to analyse the frequency of one particular type of instability, the type III flow, where the jet oscillates freely without interacting with the surface. The Strouhal number defined as $d_p f/U_\infty$ was found to be constant ≈ 0.02.

Chapter 9
References

Abraham, G. [1963]
Jet diffusion in stagnant ambient fluid, Delft Hydraulics Laboratory, Publication No. 29, Series 1, Group 14, Section 14.42.

Abraham, G. [1971]
The flow of round buoyant jets issuing vertically into ambient fluid flowing in a horizontal direction, Delft Hydraulics Laboratory, Publication No. 81, Series 1, group 14, Section 14.42.

Abramowich, G.N. [1963]
The theory of turbulent jets, (translation by scripta technica , technical editing by Lean H. Schindel) The M.I.T. Press, Massachusetts Institute of Technology, Cambridge, Massachusetts.

Albertson, M.L. , Dai, Y.B. , Jensen, R.A. & Rouse, H. [1950]
Diffusion of submerged jets, Transactions of American Society of Civil Engineers, Paper No. 2409, Vol. 115, pp 639-664

Antonia, R.A. & Bilger, R.W. [1974]
The prediction of the axisymmetric turbulent jet issuing into a co-flowing stream, The Aeronautical Quarterly, Vol. XXVI, pp. 69-80.

Ayoub, G.M. [1971]
Dispersion of buoyant jet in a flowing ambient fluid, PhD thesis, University of London.

Ayoub, G.M. [1973]
Test results on buoyant jets injected horizontally in a cross flowing stream, Water Air and Soil Pollution, Vol. 2 (1973), pp. 409-426.

Biringen,S [1975]
An experimental study of a turbulent axisymmetric jet issuing into a co-flowing air-stream. Von Kármán Institute (Rhode St. Genèse) VKI TN 110.

Brown, I. [1984]
Preliminary investigations of the performance of an ocean outfall diffuser in a crossflow,

Master's thesis, Department of Civil Engineering, University of Canterbury, Christchurch, New Zealand. Report 84-5.

Bühler, J. & Hauenstein, W. [1979]
Axisymmetric jets in a crossflow, IAHR congress, Cagliari 1979, C.c. 4.

Cameron, I. & Ho, G.E. [1985]
Disposal of wool scouring effluent in an estuarine environment,Australasian Conference on Coastal and Ocean Engineering, Christchurch, New Zealand, 2-6 December 1985, Vol. I pp. 183-192.

Cederwall, K. [1968]
Hydraulics of marine waste water disposal, Chalmers Institute of Technology, Göteborg, Sweden.

Challen, J. [1968]
Mixing in turbulent jet flows, Master's thesis, Department of Mechanical Engineering, The University of Sydney.

Chan, T.-L. & Kennedy, J.F. [1972]
Turbulent nonbuoyant or buoyant jets discharged into flowing or quiescent fluids, IIHR report No. 140, Iowa Institute of Hydraulic Research, The University of Iowa, Iowa City, Iowa.

Chu , V. H. [1975]
Three dimensional forced-plumes in a laminar cross-flow, 15th Congress IAHR, Sao Paolo, 1975, V.5, paper 2.1.

Crow S. C. & Champagne, F.H.[1971]
Orderly structure in jet turbulence, Journal of Fluid Mechanics, 48, pp. 547-591.

Fan, L.-N. [1968]
Turbulent buoyant jets into stratified or flowing ambient fluids, W.M. Keck Laboratory of Hydraulics and Water Resources, Div. of Engineering and Appl. Science, Caltech, Pasadena, California.

Fischer, H.B. , List, E.J. , Koh, R.C.Y., Imberger,J. & Brooks, N.H. [1979]
Mixing in inland and coastal water, Academic Press, New York.

Fox, D.G. [1970]
Forced plume in a stratified fluid, J. Geophys. Res., Vol. 75, pp. 6818-6835.

Gordier, R.L. [1959]
Studies on fluid jet discharging normally into moving liquid, St. Anthony Falls Hydraulic Laboratory, University of Minnesota, Technical Paper No. 28, Series B.

Hansen,J. & Schrøder, H. [1968]
Horizontal jet dilution studies by use of radioactive isotopes, Acta Polytechnica Scandinavia, Civil Engineering and Building Construction Series No. 49, Copenhagen, Denmark.

Hirst, E.A. [1971]
Analysis of round, turbulent, buoyant jets discharged to stratified, flowing ambients,. Oak Ridge National Laboratory, Report No. ORNL-4685, Oak Ridge.

Hydraulic Research Station [1977]
Horizontal outfalls in flowing water, Hydraulics Research Station report No. EX 763, Wallingford Hydraulics Research Station.

Hutter, K. [1978]
A note on entrainment in turbulent jets and plumes, Iranian Journal of Science and Technology, Vol. 7, pp 1-12, Pergamon Press Ltd.

Keffer, J.F. & Baines, W.D. [1963]
The round turbulent jet in a cross-wing, Journal of Fluid Mechanics, Vol. 15, pp. 481-496.

Kotsovinos , N. E. [1975]
A study of the entrainment and turbulence in a plane buoyant jet. PhD thesis, California Institute of Technology, Pasadena, California, Report No. KH-R-32.

Landis, F. & Shapiro, A. H. [1951]
Heat transfer and fluid mechanics Institute, Reprints of papers, p. 133.

Lee, J. H. W. & Neville-Jones, P. [1987]
Initial dilution of horizontal jet in crossflow, ASCE, Vol. 113, No. 5.

List, E.J. & Imberger, J. [1973]
Turbulent entrainment in buoyant jets and plumes, ASCE, HY 9, pp. 1461-1474.

Madni, I.K. & Pletcher, R.H. [1975]
Prediction of turbulent jets in coflowing and quiescent ambients, Transactions of the ASME Journal of Fluids Engineering, 1978, pp. 558-567.

Morton, B. , Taylor, G.I. & Turner, J. S. [1956]
Turbulent gravitaional convection from maintained and instantaneous sources, Proceedings of the Royal Society of London, A 234, pp 1-23.

Noutsopoulos, G. & Yannopoulos, P. [1985]
The round vertical turbulent buoyant jet, Civil Engineering Department, National Technical university of Athens, Greece.

Papanicolaou, P.N. [1984]
Mass and momentum transport in a turbulent buoyant vertical axisymmetric jet, PhD thesis, W.M. Keck Laboratory of Hydraulic and Water Resources, California Institute of Technology, Pasadena, California.

Patel, R.P. [1971]
Turbulent jets and wall jets in uniform streaming flow, The Aeronautical Quarterly, Vol. XXII, November 1971, pp 311-326

Platten, J.L. & Keffer, J.F. [1971]
Deflected turbulent jet flows, Transactions of the ASME Journal of Applied Mechanics.

Pratte, B.D. & Baines, W.D. [1967]
Profiles of the round turbulent jet in a crossflow, ASCE, Hydraulics division, Vol. 93, HY 6, pp. 53-64.

Priestley, C.H.B. & Ball, F.K. [1955]
Continuous convection from an isolated source of heat, Quarterly Journal of Royal Meteorological Society, Vol. 81, (348), pp. 144-157.

Rajaratnam, N. [1976]
Turbulent jets, Developments in Water Science Series, No. 5, Elsevier Scientific Publishing Co.

Richards, J.M. [1963]
Experiments on the motions of isolated cylindrical thermals through unstratified surroundings, International Journal for Air and Water Pollution, Pergamon Press, Vol. 7, pp. 17-34.

Richards, J.M . [1965]
Puff motions in unstratified surroundings, Journal of Fluid Mechanics, Vol. 21, part 1, pp. 97-106.

Robillard, L. [1971]
Mouvement périodique d'un jet bidimensionel plan dans un contre-courant et production de tourbillons alternés, Jounal de Méchanique, Vol. 10, No. 1.

Robillard, L. & Ramamurthy, A.S. [1974]
Experimental Investigation of the vortex street generated by a plane jet in a counter flow, Transactions of the ASME Jounal of Fluids Engineering, March 1974, pp. 43-48.

Rodi, W. (ed.) [1982]
Turbulent buoyant jets and plumes, HMT The Science & Applications of heat and mass transfer. Pergamon Press.

Rodi, W. & Spalding, D.B. [1970]
A two-parameter model of turbulence and its application to free jets, Wärme- und Stoffübertragung, Vol. 3, p. 85.

Rouse, H. , Yih, C.S. & Humphreys , H. W. [1952]
Gravitational convection from a boundary source, Tellus IV, (1952), pp. 201-210.

Schatzmann, M. [1976]
Auftriebsstrahlen in natürlichen Strömungen. Entwicklung eines matematischen Modells, Sonderforschungsgebiet 80, Aufbreitungs- und Transportvorgänge in Strömungen, Universität Karlsruhe, SFB 80/ T / 86.

Schatzmann, M. [1979]
An integral model of plume rise, Atmospheric Environment, Vol. 13, pp. 721-731, Pergamon Press Ltd.

Schmidt, F.H. [1957]
On the diffusion of heated jets, Tellus IX 3, pp. 378-383.

Scorer, R.S. [1959]
The behaviour of chimney plumes, International Journal for Air Pollution, Vol. 1, pp. 198-220.

Sharp, J.J. [1975]
The use of a buoyant wall jet to improve the dilution of a submerged outfall, Proceedings of the Institution of Engineers, Part 2, Vol. 59, pp. 527-534.

Smith, D.J. & Hughes, T. [1977]

Some measurements in a turbulent circular jet in the presence of a co-flowing free stream, The Aeronautical Quarterly.

Wright, S.J. [1977 I]
Effects of ambient crossflows and density stratification on the characteristic behaviour of round turbulent buoyant jets, W.M. Keck Laboratory of Hydraulics and Water Resources, Division of Engineering and Applied Science, California Institute of Technology, Pasadena, California.

Wright, S.J. [1977 II]
Mean behaviour of buoyant jet in a crossflow, ASCE HY5, May 1977, pp. 499-513.

Wygnanski, I . & Fiedler, H. [1969]
Some measurements in the self-preserving jet, Journal of Fluid Mechanics, 38, pp. 577-612.

APPENDIX A
EXPERIMENTAL DATA

List of qualitative experiments.

Abbreviations and symbols

Fr: densimetric Froude number

K : velocity ratio = U_0/U_∞

d_p: port diameter

D' : d'/d_p , where d' is distance from port to surface

M : method of recording the experiment

O is observations

P is photographs

V is video recordings

Type refers to the type of behaviour of the jet, cfr. chapter 7

f : the frequency of type III oscillations

Fr' = Fr/D'

St = $f\, d_p/U_\infty$ the Strouhal number of the oscillations

Comm: comments

Run	Fr	K	d_p	D'	M	Type	f	Fr'	St	Comm.
16	70.5	-0.036	0.91	5	P	V		14.1		
17	75.2	-0.028	0.91	5	P	V		15.04		
18	77.9	-0.027	0.89	20	O+P	IV?		3.90		
20	24.8	-0.030	0.89	20	O+P	III		1.24		
21	24.6	-0.064	0.89	20	O+P	III	.071-.187	1.23	.56-1.46	
22	24.5	-0.064	0.89	10	O+P	IV		2.45		
23	25.5	-0.125	0.89	10	O+P	IV		2.55		
24	25.2	-0.123	0.89	20	O+P	III	.10-.36	1.26	.76-.36	
25	78.7	-0.119	0.89	10	O+P	IV-V?		7.87		
26	72.0	-0.058	0.89	10	O+P	IV		7.20		
27	24.8	-0.061	0.89	10	O+P	IV?		2.48		
28	78.1	-0.122	0.89	20	O+P	III?		3.91		
29	77.6	-0.056	0.89	20	O+P	IV		3.88		
30	25.2	-0.030	0.89	10	O+P	III		2.52		
31	75.0	-0.028	0.89	10	O+P	(IV-)V	7.50			
32	24.9	-0.123	0.89	10	O+P	IV		2.49		
33	10.0	-0.114	0.89	10	O+P	III	.066-.120	1.00	1.27-2.30	
34	10.0	-0.121	0.89	20	O+P	I-III	.056-.130	0.50	1.08-2.51	
35	25.5	-0.119	0.89	10	O+P	IV		2.55		
36	5.2	-0.028	0.89	10	O+P	I		0.52		
37	5.2	-0.126	0.89	10	O+P	I		0.52		

Run	Fr	K	d_p	D'	M	Type	f	Fr'	St	Comm.
38	10.1	-0.029	0.89	10	O	I		1.01		
39	9.6	-0.059	0.89	10	O	III	.061-.190	0.96	1.23-3.84	
40	78.6	-0.118	0.89	10	O+P	IV?		7.86		
41	76.1	-0.029	0.89	10	O+P	V?		7.61		
42	78.0	-0.124	0.89	20	O+P	III(-IV?)	3.90			
43	78.0	-0.040	0.89	20	O+P	IV?		3.90		
44	50.1	-0.038	0.89	20	O+P	IV		2.52		
45	49.7	-0.029	0.89	20	O+P	IV		2.48		
46	49.0	-0.060	0.89	20	V	IV		2.45		
47	49.4	-0.120	0.89	20	V	III	.62-.98	2.47	2.42-3.84	
48	50.1	-0.058	0.89	10	V	IV-V		5.01		
49	50.8	-0.058	0.89	4.5	V	V		11.29		
50	50.8	-0.058	0.89	2.3	V	V		22.09		
51	50.7	-0.029	0.89	10	V	I-V		5.07		*1
52	50.8	-0.116	0.89	10	V	IV		5.08		
53	50.8	-0.113	0.89	4.5	V	IV		11.29		*2
54	50.8	-0.029	0.89	4.5	V	V		11.29		
55	50.8	0	0.89	4.5	O	II		11.29		
56	50.8	0	0.89	2.3	V	II		22.58		
57	50.0	0	0.89	10	V	I		5.0		
58	50.2	0	0.89	6.7	V	II		7.49		*3
59	50.8	0	0.89	4.5	V	II		11.29		
60	24.7	-0.065	0.89	4.5	V	IV-V		5.49		
61	24.7	-0.064	0.89	10	V	IV		2.47		*4
62	24.7	-0.049	0.89	10	V	IV		2.47		
63	25.1	-0.122	0.89	10	V	IV		2.51		*5
64	9.4	-0.062	0.89	10	V	I(-III)	.051-.150	0.94	1.04-3.06	
65	9.6	-0.061	0.89	4.5	V	(I-)IV		2.13		*6
66	9.6	-0.030	0.89	4.5	V	I		2.13		
67	9.6	-0.030	0.89	2.3	V	I		4.26		
68	9.8	-0.120	0.89	10	V	III	.059-.192	0.98	1.16-3.79	
69	48.3	-0.061	0.89	20	V	IV		2.41		
70	49.3	-0.121	0.89	20	V	III		2.46		*7
71	40.0	-0.029	0.89	10	V	IV		4.00		*8
72	40.0	-0.061	0.89	10	V	IV		4.00		
73	40.8	-0.122	0.89	10	V	IV		4.08		
81A	24.6	0	0.89	10	V	I		2.46		
81B	41.4	0	0.89	10	V	I		4.14		
82A	25.0	0	0.89	4.5	V	II		5.55		*9
82B	40.3	0	0.89	4.5	V	II		8.96		*10
83	40.2	-0.030	0.89	4.5	V	V		8.93		
84	40.1	-0.059	0.89	4.5	V	V		8.91		
85	30.9	-0.010	0.89	4.5	V	II		6.87		
86	29.9	-0.021	0.89	4.5	V	II		6.64		
87	40.0	-0.021	0.89	10	V	IV		4.00		*11
88	40.1	-0.050	0.89	10	V	IV		4.01		*12
89	75.1	0	0.89	10	V	II		7.51		
90	76.1	-0.087	0.89	4.5	V	V		16.91		
91	5.0	-0.121	0.89	4.5	V	I		0.50		
92	20.4	0	0.89	10	V	I		2.04		
93	30.4	0	0.89	10	V	I		3.04		
95	48.9	0	0.89	10	V	I		4.89		
96	29.8	-0.020	0.89	10	V	IV		2.98		*13
97A	10.4	-0.030	0.89	10	V	I		1.04		
97B	5.2	-0.029	0.89	10	V	I		0.52		*14
98A	5.3	+0.030	0.89	10	V	I		0.53		
99	29.9	0	0.89	21.9	O	I		1.37		
100	10.1	-0.095	0.89	4.5	V	IV		2.24		
113	45.0	-0.140	0.30	3-11	O	IV		4.1-15.0		*15

Run	Fr	K	d_p	D'	M	Type	f	Fr'	St	Comm.
125	55.7	+0.110	0.58	5.2	V	I-II		10.71		
126	54.6	+0.012	0.58	5.2	V	(I-)II		10.5		*16
127	∞	+0.019	0.58	22.4	V	II		∞		*17
128	98.1	+0.055	0.58	5.2	V	I-II		18.87		
129	76.1	+0.084	0.58	5.2	V	I-II		14.64		*18
130	40.8	+0.077	0.58	5.2	V	I-II		7.85		*19
131	56.8	+0.061	0.58	10.3	V	I(-II)		5.52		
132	103.8	+0.062	0.58	20.7	V	I		5.01		
133	53.9	+0.059	0.58	10.3	V	I		5.23		
230	60.8	-0.019	0.34	10.0	V	I-V		6.08		
231	30.1	-0.020	0.34	10.0	V	IV-V		3.01		
232	30.1	-0.030	0.34	10.0	V	IV		3.01		
233	30.1	-0.010	0.34	10.0	V	I		3.01		
234	60.8	-0.010	0.34	10.0	V	II		6.08		
235	30.1	-0.019	0.34	10.0	V	I-V		3.01		
236	13.4	-0.052	0.34	10.0	V	III	.040-.130	1.34	.30-.97	

*1: I in first half and V in second half of run
*2: very close to constant clinging
*3: not much deformed
*4: or I-V
*5: just touched the surface lightly
*6: I far most of the time
*7: a single cling
*8: behaved as V when clinging
*9: (I-V) not much deformed
*10: V very pronounced
*11: I-IV-V
*12: I-IV-V
*13: I much of the time
*14: In same tankfull as 97A
*15: positively buoyant effluent in flume
*16: just touched the surface
*17: Fr is probably effectively finite because of small temperature differences.
*18: vortex street behind port?
*19: smaller velocities than in 129.

List of concentration measurement experiments.

Run	Fr	K	d_p	x/d_p	y/d_p	s/d_p	$\lambda b/d_p$	S_{CL}	Comments
101	10.3	.000	0.89	28.4	10.0	31.2	3.92	8.7	
102	10.5	.000	0.89	34.4	19.8	42.1	5.49	14.0	
103	10.5	.000	0.89	31.6	14.8	36.5	5.20-5.12	12.9-12.3	*1
104	10.5	.000	0.89	24.3	5.6	25.6	3.24	6.3	
105	10.5	.000	0.89	37.5	24.4	48.3	6.36	17.4	
106	10.5	.000	0.89	37.5	24.7	48.3	6.21	18.0	
107	13.6	.030	0.89	47.2	17.4	52.3	5.23	11.9	
108	10.5	.029	0.89	41.4	19.7	46.7	4.88	12.7	
109	10.5	.060	0.89	48.0	17.4	51.6	5.18	15.0	
110	10.5	.029	0.89	51.7	31.8	62.6	6.92	23.7	
111	10.5	.060	0.89	75.4	35.4	83.4	9.66	44.0	
112	11.2	.060	0.89	51.2	19.3	57.5	5.36	16.8	
114	10.1	-.030	0.89	16.0	4.7	17.2	2.92	5.6	
115	10.1	-.030	0.89	28.4	19.3	37.1	-	≈21.9	*2
118	10.1	-.030	0.89	29.8	17.4	33.9	5.81	15.4	
122	10.1	-.030	0.50	25.4	47.2	65.0	11.30	59.0	
134	8.73	-.031	0.58	9.5	40.5	77.6	14.38	67.0	

Run	Fr	K	d_p	x/d_p	y/d_p	s/d_p	$\lambda b/d_p$	S_{CL}	Comments
137	10.4	.062	0.89	43.8	8.1	34.0	3.62	8.0	
139	25.2	.065	0.58	91.7	12.6	92.2	7.48	21.9	
140	25.2	.065	0.58	132.2	22.8	134.1	12.12	43.0	
141	25.2	.000	0.58	64.5	22.9	70.7	9.41	20.5	
142	∞	.0264	0.45	108.4	0	108.4	11.16	-	
143	∞	.0264	0.45	86.2	0	86.2	9.82	-	
144	∞	.0264	0.45	188.4	0	188.4	14.0	-	
145	∞	.0264	0.45	254.4	0	254.4	21.3	65.4	
146	∞	.000	0.45	254.4	0	254.4	38.16	59.0	
147	∞	.0264	0.45	254.4	0	254.4	19.69	53.9	
148	∞	.0264	0.45	145.6	0	145.6	13.87	35.3	
149	∞	.0264	0.45	217.6	0	217.6	18.00	48.8	
150	∞	.000	0.45	217.6	0	217.6	16.71	52.6	
151	∞	.000	0.45	103.3	0	103.3	13.80	24.3	
152	∞	.0061	0.45	103.3	0	103.3	12.89	23.3	
153	∞	.0016	0.20	217.5	0	217.5	28.30	45.3	
154	∞	.234	0.80	139.6	0	139.6	5.44	27.6	
155	∞	.1632	0.80	139.6	0	139.6	6.39	28.6	
157	∞	.3158	0.80	139.6	0	139.6	4.91	32.3	
158	∞	.0563	0.45	267.8	0	267.8	15.33	56.2	
159	∞	.010	0.45	150.0	0	150.0	17.71	36.3	
160	∞	.656	0.80	146.3	0	146.3	3.68	35.6	
164	∞	.020	0.24	133.3	0	133.3	17.7	49.2	30^o
165	∞	.128	0.24	134.6	51.3	125.8	17.5	47.1	30^o
166	∞	.020	0.24	151.0	60.0	163.8	19.7	43.5	30^o
167	∞	.020	0.24	173.6	66.6	186.7	21.2	52.1	30^o
170	∞	.018	0.24	81.9	38.8	91.7	11.1	21.8	30^o
173	∞	.020	0.24	112.5	45.8	120.8	12.1-15.4	74.2-80.2	30^o *3
174	∞	.020	0.24	115.4	48.8	125.8	15.0	32.4	30^o
177	∞	.0133	0.24	252.9	90.0	270.8	31.7	73.3	30^o
178	∞	.020	0.24	261.3	77.1	270.8	30.1	76.0	30^o
180	∞	.020	0.24	249.2	76.3	262	29.1	77.1	30^o
186	∞	.040	0.24	243.3	78.3	264.6	29.6	142.0	60^o
195	1.25	1.00	0.611	57.3	15.9	58.6	5.6	120.2	
196	1.25	1.00	0.611	73.7	18.0	63.8	6.61	191.1	
197	1.25	1.00	0.611	42.2	13.7	42.2	2.98	89.9	
202	2.07	1.00	0.611	69.9	13.4	69.9	4.78	86.2	
203	2.07	1.00	0.611	91.7	16.0	91.7	5.94	133.8	
204	2.07	1.00	0.611	47.5	11.1	47.5	3.91	59.2	

Comments:
*1: Two runs in one
*2: Cross section center on edge of probes, inaccurate.
*3: Too few points, inaccurate.

Some of the runs were made with non-buoyant effluent and with an angle of either 30^o or 60^o between the port and horizontal. These cases have not been modelled in this work.

List of trajectory data recorded over large distances for jets in a coflow and recorded by video.

Run	d_p	Δ_o/g	U_∞/U_o	Fr
205	0.24	0.0235	0.125	27.0
206	0.24	0.0235	0.250	13.6
207	0.24	0.0235	0.125	27.1
208	0.24	0.0235	0.030	112.0

Run	d_p	Δ_o/g	U_∞/U_o	Fr
209	0.24	0.0235	1.000	3.39
210	0.24	0.0235	0.500	6.66
211	0.60	0.0235	1.00	2.13
212	0.24	0.0235	0.0185	181.4
213	0.62	0.0240	0.134	15.4
214	0.62	0.0240	0.0344	60.2
215	0.62	0.0240	0.0669	31.0
216	0.338	0.0240	1.00	2.82
217	0.62	0.0240	0.250	8.28
218	0.62	0.0240	1.00	2.09
221	0.335	0.0240	0.125	58.2
222	0.335	0.0240	0.125	14.6
223	0.620	0.0240	1.000	2.13

Run 205

x/d_p	41.7	83.3	125	167	335	419	502	544	682
y/d_p	4.2	9.2	10.8	13.3	25.4	30.0	37.1	38.8	54.2-55.0

x/d_p	765	849
y/d_p	60.4-62.5	62.5-72.9

Run 206

x/d_p	83.3	167	343	426	509	593	719	802	969
y/d_p	6.3	12.5	27.9	37.5	43.8	50.8	57.1	60.4	75.4

Run 207

x/d_p	83.3	125	167	208	235	250	319	402	485	569
y/d_p	4.6	6.7	10.8	13.8	17.9	20.0	26.7	31.7	40.8	47.1
x/d_p	614	652	780	864	947	1030	1114	1354	1521	1688
y/d_p	52.5	52.5	60.8	69.2	72.5	77.5	80.4	93.8	105	116

Run 208

x/d_p	125	167	208	250	266	308	350	391	475	532
y/d_p	3.8	7.1	7.9	10.4	9.6	11.7	15.4	16.3	21.7	28.3
x/d_p	558	615	699	782	865	870	954	1037	1195	1204
y/d_p	30.4	36.3	42.5	52.7	56.3	62.5	66.7	75.0	87.5	89.6
x/d_p	1361	1611								
y/d_p	97.9	112.5								

Run 209

x/d_p	176	259	343	426	468	635	635	786	801	828
y/d_p	16.7	28.3	30.0	32.1	36.7	32.1	45.4	48.8	49.6	51.3

x/d_p	911	994	1119							
y/d_p	55.0	62.5	69.6							

Run 210

x/d_p	83.3	125	167	238	404	529	571	612	696	779
y/d_p	8.8	13.8	17.1	23.8	33.3	41.3	46.7	45.4	50.0	52.1
x/d_p	862									
y/d_p	55.4									

Run 211

x/d_p	16.2	226	260	283	310	317	350	383	383	449
y/d_p	19.5	25.0	30.0	27.0	36.3	30.3	33.7	33.7	36.8	40.7
x/d_p	483									
y/d_p	42.7									

Run 212

x/d_p	167	250	344	385	427	466	510	633	701	785
y/d_p	4.2	5.0	12.9	15.8	15.8	20.8	22.9	32.9	40.0	50.8
x/d_p	868	1005	1172	1191						
y/d_p	57.1	66.7	81.3	81.3						

Run 213

x/d_p	71.9	104	137	153	169	202	250	254	282	302
y/d_p	7.9	11.9	17.9	15.3	22.2	21.9	31.0	33.1	33.7	39.7
x/d_p	315	350	355	383	387	415	419			
y/d_p	39.0	45.2	44.4	48.9	47.6	53.2	51.3			

Run 214

x/d_p	60.5	92.7	125	157	190	222	224	256	288	298
y/d_p	4.0	7.3	11.1	15.3	19.4	23.4	18.1	22.3	27.1	25.2
x/d_p	321	330	337	353	362	378	395	411	427	
y/d_p	33.2	32.6	36.5	40.5	39.0	39.5	44.4	44.7	48.1	

Run 215

x/d_p	64.2	96.5	129	177	209	221	253	280	285	301
y/d_p	2.6	7.6	11.9	20.2	24.4	28.2	33.4	37.1	38.9	40.0

x/d_p	313	317	334	345	350	361
y/d_p	40.8	41.1	44.4	46.1	45.3	49.8

Run 216

x/d_p	59.2	118	131	178	190	249	309	368	375	427
y/d_p	7.70	15.4	18.4	20.7	21.9	24.3	27.3	30.5	29.6	34.4

x/d_p	435	494	553	612	671
y/d_p	32.6	34.4	37.0	39.4	42.7

Run 217

x/d_p	43.4	59.5	91.8	124	156	189	189	237	286	291
y/d_p	4.4	7.4	12.3	17.6	22.4	27.4	26.6	31.8	35.5	36.9

x/d_p	339	388	403	452	500
y/d_p	41.1	45.7	44.8	50.0	55.0

Run 218

x/d_p	48.4	80.7	113	128	176	208	241	255	304	336
y/d_p	7.3	13.4	16.6	16.6	20.3	22.7	25.5	26.8	29.8	31.5

x/d_p	368	383	431	463	496
y/d_p	33.4	33.4	35.5	39.2	40.3

Run 221

x/d_p	1298	1417	1739	1829	1919	2367	2456	2546
y/d_p	36.4	40.0	51.3	53.7	56.7	67.2	70.5	72.5

Run 222

x/d_p	119	179	239	240	300	330	359	396	449	456
y/d_p	17.9	24.8	37.9	37.3	45.4	49.3	53.1	57.6	64.2	66.3

x/d_p	554	614	765
y/d_p	78.2	84.8	100

Run 223

x/d_p	79.0	127	176	206	222	271	319	340	384	388
y/d_p	12.7	16.1	21.3	22.1	24.5	28.4	31.9	33.9	37.9	36.5

x/d_p	437
y/d_p	39.0

APPENDIX B

DIMENSIONAL ANALYSIS TO DERIVE TRAJECTORIES IN THE XY- PLANES AND YZ-PLANES IN MOMENTUM DOMINATED FLOWS.

1. The xy-trajectory in the momentum dominated part of a buoyant jet in still ambient.

Eqs. (4.2.6) and (4.2.7) for pure jets in still ambient are

$$\frac{u_m}{Q/M} \sim \left(\frac{x}{l_{QM}}\right)^{-1} \tag{B1}$$

$$\frac{b}{l_{QM}} \sim \frac{x}{l_{QM}} \tag{B2}$$

They can be rewritten as

$$\frac{u_m}{B^{1/2}/M^{1/4}} \sim \left(\frac{x}{l_{MB}}\right)^{-1} \tag{B3}$$

$$\frac{b}{l_{MB}} \sim \frac{x}{l_{MB}} \tag{B4}$$

In this type of flow $U_\infty = 0$, $\delta = 0^o$, $\beta = 0^o$, $s' = s \approx x$, $v_{vm} = 0$, $u_{em} = u_{sm}$.

Eq. (6.2.10), the y-momentum equation,becomes

$$\frac{d}{dx}\left[I_m u_{em}^2 b^2 \sin\beta\right] = I_\Delta \Delta_m b^2 \tag{B5}$$

And eq. (6.2.11), the buoyancy flux conservation equation becomes

$$I_{q\Delta} \Delta_m u_{em} b^2 = B \tag{B6}$$

Inserting (B3) , (B4) and (B6) in (B5) and using $\sin\beta \approx dy/dx$ (cfr. eq. (6.2.18)) yields

$$\frac{y}{l_{MB}} \sim \left(\frac{x}{l_{MB}}\right)^3 \qquad \text{(B7)}$$

2. The xy-trajectory in MDNF in co-, cross- and counterflowing jets.

Eq. (B7) must also hold in these cases because (B1) , (B2) , (B5) and (B6) still apply. (B7) can be rewritten for that purpose:

$$\frac{y}{l_{BU_\infty}} \sim \left(\frac{x}{l_{M_e U_\infty}}\right)^3 \qquad \text{(B8)}$$

Note that y and x thereby become non-dimensionalised by different length scales.

3. The xy-trajectory in the MDFF of a coflowing jet.

In this type of flow $\beta \approx 0^o$, $\delta \approx 0^o$, $s' \approx s \approx x$, $v_{vm} \approx 0$, $u_{sm} \approx u_{em}$ and $u_{em} << U_\infty$.
Eqs. (4.5.31) and (4.5.32) apply :

$$\frac{u_{em}}{U_\infty} \sim \left(\frac{x}{l_{M_e U_\infty}}\right)^{-2/3} \qquad \text{(B9)}$$

$$\frac{b}{l_{M_e U_\infty}} \sim \left(\frac{x}{l_{M_e U_\infty}}\right)^{1/3} \qquad \text{(B10)}$$

Equation (6.2.10) , the y-momentum equation becomes:

$$\frac{d}{dx}\left[I_q U_\infty u_{em} \sin\beta\, b^2 \right] = I_\Delta \Delta_m b^2 \qquad \text{(B11)}$$

(Ignoring first term in (6.2.10) because $u_{em} << U_\infty$).

Equation (6.2.11) , the buoyancy flux conservation equation becomes

$$I_\Delta U_\infty b^2 \Delta_m = B \tag{B12}$$

(Ignoring first term in (6.2.11) because $u_{em} << U_\infty$).

Inserting (B9) , (B10) and (B12) in (B11) yields:

$$\sin\beta \sim \frac{x}{l_{M_e U_\infty}} \frac{l_{BU_\infty}}{l_{M_e U_\infty}} \tag{B13}$$

Equations (6.2.18) and (6.2.19) become

$$\frac{dy}{dx} = \frac{u_{em} \sin\beta}{U_\infty + u_{em}\cos\beta} \approx \frac{u_{em}\sin\beta}{U_\infty}$$

When this is inserted in (B13) then

$$\frac{y}{l_{BU_\infty}} \sim \left(\frac{x}{l_{M_e U_\infty}}\right)^{4/3} \tag{B14}$$

Note that x and y again are non-dimensionalised by different length scales.

4. The xy-trajectory in the MDFF of a counterflowing jet.

The equations will be the same as for the coflowing case but x will have the opposite sign. Eq. (B14) therefore also applies to counterflows.

5. xy- or yz-trajectories in MDFF of a crossflowing jet.

Equations (4.5.16), (4.5.17) and (4.5.19) for line momentum puffs are:

$$\frac{u_{em}}{U_\infty} \sim \left(\frac{x}{l_{M_e} U_\infty}\right)^{-2} \tag{B15}$$

$$\frac{b}{l_{M_e} U_\infty} \sim \frac{x}{l_{M_e} U_\infty} \tag{B16}$$

$$\frac{x}{l_{M_e} U_\infty} \sim \left(\frac{z}{l_{M_e} U_\infty}\right)^{1/3} \tag{B17}$$

In this type of flow $\delta \approx 90^o$, $\beta \approx 0^o$, $s' \approx s \approx z$, $u_{sm} \approx 0$, $v_{vm} \approx u_{em}$, $u_{em} << U_\infty$.
Then eq. (6.2.27), the y-momentum flux equation becomes

$$\frac{d}{dz}\left[I_v U_\infty u_{em} b^2 \sin\beta\right] = I_\Delta \Delta_m b^2 \tag{B18}$$

Eq. (6.2.28), the buoyancy flux conservation equation becomes

$$I_\Delta U_\infty \Delta_m b^2 = B \tag{B19}$$

Inserting (B15), (B16), (B17) and (B19) in (B18) yields

$$\left(\frac{z}{l_{M_e} U_\infty}\right)^{-1} \left(\left(\frac{z}{l_{M_e} U_\infty}\right)^{-2/3} \left(\frac{z}{l_{M_e} U_\infty}\right)^{2/3} \sin\beta \right) \sim \frac{l_B U_\infty}{l_{M_e} U_\infty} \tag{B20}$$

Using $dy/dx \approx \sin\beta$ (cfr. (6.2.29) and (6.2.30) in (B20) yields

$$\frac{y}{l_{BU_\infty}} \sim \left(\frac{x}{l_{M_e U_\infty}}\right)^4 \sim \left(\frac{z}{l_{M_e U_\infty}}\right)^{4/3} \tag{B21}$$

APPENDIX C
ASSUMPTIONS

Assumptions in the calculations.

1. The flow is incompressible.

2. The variations of the fluid density throughout the flow field are small compared to the reference density. This implies that the density variation can be neglected when considering the inertia terms and thus the conservation of mass flux can be replaced by the conservation of volume flux. This is called the Boussinesq approximation.

3. Within the range of variation the density of the fluid is assumed to be a linear function of salt concentration .

4. Longitudinal turbulent transport ($\overline{u'c'}$) is small compared to longitudinal convective transport $\overline{uc}$. (However, Papanicolaou [1984] showed that $\overline{u'c'}$ is about 15% of $\overline{uc}$. This has been accounted for by subsequently adjusting the cross sectional constants $I_{q\Delta}$ and I_{qc}, see appendix D).

5. The flow is fully turbulent such that molecular transports can be neglected with respect to turbulent transports.

6. The pressure in the flow field is hydrostatic.

7. The curvature of the trajectory is small, i.e. the ratio of the local characteristic width b is small as compared with the radius of curvature of the trajectory.

8. The flow region is sufficiently long and thin for all changes in the flow to occur slowly, i.e. the boundary approximations can be made in which gradients in the tangential direction are much smaller than those in the radial direction. This approximation also implies that the tangential velocity is much greater than the radial velocity.

9. In a moving environment we will assume that as long as the ambient velocity is perpendicular to the local excess velocity then the jet will be merely advected by the ambient flow.

APPENDIX D

THE RELATIONSHIP BETWEEN COEFFICIENTS IN CHAPTER 5 AND CROSS SECTIONAL CONSTANTS.

MDNF still ambient, coflow, crossflow and counterflow.

In this type of flow $\beta \approx 0^o$, $\delta \approx 0^o$, $s' \approx s \approx x$, $u_{em} \approx u_{sm}$, $v_{vm} \approx 0$, $u_{em} >> U_\infty$.

The x-momentum equation becomes (cfr. eqs. (6.2.9) , (6.2.26) and (6.2.36)):

$$I_m u_{em}^2 b^2 = M_e \tag{D1}$$

The y-momentum equation becomes (cfr. eqs. (6.2.10) , (6.2.27) and (6.2.37)):

$$\frac{d}{dx}[I_m u_{em}^2 b^2 \sin\beta] = I_\Delta \Delta_m b^2 \tag{D2}$$

The buoyancy flux conservation equation becomes (cfr. eqs. (6.2.11), (6.2.28) and (6.2.38)): (Irrelevant when B=0)

$$I_{q\Delta} u_{em} \Delta_m b^2 = B \tag{D3}$$

Tracer flux conservation (relevant when B=0):

$$I_{qc} u_{em} c_m b^2 = QC_o \tag{D4}$$

Eq. (D4) is eq. (D3) with Δ replaced by c.

The growth of width equation is (cfr.(6.3.10) with $u_{em} >> U_\infty$)

$$db/dx = k = 0.109 \tag{D5}$$

The geometric relationship becomes (cfr. eqs. (6.2.18), (6.2.30) or (6.2.40)):

$$dy/dx \approx \sin\beta \tag{D6}$$

There is an additional geometric relationship for crossflows (cfr. (6.2.31)):

$$dz/dx \approx U_\infty/u_{em} \tag{D7}$$

By solving the system of equations (D1)-(D7) the following solutions are found:

$$\frac{y}{l_{BU_\infty}} = \frac{I_\Delta I_m^{1/2} k}{6 I_{q\Delta}} \left(\frac{x}{l_{M_e U_\infty}} \right)^3 \tag{D8}$$

$$\frac{S_{CL} Q}{U_\infty l_{M_e U_\infty}^2} = \frac{I_{q\Delta} k}{I_m^{1/2}} \left(\frac{x}{l_{M_e U_\infty}} \right) \tag{D9}$$

Crossflow only:

$$\frac{x}{l_{M_e U_\infty}} = \left(\frac{2}{I_m^{1/2} k} \right)^{1/2} \left(\frac{z}{l_{M_e U_\infty}} \right)^{1/2} \tag{D10}$$

For co-, cross- and counterflow eqs. (D8) and (D9) can also be written as:

$$\frac{y}{l_{BU_\infty}} = \frac{I_\Delta I_m^{1/2} k}{6 I_{q\Delta}} \left(\frac{x}{l_{M_e U_\infty}} \right)^3 \tag{D11}$$

$$\frac{S_{CL} Q}{U_\infty l_{M_e U_\infty}^2} = \frac{I_{q\Delta} k}{I_m^{1/2}} \left(\frac{x}{l_{M_e U_\infty}} \right) \tag{D12}$$

When equations (D8)-(D12) are compared with the equations in chapter 5 it can be seen that

$$C_{a1} = C_{b1} = C_{c1} = C_{d1} = \frac{I_{q\Delta} k}{I_m^{1/2}} \tag{D13}$$

$$C_{a2} = C_{b2} = C_{c2} = C_{d2} = \frac{I_\Delta I_m^{1/2} k}{6 I_{q\Delta}} \tag{D14}$$

$$C_{c3} = \left(\frac{2}{I_m^{1/2} k} \right)^{1/2} \tag{D15}$$

For non-buoyant flows $I_{q\Delta}$ and I_Δ are replaced by I_{qc} and I_c which are of the same value.

Eliminating k:

$$\begin{Bmatrix} C_{a1} \\ C_{b1} \\ C_{c1} \\ C_{d1} \end{Bmatrix} = \frac{6 I_{q\Delta}^2}{I_\Delta I_m} \begin{Bmatrix} C_{a2} \\ C_{b2} \\ C_{c2} \\ C_{d2} \end{Bmatrix} \tag{D16}$$

$$C_{c3} = \frac{I_\Delta^{1/2}}{\sqrt{3} I_{q\Delta}^{1/2}} C_{c2}^{-1/2} \tag{D17}$$

MDFF in coflow.

In this type of flow $\beta \approx 0^o$, $\delta \approx 0^o$, $s' \approx s \approx x$, $u_{em} \approx u_{sm}$, $v_{vm} \approx 0$, $u_{em} << U_\infty$.

The x-momentum equation becomes (cfr. eq. (6.2.9))

$$I_q U_\infty u_{em} b^2 = M_e \tag{D18}$$

The y-momentum equation becomes (cfr. (6.2.10)):

$$\frac{d}{dx} [I_q U_\infty u_{em} b^2 \sin\beta] = I_\Delta \Delta_m b^2 \tag{D19}$$

The buoyancy flux conservation equation becomes (cfr. (6.2.11)):

$$I_\Delta U_\infty \Delta_m b^2 = B \tag{D20}$$

The tracer flux conservation equation becomes (relevant when B=0):

$$I_c U_\infty c_m b^2 = QC_o \tag{D21}$$

(Which is (D20) with Δ_m replaced by c_m and $B=Q_o\Delta_o$ replaced by QC_o).

The growth of width equation (eq. (6.3.10) with $u_{em}<<U_\infty$) becomes:

$$db/dx = k\, u_{em}/U_\infty \tag{D22}$$

The geometric relationship becomes (cfr. eq. (6.2.18)):

$$dy/dx \approx \sin\beta\, u_{em}/U_\infty \tag{D23}$$

The system of equations (D18)-(D23) is solved and the following solutions are found:

$$\frac{y}{l_{BU_\infty}} = \frac{3^{1/3}}{4 I_q^{1/3} k^{2/3}} \left(\frac{x}{l_{M_e U_\infty}} \right)^{4/3} \tag{D24}$$

$$\frac{S_{CL} Q}{U_\infty l_{M_e U_\infty}^2} = I_\Delta \left(\frac{3k}{I_q} \right)^{2/3} \left(\frac{x}{l_{M_e U_\infty}} \right)^{2/3} \tag{D25}$$

Similar equations will be expected for jets in a counterflow but with a change of sign for x.
For non-buoyant flows I_Δ is replaced by I_c.

When eqs. (D24) and (D25) are compared with the formulae in chapter 5 then it can be seen that:

$$C_{b4} = C_{d4} = I_\Delta \left(\frac{3k}{I_q} \right)^{2/3} \tag{D26}$$

$$C_{b5} = C_{d5} = \frac{3^{1/3}}{4 I_q^{1/3} k^{2/3}} \tag{D27}$$

Eliminating k yields:

$$\begin{Bmatrix} C_{b5} \\ C_{d5} \end{Bmatrix} = \frac{3 I_\Delta}{4 I_q} \begin{Bmatrix} C_{b4} \\ C_{d4} \end{Bmatrix}^{-1} \tag{D28}$$

MDFF in a crossflow.

In this type of flow $\beta \approx 0^o$, $\delta \approx 90^o$, $u_{sm} \approx 0$, $v_{vm} \approx u_{em}$, $u_{em} << U_\infty$, $s' \approx z$.

The x-momentum equation , eq. (6.2.26) becomes

$$I_v U_\infty u_{em} b^2 = M_e \tag{D29}$$

The y-momentum equation, eq. (6.2.27) becomes:

$$\frac{d}{dz}[I_v U_\infty u_{em} b^2 \sin\beta] = I_\Delta' \Delta_m b^2 \tag{D30}$$

The buoyancy flux equation, eq. (6.2.28) becomes:

$$I_\Delta' U_\infty \Delta_m b^2 = B \tag{D31}$$

The tracer conservation equation is (relevant when B=0):

$$I_c' U_\infty c_m b^2 = QC_o \tag{D32}$$

Eq. (D32) is eq. (D31) with Δ replaced by c and dashes indicate that the cross sectional constants refer to vortex pair distribution.
The growth of width equation is (cfr. (6.3.6)):

$$db/dx = m \approx 0.30 \tag{D33}$$

The geometric relationships (6.2.29) - (6.2.31) become:

$$dy/dx \approx \sin\beta \tag{D34}$$

$$dx/dz \approx u_{em}/U_\infty \tag{D35}$$

The system of equations (D29)-(D35) is solved and the following solutions are found:

$$\frac{z}{l_{M_e}U_\infty} = \frac{I_v m^2}{3}\left(\frac{x}{l_{M_e}U_\infty}\right)^3 \tag{D36}$$

$$\frac{y}{l_{BU_\infty}} = \frac{3^{1/3}}{4 I_v^{1/3} m^{2/3}}\left(\frac{z}{l_{M_e}U_\infty}\right)^{4/3} \tag{D37}$$

$$\frac{S_{CL}Q}{U_\infty l_{M_e}^2 U_\infty} = I_\Delta' m^2\left(\frac{x}{l_{M_e}U_\infty}\right)^2 \tag{D38}$$

Comparing eqs. (D36)-(D38) with the equations in chapter 5 yields:

$$C_{c4} = I_\Delta' m^2 \tag{D39}$$

$$C_{c5} = \frac{3^{1/3}}{4 m^{2/3} I_v^{1/3}} \tag{D40}$$

$$C_{c6} = \left(\frac{m^2 I_v}{3}\right)^{-1/3} \tag{D41}$$

Eliminating m:

$$C_{c5} = \frac{3^{1/3}}{4 I_v^{1/3}}\left(\frac{C_{c4}}{I_\Delta'}\right)^{-1/3} \tag{D42}$$

$$C_{c6} = \left(\frac{3 I_\Delta'}{I_v}\right)^{1/3} C_{c4}^{-1/3} \tag{D43}$$

BDNF in still ambient, coflow, crossflow and counterflow.

In this type of flow $\delta \approx 0^o$, $\beta \approx 90^o$, $s' \approx y$, $u_{sm} \approx u_{em}$, $v_{vm} \approx 0$, $u_{em} >> U_\infty$.

The y-momentum equation becomes (cfr. (6.2.10) , (6.2.27) and (6.2.37)):

$$\frac{d}{dy}[I_m u_{em}^2 b^2] = I_\Delta \Delta_m b^2 \qquad \text{(D44)}$$

The buoyancy flux conservation equation becomes (cfr. (6.2.11) , (6.2.28) and (6.2.38)):

$$I_{q\Delta} u_{em} \Delta_m b^2 = B \qquad \text{(D45)}$$

The geometric relationship is for coflows and counterflows (cfr. (6.2.18) + (6.2.19) or (6.2.39)+(6.2.40)):

$$dy/dx = u_{em}/U_\infty \qquad \text{(D46)}$$

(D46) becomes for still ambient cases where $U_\infty = 0$:

$$dy/dx \rightarrow \infty \qquad \text{(D47)}$$

For crossflows the geometric relationships are (cfr. (6.2.29)-(6.2.31)):

$$dy/dz = u_{em}/U_\infty \qquad \text{(D48)}$$

$$dy/dx \rightarrow \infty \qquad \text{(D49)}$$

The growth of width is in all cases (cfr. (6.3.10)):

$$db/dy = k \qquad \text{(D50)}$$

Solving eqs. (D44)-(D50) yields the following solutions (after assuming u_{em} to be a power of y):

coflow and counterflow (with a change of sign for x):

$$\frac{y}{l_{BU_\infty}} = \left(\frac{9 I_{q\Delta} I_m k^2}{16 I_\Delta}\right)^{1/4} \left(\frac{x}{l_{BU_\infty}}\right)^{3/4} \tag{D51}$$

still ambient:

$$\frac{x}{l_{MB}} = \frac{x_{max}}{l_{MB}} \tag{D52}$$

crossflow:

$$\frac{x}{l_{BU_\infty}} = \frac{x_{max}}{l_{BU_\infty}} \tag{D53}$$

(x_{max} can not be found explicitly from this analysis).

Crossflow:

$$\frac{y}{l_{BU_\infty}} = \left(\frac{9 I_{q\Delta} I_m k^2}{16 I_\Delta}\right)^{1/4} \left(\frac{z}{l_{BU_\infty}}\right)^{3/4} \tag{D54}$$

Still ambient:

$$\frac{S_{CL} Q}{l_{MB} M^{1/2}} = I_{q\Delta} \left(\frac{3 I_\Delta}{4 I_{q\Delta} I_m k^2}\right)^{1/3} k^2 \left(\frac{y}{l_{MB}}\right)^{5/3} \tag{D55}$$

General(coflow, crossflow and counterflow):

$$\frac{S_{CL} Q}{U_\infty l_{BU_\infty}^2} = I_{q\Delta} \left(\frac{3 I_\Delta}{4 I_{q\Delta} I_m k^2}\right)^{1/3} k^2 \left(\frac{y}{l_{BU_\infty}}\right)^{5/3} \tag{D56}$$

Comparing eqs. (D51)-(D56) with the equations in chapter 5 gives

$$C_{a7} = C_{b7} = C_{c7} = C_{d7} = I_{q\Delta}\left(\frac{3I_\Delta}{4I_{q\Delta}I_m}\right)^{1/3} k^{4/3} \tag{D57}$$

$$C_{b8} = C_{c8} = C_{d8} = \left(\frac{9I_{q\Delta}I_m}{16I_\Delta}\right)^{1/4} k^{1/2} \tag{D58}$$

Eliminating k yields:

$$\begin{Bmatrix} C_{b7} \\ C_{c7} \\ C_{d7} \end{Bmatrix} = \frac{4I_\Delta}{3I_m} \begin{Bmatrix} C_{b8} \\ C_{c8} \\ C_{d8} \end{Bmatrix}^{8/3} \tag{D59}$$

<u>BDFF in coflow, crossflow and counterflow.</u>

In this type of flow $\beta \approx 0^o$, $\delta \approx 90^o$, $u_{sm} \approx 0$, $v_{vm} \approx u_{em}$, $u_{em} << U_\infty$. Coflow and counterflow: $s' \approx x$, crossflow: $s' \approx z$.

The y-momentum equation becomes for a coflow and counterflow (cfr. (6.2.10) and (6.2.37)):

$$\frac{d}{dx}[I_v U_\infty u_{em} b^2] = I_\Delta' \Delta_m b^2 \tag{D60}$$

The y-momentum equation becomes for a crossflow (cfr. (6.2.27)):

$$\frac{d}{dz}[I_v U_\infty u_{em} b^2] = I_\Delta' \Delta_m b^2 \tag{D61}$$

The buoyancy flux conservation equation becomes (cfr. (6.2.11),(6.2.28) and (6.2.38)):

$$I_\Delta' U_\infty \Delta_m b^2 = B \tag{D62}$$

The geometric relationship is for coflow and counterflow (cfr. (6.2.18)+(6.2.19) or (6.2.39)+(6.2.40)):

$$dy/dx = u_{em}/U_\infty \tag{D63}$$

The geometric relationships for a crossflow (cfr. (6.2.29)-(6.2.31)):

$$dy/dx \rightarrow \infty \tag{D64}$$

$$dy/dz \approx u_{em}/U_\infty \tag{D65}$$

The growth of width equation is common for coflow, crossflow and counterflow (cfr. (6.3.8)):

$$db/dy = m \approx 0.30 \tag{D66}$$

Solving (D60)-(D66) yields the following solutions:

Coflow:

$$\frac{y}{l_{BU_\infty}} = \left(\frac{3}{2 I_v m^2}\right)^{1/3} \left(\frac{x}{l_{BU_\infty}}\right)^{2/3} \tag{D67}$$

(Applies also to counterflows with a change of sign for x).

Crossflow:

$$\frac{y}{l_{BU_\infty}} = \left(\frac{3}{2 I_v m^2}\right)^{1/3} \left(\frac{z}{l_{BU_\infty}}\right)^{2/3} \tag{D68}$$

Coflow, crossflow and counterflow:

$$\frac{S_{CL} Q}{U_\infty l_{BU_\infty}^2} = I_\Delta' m^2 \left(\frac{y}{l_{BU_\infty}}\right)^2 \tag{D69}$$

Comparing (D67)-(D69) with the equations in chapter 5 yields:

$$C_{b9} = C_{c9} = C_{d9} = I_\Delta' m^2 \tag{D70}$$

$$C_{b10} = C_{c10} = C_{d10} = \left(\frac{3}{2 I_v m^2}\right)^{1/3} \tag{D71}$$

Eliminating m yields:

$$\begin{Bmatrix} C_{b10} \\ C_{c10} \\ C_{d10} \end{Bmatrix} = \left(\frac{3 I_\Delta'}{2 I_v}\right)^{1/3} \begin{Bmatrix} C_{b9} \\ C_{c9} \\ C_{d9} \end{Bmatrix}^{-1/3} \tag{D72}$$

In chapter 6 it was assumed that the distribution of u_s was Gaussian:

$$u_s = u_{sm} e^{-\left(\frac{r}{b}\right)^2} \tag{D73}$$

The distribution of Δ_m and c_m in category I flows were also assumed Gaussian. Using the definitions of the cross sectional constants, eqs. (6.2.12)-(6.2.17) yields:

$I_m = \pi/2$

$I_q = \pi$

$I_{q\Delta}=I_{qc}=(\pi\lambda^2/(1+\lambda^2)) * 1.15$ (cfr. Papanicolaou p. 174)

$I_\Delta = I_c = \pi\lambda^2$

$I_{q\Delta}$, I_{qc} , I_Δ and I_c must be expected to change when the distribution of Δ or c changes from Gaussian to what corresponds to vortex-pair distribution of the velocity. The constants are then denoted $I_{q\Delta}'$, I_{qc}' , I_Δ' and I_c'. However, for the sake of simplicity it is decided that

$I_{q\Delta} = I_{q\Delta}' = I_{qc} = I_{qc}' = (\pi\lambda^2/(1+\lambda^2)) * 1.15$ and $I_\Delta = I_\Delta' = I_c = I_c' = \pi\lambda^2$

The cross sectional constant I_v then remains to be determined. I_v can be found from the coefficients C_{c6} , C_{c5} , C_{b10} or C_{c10} which all contain I_v. The data for C_{b9} , C_{b10} and C_{c6} must be considered to be of the best quality and they yield $I_v \approx 4.2$.

The spreading coefficient λ is assumed not to vary with the velocity distribution and it is assumed to be equal to 1.2. The value of k is 0.109 and the value of m is 0.30.

The above constants were used to calculate the theoretical values of the coefficients in table 5.5.

APPENDIX E

SOLUTION OF THE BASIC EQUATIONS IN COMPOSITE JETS.

Pure jet in a coflow.

The basic equations become (cfr. eqs. (6.4.1), (6.4.2) and (6.4.3)):

$$I_m u_{em}^2 b^2 + I_q u_{em} U_\infty b^2 = M_e \tag{E1}$$

$$I_c U_\infty c_m b^2 + I_{qc} u_{em} c_m b^2 = C_o Q \tag{E2}$$

$$\frac{db}{dx} = k \frac{u_{em}}{U_\infty + u_{em}} \tag{E3}$$

Eqs. (E1) and (E2) can be rewritten:

$$\frac{dx}{d u_{em}} = -\frac{M_e^{1/2}}{2} \frac{2 I_m u_{em} + I_q U_\infty}{(I_m u_{em}^2 + I_q u_{em} U_\infty)^{3/2}} \frac{U_\infty + u_{em}}{k u_{em}} \tag{E4}$$

Using $I_q = 2 I_m = \pi$ and integrating yields:

$$\left(\frac{1}{2}\left(\frac{u_{em}}{U_\infty}\right)^2 + \left(\frac{u_{em}}{U_\infty}\right)\right)^{-1/2} \left[\frac{8k}{3\sqrt{\pi}}\left(\frac{u_{em}}{U_\infty}+1\right) - \frac{2k}{3\sqrt{\pi}}\left(\frac{u_{em}}{U_\infty}\right)^{-1} + \frac{2k}{\sqrt{\pi}}\frac{u_{em}}{U_\infty}\right] = \frac{x}{l_{M_e} U_\infty} + c_4 \tag{E5}$$

where c_4 is an integration constant.

Similarly, rewriting (E1) and (E3) and using $I_q = 2 I_m = \pi$ yields:

$$\frac{dx}{db} = k^{-1} \frac{\left(\frac{\pi}{2}\left(\frac{b}{l_{M_e} U_\infty}\right)^2 + 1\right)^{1/2}}{-\left(\frac{\pi}{2}\right)^{1/2} \frac{b}{l_{M_e} U_\infty} + \left(\frac{\pi}{2}\left(\frac{b}{l_{M_e} U_\infty}\right)^2 + 1\right)^{1/2}} \tag{E6}$$

Eq. (E6) yields after integration:

$$k^{-1}\left[\frac{b}{l_{M_e}U_\infty}+\frac{\pi}{6}\left(\frac{b}{l_{M_e}U_\infty}\right)^3+\frac{1}{6\sqrt{\pi}}\left[\left(\frac{b}{l_{M_e}U_\infty}\right)^2+2\right]^{3/2}\right]=\frac{x}{l_{M_e}U_\infty}+c_5 \tag{E7}$$

where c_5 is an integration constant.

Finally, eq. (E2) yields:

$$\frac{S_{CL}Q}{U_\infty l^2_{M_e}U_\infty}=\left(I_c+I_{qc}\frac{u_{em}}{U_\infty}\right)\left(\frac{b}{l_{M_e}U_\infty}\right)^2 \tag{E8}$$